By Architects. For Architects.
By Engineers. For Engineers.

Architecture
Civil and Structural Engineering
Mechanics of Materials
Building and Construction
Urban Planning and Development
Transportation Issues in Construction
Geotechnical Engineering and Engineering Geology
Designing, Operation and Service
of Construction Site Engines

# Architecture and Engineering

## Volume 7  Issue 1 (2022)

ISSN: 2500–0055

# CONTENTS

# Civil Engineering

## EULER'S POWER CALCULATIONS OF "NATURAL FORCES" TO RAISE WATERS WITH PISTON PUMPS

Sylvio R. Bistafa

University of São Paulo, Polytechnic School, Department of Mechanical Engineering
05508-030, São Paulo, SP, Brazil

E-mail: sbistafa@usp.br

**Abstract**

**Introduction:** In a 1754 publication, *Discussion plus particulière de diverses manières d'elever de l'eau par le moyen des pompes avec le plus grand avantage* (Very detailed explanation of the different methods of raising water through pumps with the greatest effectiveness), Leonhard Euler (1707–1783) made extensive use of the concept of mechanical power in estimates of the power needed to raise waters with piston pumps, by means of natural forces such as human and horse force, running waters, and windmills. **Purpose of the study:** We aimed to revisit this publication to show to the modern reader Euler's pioneering approach in providing rational calculations of the power of natural forces needed to drive different machines to raise waters with piston pumps. **Methods:** After a brief historical review on the use of natural forces to drive machines and the evolution of the concept of mechanical power, the method employed was the examination and an annotated reproduction of the main formulation using Euler's original notation and ways of scientific writing of the time. **Discussion:** We address the evolution of hydropower and wind power, particularly for the generation of electricity, and also show that despite of its much lower attractiveness, there have been some attempts in the use of human and animal power in developing countries, particularly in applications that do not require large and constant amounts of power inputs.

**Keywords**

Piston pumps to raise water, history of piston pumps, power of natural forces, history of hydraulic machines.

### Introduction

The need of providing mechanical power to drive machines has been a pressing issue for humans since the earliest civilizations as it is still today. In classical antiquity, virtually all work was done by man-power or animal power. Water power was used for pumping and in ancient industrial processes but probably not much before the first century BC (Landels, 1978). The dates are uncertain, but it is said that as early as 1700 BC, Hammurabi used windmills for irrigation in the plains of Mesopotamia (Golding, 1976). There is evidence that wind power was used in Afghanistan around 700 AD and by the Chinese back in 1200 AD (Golding, 1976). Harnessing water power and using it to drive machinery were apparently not explored until the early part of the first century BC. According to the geographer Strabo, a water-mill was built in the Pontus (near the modern Niksar, N. central Turkey) (Landels, 1978). The conceptions of these machines were probably transmitted and perfected from generation to generation. Certainly, there were virtually no guidelines to estimate the required inputs (force, work, and power) to achieve the desired outputs (flow rate, head, pressure, and efficiency); in other words, the technological

knowledge as is known today was non-existent, and, perhaps, not even thought of.

It is argued (Landels, 1978) that the Mediterranean world, and particularly the Roman Empire, was dominated by the Greek culture, which might have had important effects on the scientific thought. This was characterized by a liking for stability, rest and permanence, and an opposing dislike of change and movement, which caused people to set a high value on the permanent and stable. As a result, their understanding of static conditions (e.g., hydrostatics) and mechanical problems not involving movement was acute, whereas their ideas on dynamics (e.g., ballistics) were incomplete and inaccurate. They spoke of velocities but hardly even began to study acceleration, which impaired the notion of inertia and kinetic energy.

The study of motion was also impaired by the lack of devices to measure short intervals of time, of the order of seconds. Moreover, philosophers of the time, such as Plato, and their followers adopted an anti-physical attitude, exalting the "pure" and theoretical sciences (such as geometry and astronomy), looking down on any research that was mechanical, or which had practical applications (Landels, 1978).

### First Notions of Force, Work, and Power

It is possible to say that this state of affairs began to change with Galileo Galilei (1564–1642) and a mechanical treatise of his authorship, referred to by the author himself as *Mechanics (Le mecaniche)*, which consisted of handwritten texts, copies of which obtained wide circulation in Europe in the first half of the 17th century, and eventually was published in 1634 in French by Marin Mersenne (1588–1648) under the title *Les Mécaniques de Galilée*, a year after the conviction of Galileo by the Holy Inquisition. Along with Galileo, he referred to mechanics in the plural to designate the part concerned with machines, as distinct from the denomination in the singular — mechanic — understood as the general theory for the conditions of rest (equilibrium) and natural motion of physical bodies.

According to Mariconda (2008), the original manuscript by Galileo was considered lost. Nonetheless, two copies appeared, one in a short version and another in a long version, the former written in 1593/1594, and the latter written in 1601/1602. Based on secondary sources that examined these publications, Mariconda showed that the basic explanation scheme employed by Galileo consists in showing that, as for the machines known at Galileo's time (lever, pulley, wedge, screw, inclined plane, and capstan), all can be reduced to a system of simple levers. The lever principle is extended from the static to the dynamic case, and the effect of velocity on the motive power is considered, where the motive power is the product of the weight (force) of a body and its velocity, taken by Galileo as a measure of the power being used.

Galileo's approach differed from the works of his predecessors in his strategy of introducing idealized conditions with the basic objective of eliminating friction, in order to think of an ideal machine. Galileo's predecessors knew that friction reduces performance (yield) of a machine, but none of them were led to, or were able to, think about the following problem: what would happen with a perfect machine? Or, more simply, what would happen with a frictionless machine?

Thus, according to Galileo's conception of machines, they all have the function of transmitting and applying force or power as effectively as possible. In this conception, it is possible to develop a quantitative evaluation for the performance of machines in terms of the product of the driving force used and speed, which corresponds to an important step towards the quantification of the power of a machine and opens the way for the elaboration of concepts such as work and energy, which are fundamental for the development of modern engineering.

It is generally accepted that the concept of force was first formally introduced into physics with Newton's second law of motion. Similar to "quantity of matter", the product of density and volume, Newton (1643–1727) proposed "quantity of motion" as a measure of the same, arising from velocity and quantity of matter conjointly ($mv$).

Since the quantity of motion is a scalar, Newton's definition implicitly treated velocity $v$ as scalar speed rather than vector velocity $\vec{v}$. Hence the quantity of motion is not precisely identical to the modern concept of momentum, which is a vector quantity given by $m\vec{v}$. Based on the scalar quantification of "motion", Newton had to acknowledge that, contrary to the teachings of Descartes, the "quantity of motion" is not conserved.

The concept of work (force times distance), and power (work per unit of time) may have been first introduced by Descartes (1596–1650) as indicated by Belidor[a], in his famous *Architecture Hydraulique* (de Belidor, 1819). In the first chapter (§ 85), the concept was discussed by Belidor, with the subtitle "Descartes Principle for Mechanics", and it is presented as follows (Fig. 1): "… a body only has force as long as it is in motion, and this force will be all the greater when it will have, at the same time, more mass and more speed, as a rectangle will have more surface when it has a larger base and a greater height. Or, since this surface is expressed by the product of these two dimensions, similar is the force of a body, which is also called its 'quantity of motion', and should be expressed by the product of its mass and its speed…"

In § 89 Belidor generalized the Descartes Principle considering power ($P = Fv$) rather than quantity of motion ($mv$), to read: "… in the state of equilibrium, the force and the weight will be as the reciprocal ratio of their speed; and, therefore, the quantity of motion of the force will be equal to that of the weight …" This translates to the equality of powers: $P_{in} = P_{out}$. In the subsequent paragraphs, de Belidor applied this principle to several simple mechanical machines such as: levers, pulleys, cranks, etc. Fig. 2 is an image of an ancient crane, composed of several mechanical elements for power conversion.

In § 99 Belidor exemplified the mechanical principle by applying it to a hoisting machine: "… a force of 25 livres[b] may aid a machine to hoist a weight of 500 livres, if the weight is only one foot of a way in

---

[a] Bernard Forest de Belidor (1697–1761), a military engineer, taught mathematics at the artillery school at La Fère where he authored several textbooks. Seeking to introduce mathematics into practical engineering, he wrote *La science des ingénieurs* (1729) and *Architecture hydraulique* (1737–1739).

[b] The livre poids de marc or livre de Paris was equivalent to about 489.5 grams and was used between the 1350s and the late 18th century.
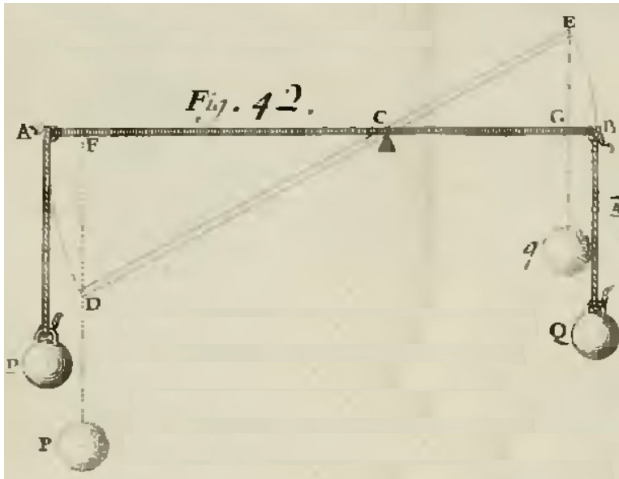
Fig. 1. de Belidor's illustration of the Descartes Principle for Mechanics (de Belidor, 1819)



Fig. 2. Ancient crane hoisting a load with the aid of the human power applied to the paddles of the turning wheel (source: https://www.gruasyaparejos.com/en/construction-crane/ancient-crane/)

the time that the force will make 20 (feet): or else, a weight of 50 livres will raise a weight of 500 livres, if the former has a velocity ten times greater than that of the 500 livres weight …"

However, Claude-Louis Navier (1785–1836), the reviewer of the new edition of *Architecture Hydraulique*[c] , an academic at the *École Nationale des Ponts et Chaussées and École Polytechnique,* in a footnote following this paragraph, reproached de Belidor for his interpretation of the Descartes Principle and rephrased it in more rigorous terms by substituting speeds for virtual velocities, followed by other considerations. Nonetheless, de Belidor recast it in terms of power, perhaps because he was more interested in the practical applications of the  principle.

**Definition of power:** if a constant force $F$ is applied throughout a distance $d$, the work done $T$ is defined as $T=F \cdot d$. In turn, the power $P$ is defined as the work done per unit of time, $P=\dfrac{T}{t}=\dfrac{F \cdot d}{t}=F \cdot 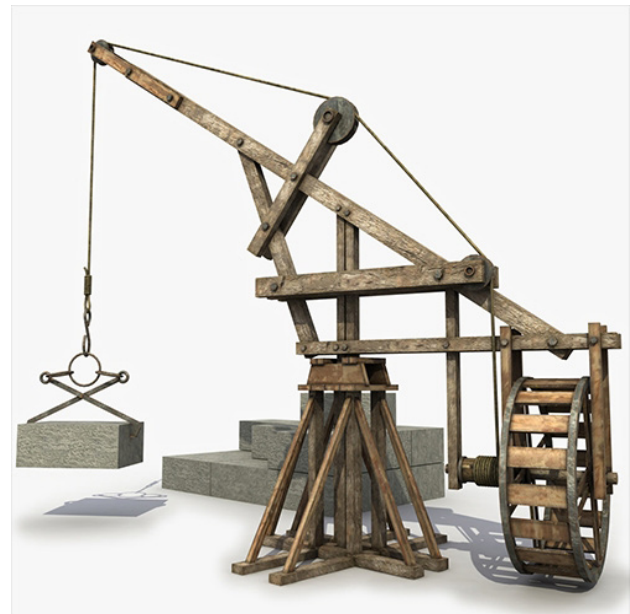v$ , where $v$ is the speed. For a distance $d$ equal to one meter, a force $F$ equal to one newton, and for a unit of time of one second, the power is equal to one watt: $1W=1N \cdot 1 \; m/s$.

Another common and traditional measure of power is the horsepower (hp)[d], comparing to the power of a horse (Fig. 3); one mechanical horsepower equals about 735.5 watts. This means that a horse is capable of raising a load of 75 kg (165 lbf) to a height of 1 m (3.28 ft) in 1 s. Since the normal gravity is equal to 9.80665 m/s², then a force of 735.5 N is necessary to raise a mass of 75 kg, which at a velocity of 1 m/s, would require a power of  foot-pounds per second (FPS).

When considering human-powered equipment, a healthy human can produce about 1.2 hp (0.89 kW) "briefly" and sustain about 0.1 hp (0.075 kW) "indefinitely".

[c]  In the 1810s, de Belidor's two works, *La science des ingénieurs* (1729) and *Architecture hydraulique* (1737–1739) were issued in revised and expanded editions by Navier, who had been recruited by the École des Ponts et Chaussées to edit the works of his great-uncle, the great French engineer Émiland Gauthey. By 1813 Navier completed this task and also issued a revised and expanded edition of Belidor's *La science des ingénieurs*. Navier's success as an editor of Belidor's *Science des ingénieurs* and Gauthey's works led their publisher, Firmin Didot, to invite him to prepare a revised edition of Belidor's *Architecture hydraulique.* Navier sought to correct the errors found in this work and give it a mathematical sophistication that would make it useful to the graduates of the École Polytechnique. Navier's contributions to the *Architecture hydraulique* are confined to the first volume, which contains notes and commentary equal or surpassing the original text in length. The remaining volumes consist of reissues, with new titles dated 1810, of the edition published in 1780 (text adopted from Jeremy Norman's Historyofscience.com, *https://www.jnorman.com/cgi-bin/hss/38462.html,* accessed on March 9, 2017).

[d]  Until the mid-18th century, most demanding labor required horses. With the advent of the steam engine, machinery began to replace horses for various tasks. But many people resisted this change; they were skeptical about the efficiency of the new machines. Inventor James Watt (1736–1819) knew this and capitalized on it when marketing his improved steam engine. Watt noticed people's reticence to adopt the new technology and decided to make a measurement comparison that potential buyers could relate to: horses. But instead of figuring out exactly how much power a horse really produced, he estimated it. Watt guessed that a pony could lift an average of 220 lbf (pound-force) 100 ft. per minute (220 lbf x 100 ft./min. = 22,000 lbf x ft./min.). From there, he extrapolated that a horse could lift 50 percent more than a pony, bringing the estimated power of a horse, or horsepower, to 33,000 lbf x ft/min = 550 lbf x ft./s. Regardless of how accurate his measurements actually were (some neigh-sayers disagreed with them because no horse could sustain that level of effort for an extended period of time), the comparison was an effective one, and the term stuck (text adopted from "The History of Horsepower" by Paul Humphreys, https://www.thecompressedairblog.com/the-history-of-horsepower, accessed on March 10, 2021).

**Euler's Calculations of Mechanical Power from "Natural Forces"**

Leonhard Euler (1707–1783) was, perhaps, the first to formally introduce mechanical power as a measure of the capacity of natural forces to drive piston pumps by means of humans, horses, running waters, and windmills (Euler, 1754). This is a most remarkable publication from the engineering point of view, because Euler was capable of providing detailed calculations on how to design systems to extract power from these natural sources, which can well serve as an introductory historic chapter to any textbook on the evolution of machinery for raising waters.

Euler began by invoking his previous memoir on raising waters with piston pumps (Euler, 1754b), in which he had developed the analytical tools necessary for determining the pressures that the piping system should sustain according to the required raising height and volume flow rate. From these, and from the pump dimensions, he was able to determine the piston velocity and the effort exerted by the pump's piston per second (equal to the work done per second during the pump's piston motion, or the supplied power).

Fig. 4 shows a conception of a pair of piston pumps that operate out of phase in their delivery and aspiration cycles, in order to provide a continuous flow of water through the piping system. In this figure, $F$ is the force applied to the lever that is supposed to move with a velocity $a$, and $K$ is the resulting force applied to the piston that is supposed to move with a velocity $\zeta$, such that $K\zeta = Fa$. The pumping system is supposed to have the following characteristics: piston diameter = $a$, piston excursion = $b$, diameter of the piping system = $c$, height of the reservoir = $g$, length of the pipe = $l$, cycling time of the piston = $t$, flow rate per hour = $M$, and pressure inside the pipe at the pump exit = $p$.

Next, Euler wrote the following formulas, which he had obtained in his previous memoir (Euler, 1754b). For the cycling time of the piston:

$$t = \frac{0.4484 a^2 \sqrt{bl}}{c\sqrt{\left(K - \frac{\pi a^2}{4}g\right)}}(s),\qquad(1)$$

for the flow rate:

$$M = \frac{3600 F \propto}{\lambda g}\left(\frac{ft^3}{h}\right),\qquad(2)$$

and for the pressure at the pump exit:

$$p = \frac{4K}{\pi a^2}(ft),\qquad(3)$$

where the force $K$ is given in cubic ft of water.

Euler also defined two additional parameters: the ratio of pressures $\lambda$, and the ratio of velocities $i$, which are written as follows:

$$\lambda = \frac{p}{g},\qquad(4)$$

$$i = \frac{\zeta}{\propto},\qquad(5)$$

and from this latter expression, the following relations hold: $\zeta = \frac{2b}{t} = i \propto$ and $t = 2b/i \propto$.

Setting the number of all pumps to be used = $2n$, where $n$ is the number of pairs of pumps, Euler then provided the following additional formulas:

$$\lambda = \frac{1}{2} + \sqrt{\left(\frac{1}{4} + \frac{0.0815 F \propto^2 il}{bc^2 g^2}\right)},\qquad(6)$$

for the piston diameter:

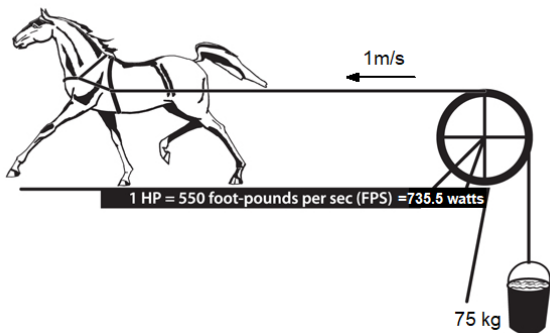$$a = \sqrt{\frac{1.2732 F}{\lambda ing}},\qquad(7)$$



Fig. 3. One horsepower is needed to lift 75 kilograms (of water) by 1 meter in 1 second (adopted from https://aces.nmsu.edu/pubs/_m/M227/welcome.html)
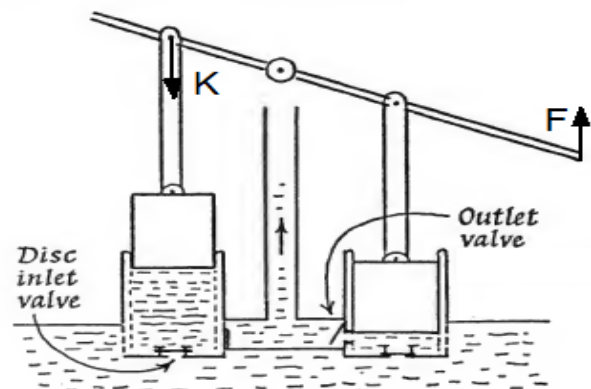


Fig. 4. A pair of piston pumps operating out of phase to provide a continuous flow of water through the piping system (Landels, 1978)

for the force acting on the piston:

$$K = \frac{1}{4}\lambda\pi a^2 g,$$ (8)

and for the piston velocity:

$$\zeta = \frac{1.2732\, F\alpha}{\lambda a^2 g}.$$ (9)

It will become clearer later that $1/\lambda$ is a measure of the system efficiency, which was extensively used by Euler for the optimization of the pumping system performance.

**Man-power:** by defining $f$ as a force that a man is capable to deliver at rest and $\varphi$ as the greatest velocity that a man can walk without too much fatigue, such that if a man has to walk at such velocity, he would be unable to exert any force, because all his efforts will be consumed through this course of walk. If $\omega$ is a velocity smaller than $\varphi$ and $\rho$ is the force that a man can proceed with the velocity $\omega$, then, the relation between the forces $f$ and $\rho$, can be obtained from the velocities $\varphi$ and $\omega$, by considering the following conditions:

1. If $\omega$ = 0, then $\rho = f$,
2. If $\omega = \varphi$, , then $\rho = 0$.

Euler then proposed the following ad-hoc analytical expression for $\rho$:

$$p = f\left(1 - \frac{\omega}{\varphi}\right)^2.$$ (10)

To find the velocity that would correspond to the maximum deliverable power (which Euler called the greatest "moment of motion"), he proposed the differentiation with respect to $\omega$ of the following expression (which corresponds to the deliverable power):

$$f\omega\left(1 - \frac{\omega}{\varphi}\right)^2,$$ (11)

under the supposition that the velocity $\omega$ is the variable that should be maximized, $\omega = \frac{1}{3}\varphi, p = \frac{4}{9}f,$

and then the maximum deliverable power is $= \frac{4}{27}f\varphi$.

Considering that a man at rest can exert an effort of 60 lbf, and that without too much fatigue, he is able to follow a path at 6 ft per second, then $f$ = 60 lbf and $\varphi$ = 6 ft. Then, to apply most advantageously the force of a man to a given machine, it will be necessary for him to march at 2 ft per second, and the force will assume the following value:

$\frac{4}{9}\cdot 60\,lb = 26\ 67\,lb$ [e]. Reducing this force to the weight of a volume of water, at a ratio of 70 lbf per cubic ft, this force will be equivalent to $\frac{8}{21}$ cubic ft (of water). Therefore, we can say that the force of a man is applied in the most advantageous way with a velocity of 2 ft per second, carrying a weight of $\frac{3}{8}\,ft^3$ of water.

If the number of men that one wishes to employ in a machine is set = $m$, and these men put the machine into motion with a velocity of 2 ft per second, their force (= $F$) will be $F = \frac{3m}{8}$ cubic ft of water, and the force that drives each pump will be $K = \frac{3m}{8in}$ cubic ft of water. For a velocity of 2 ft per second, $\alpha = 2$, and the power of this force will be $F\alpha = \frac{3}{4}m$. As a consequence, according to Eq. 2, the amount of water that will be raised in one hour will be $M = \frac{2700m}{\lambda g}$. Since a portion of that force will be used to overcome friction and raise the pistons to admit water by suction, the quantity $M$ will be a little less, or it will be necessary to employ a few more men to overcome the obstacles.

Substituting $F\alpha^2 = \frac{3}{2}m$ into Eq. 6, we obtain the following:

$$\lambda = \frac{1}{2} + \sqrt{\left(\frac{1}{4} + \frac{0.1222\,mil}{bc^2 g^2}\right)}.$$ (12)

Based on Eq. 7, we also obtain the diameter $a$ of each piston:

$$a = \sqrt{\frac{0.4774\,m}{\lambda ing}}.$$ (13)

According to Eq. 4, the pressure that the pipe should sustain at its lower end $\rho$ will be equivalent to the height $\lambda g$.

**Example of application**: by putting $m$ = 1 (one man driving pumps), $i = \frac{\zeta}{\alpha} = \frac{6}{2} = 3$, $n$ = 1, (one pair of pumps), and $g$ = 30 $ft$ in Eq. (13), we will obtain $\lambda = \frac{0.053}{a^2}$. By assuming $b$ = 1 $ft$ , $c = \frac{1}{12}ft = 1in$ , and $l$ = 45 $ft$, we will obtain $\lambda$ = 2.20 and $a$ = 0.155 $ft$. Based on Eq. 2, the flow rate will be $M = 41\ ft^3/h$, and based on Eq. 4, the pressure that the pipe should sustain at the pump exit will be $\rho = \lambda g = 66\ ft$. These results show that a man driving a pair of pumps, such as that shown in Fig. 4, is capable of rising 41 $ft^3$ of water per hour to a height of 30 $ft$ through a pipe with a diameter of 1 $in$ and 45 $ft$ in length. The piston of each pump will have a diameter of 0.155 $ft$, each running into a cylinder of 1 $ft$ in height. Of course, these results do not take into account the friction between the piston and the walls of the cylinders,

---

[e] These values would give approximately 0.1 hp (0.075 kW), which is the same value that has been proposed for the human power as mentioned earlier.

the friction of the water flowing through the pipe, and the power needed to raise the pistons to admit water by suction.

**Horsepower:** considering that for a horse $f=420 lbt$ and $\varphi=12\ ft$, and based on the same power model established for a man (Eqs. 10 and 11), Euler found that the force of a horse is applied in the most advantageous way, with a velocity of 4 $ft/s$, carrying a weight $2\frac{2}{3}\ ft^3$ of of water (186.5 $lbf$).

Then, for a horse, the corresponding formula for $\lambda$ (Eq. 6) is as follows:

$$\lambda = \frac{1}{2} + \sqrt{\left(\frac{1}{4} + \frac{3.4773\,mil}{bc^2g^2}\right)}, \qquad (14)$$

and, from Eq. 7, the diameter of each piston $a$ will be as follows:

$$a = \sqrt{\frac{3.3952\,m}{\lambda ing}}. \qquad (15)$$

**Running water power:** the points *A, B, C, D, E, etc.* along the circumference of the water wheel with the center at *0* are considered (Fig. 5), which is garnished with paddles *Aa, Bb, Cc, etc* receiving successive impulses of the running water *lm*: such that the water wheel by its motion drives the machine under consideration. Then, *m* is set as the center of the efforts of the water on the paddle *Aa*, which will fall roughly in its middle.

Let us set: the radius of the water wheel *0m=r*, the height of the paddle *Aa=h*, the length of the paddles, or the width of the water wheel $= f$, and the surface of each paddle $= fh$ velocity of the water wheel at point *m = v* in *ft* per second, velocity of the running water *lm = e* in *ft* per second.

Let us also consider that the paddle *Aa* is in the vertical position, and that the water hits only this paddle, such that the neighboring paddles *Hh*, *Bb* are above the free surface of the river.

Based on these definitions, the relative velocity of the water on the paddle will be equal to *(e − v)ft/s*, which is due to the height *u*. Considering that a weight falling from a height of 15.625 *ft* gives a velocity of 31.25 *ft/s*, then $\frac{(e-v)^2}{u} = \frac{31.25^2}{15.625}$, from which

we have that $\frac{15.625(e-v)^2}{31.25^2} = \frac{(e-v)^2}{62.5} = \frac{2}{125}(e-v)^2$. The force of the water on this paddle will be equal to the weight of a volume of water $= \frac{2\,fh}{125}(e-v)^2$, from which the power ("moment of motion") is $= \frac{2\,fhv}{125}(e-v)^2$; and this will be as high as possible if $v = \frac{1}{3}e$. Therefore, to take this advantage, it will be necessary to arrange the machine in such a way that the wheel turns with such motion that the velocity at the center of the paddles is equal to one-third of the velocity of the running water; and then the force of the water that is applied to the wheel will be $= \frac{4}{9}\frac{2e^2\,fh}{125} = \frac{8}{1125}e^2\,fh$.

If our machine is set into motion by such a water wheel, we will have the force $F = \frac{8}{1125}e^2\,fh$ and the velocity of the wheel at a distance *0m=r* will be $= \frac{1}{3}e$, which is the value of *a*, that is $a = \frac{1}{3}e$ and $F\alpha = \frac{8}{3375}e^3\,fh$. Therefore, the amount of water that could be raised in one hour by this machine is $M = \frac{8 \cdot 3600}{3375\lambda g}e^3\,fh = \frac{123}{15}\frac{e^3\,fh}{g\lambda}$.

Then, for the water wheel, the corresponding formulas for $\lambda$ and the diameter of the piston *a* are as follows:

$$\lambda = \frac{1}{2} + \sqrt{\left(\frac{1}{4} + \frac{ie^4\,fhl}{15529bc^2g^2}\right)}; \qquad (16)$$

$$a = \sqrt{\frac{2e^2\,fh}{221\lambda ing}}. \qquad (17)$$

According to Euler, a machine of this kind was put into practice at the Notre-Dame bridge in Paris (Fig. 6) to raise water to a height of 81 *ft* above the level of the Seine River. It was composed of two water wheels pushed by the flow of the river, each one driving a separate equipment.

Euler then commented that these wheels are similar to the one considered here, which according to a description by M. de Belidor[g] had the height *h* of the paddles equal to 3 *ft* and their width *f* equal

---

[g] de Belidor himself, in the *Avant-Propos* of the 1739 edition of *Architecture Hydraulique* (Vol. 2), reported on a call to the Notre-Dame facility: "… Messrs. The Provost of Merchants & Aldermen of the City of Paris having learned that I had commented on faults in the pumps of the machine applied to the bridge Notre-Dame, which supplies water from the Seine river to the greater number of public fountains, made me the honor of inviting me in 1737 to communicate to them my views on how to rectify this machine, in order to make it capable of a bigger product. As in working on the project that we carried out, it happened to me make several new discoveries on the movement of waters and the perfection of machines suitable for raising them, I have believed it necessary to suspend the printing of this Volume in order to infer them, and at the same time make essential corrections in several places, based on a few hydraulic principles, commonly received, the error of which I saw, as we can convince ourselves…"

to 18 $ft$. The velocity of the river $e$ was estimated as 9 $ft/s$, and g=81 $ft$, which was equal to the length of the pipe $l$, because it was mounted vertically. Euler then argued that this machine would be capable of delivering the amount of water $M = \dfrac{4147}{\lambda} ft^3/h$, if "well managed", and twice this value considering both equipments, which increases as the value of $\lambda$ is reduced.

However, according to Euler, the system proved to be capable to raise only 2400 $ft^3/h$, which de Belidor himself recognized that it was too little, and among other considerations, he attributed this result to the slow motion of the wheels, because just one-third of the paddles was immersed into the river, and not up to their centers. Corrections in the valves were also considered to reduce the flow resistance, and by these corrections, Belidor expected to more than double the output of the system.

The value $\lambda$ of estimated by Euler for this system, considering both equipments, was $\lambda = \dfrac{8294}{2400} = 3\dfrac{1}{2}$, and, therefore, the pipe had to resist a pressure corresponding to more than three times the water column. Euler then concluded that the machine was highly defective in delivering much less water than it was desired, and as a consequence, the pressure inside the pipe increased considerably, which could cause the "destruction of the machine".

Here, it is possible to consider that $1/\lambda$ is a measure of the system efficiency; then $1/\lambda \times 100\% = 1/3\dfrac{1}{2} \times 100\% \approx 28\,6\%$, which seems to be a reasonable estimate for the efficiency of a system of this sort.

Next, Euler proposed to improve the performance of the machine by reducing the value of $\lambda$ as much as possible. His strategy was to increase the number of cycles for each complete turn of the wheel. He began by calculating the value of $\lambda$ for $e = 9$, $f = 18$, $h = 3$ $l = g = 81$ and by considering that for each turn of an 8.5 $ft$ radius wheel (with a peripheral velocity of 3 $ft/s$), each piston would accomplish $\mu$ cycles per turn of the wheel, giving then the following result:

$$\lambda = \frac{1}{2} + \sqrt{\left(\frac{1}{4} + \frac{\mu}{95c^2}\right)}. \qquad (18)$$

By this approach, the value of $\lambda$ for $c = \sqrt{2}$ would be reduced to 1.03 for $\mu = 6$ and to 1.002 for $\mu = 4$. According to the machine description, the piston excursion $b=1.5\,ft$, which would result in a flow rate of 8052 $ft^3/h$ for both wheels for $\mu = 6$. Euler then considered that this output would be less, about 7200 $ft^3/h$, on account of the force required to overcome friction but, nonetheless, would triple the current output of the machine.

Euler finished this section by providing general design formulas for pumping water by means of
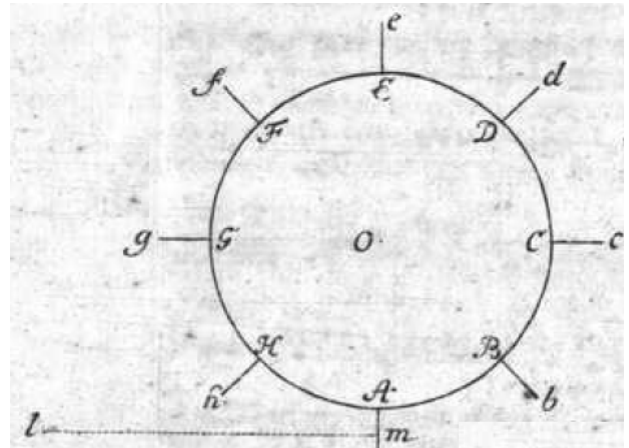


Fig. 5. Water wheel (Euler, 1754)



Fig. 6. Pompe Notre-Dame (Notre-Dame Pump) originally built in 1670 and reconstructed in 1708. This pump raised waters from the Seine into many public fountains and monuments, and it is said that it would allow the fountains to shoot water from 12 up to 50 feet in the air. Here shown in 1861, the pump looks rather destitute and neglected next to the Pont-Notre Dame. The Pont underwent much renovation during the 19th century, while the pump itself remained virtually untouched (source: https://fr.wikipedia. org/wiki/Fichier:Pompe_Notre-Dame,_vue_prise_de_la_ vo%C3%BBte_du_quai_de_G%C3%AAvres_en_1861.jpg)
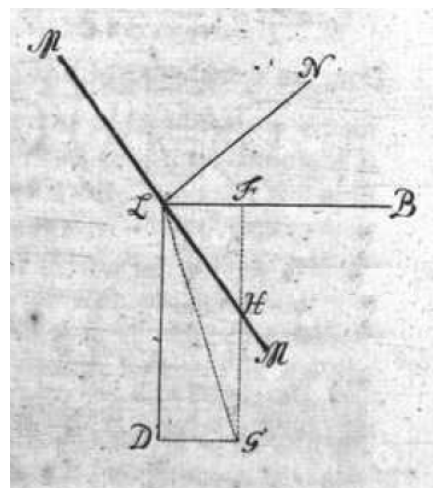


Fig. 7. Geometrical elements of the sail of a windmill (Euler, 1754)

water wheels, by substituting $i$ in Eqs. 16 and 17 with $\dfrac{\mu b}{\pi r}$. This substitution is based on an ad-hoc assumption of the wheel turning with a peripheral velocity equal to one-third of the velocity of the river. However, Euler omitted the conditions on how to make the wheel to turn at this desired velocity. This would require a more complex and detailed calculation of the inertia of the system, including the mechanical characteristics of the water wheel itself, and other considerations such as friction (fluid and mechanical), which Euler was unable or had no desire to establish at that time.

**Windmill power:** Fig. 7 shows a view perpendicular to the keel of the sail of a windmill, where $MLM$ is a section of the sail, the point $L$ belongs to the keel, and the line $LB$ represents the direction of the motion of point $L$. It is clear that the wind direction is in the same plane and that it is perpendicular to the line $LB$. The width of the sail $MM = y$, the inclination of the wind or angle $D\hat{L}N = \varphi$, the wind velocity $DL = e$, and the velocity of the point $L$ of the sail $LF = v$; and since the sail "escapes" in part from the action of the wind, then one finds from the rules of mechanics that the effect would be the same if the wind is expressed by the diagonal $GL$, falling into the same direction $GL$ when the sail is considered at rest.

The force of the wind on the line $MM$ will be $= GL^2 \cdot sin^2\ GLM \cdot y$, which Euler showed that it can be written as $= y(e\ sin\varphi - v\ cos\varphi)^2$, and if the letters $e$ and $v$ are given in $ft/s$, this force will be equal to the weight of a volume of air, and then $= \dfrac{2}{125} y \left( e\sin\varphi - v\cos\varphi \right)^2$. But since air is about 800 times lighter that water, this force will be reduced to a mass of water whose volume $= \dfrac{1}{50000} y \left( e\sin\varphi - v\cos\varphi \right)^2$ in feet square, and assuming the width of the sail $MM = y$ is also expressed in feet, then, since we have considered it to be a line, the effect of one dimension out of three is still missing.

Since this force is in the direction $LN$, its component, which drives the line $MM$ in the direction of the motion $LB$ will be $= \dfrac{y\cos\varphi}{50000} \left( e\sin\varphi - v\cos\varphi \right)^2$, and if we call the infinitesimal width of this line $dx$, then the infinitesimal resultant force that makes the sail to turn in the direction $LB$ will be $= \dfrac{ydx\cos\varphi}{50000} \left( e\sin\varphi - v\cos\varphi \right)^2 ft^3$ of water.

Fig. 8 is the frontal view of the sail $OAABB$ of a windmill, and Fig. 9 is an image of a real windmill, showing the elements of the sail considered in Fig. 7.

In these figures, $0D$ is the axis around which the sail turns, such that the sail falls into the wind direction. Here, $0CD = f$ is the sail span, and $OL = x$ is any section along the span, where the width $MLM=y$, and where the inclination of the wind direction over the element $MMmm$ is $=\varphi$. The velocity at the tip $D$ of the sail will be set as $u$, and since $u:f=v:x$, then the velocity of point $L$ will be $v = \dfrac{xu}{f}$; therefore, the wind force over the element $MMmm=ydx$ in the direction of the motion will be $= \dfrac{ydx\cos\varphi}{50000} \left( e\sin\varphi - \dfrac{xu}{f}\cos\varphi \right)^2 ft^3$ of water, where $e$ is the wind velocity in $ft/s$. This element of force, when multiplied by the velocity $\dfrac{xu}{f}$, will give the element of the moment of motion for the force (element of power) of the wind over the sail, which will be $= \dfrac{xuydx\cos\varphi}{50000f} \left( e\sin\varphi - \dfrac{xu}{f}\cos\varphi \right)^2$.

Since, ordinarily, the angle $\varphi$ is the same over the entire span of the sail, and assuming that the sail has the same width $AA=BB=h$, and because $y=h$, the element of the moment of motion (element of power) will be given by

$$\frac{hu\cos\varphi}{50000f} xdx \left( e^2\sin^2\varphi - \frac{2eux}{f}sin\varphi\ cos\varphi + \frac{u^2x^2}{f^2}\cos^2\varphi \right),$$

which after integration gives

$$\frac{hu\cos\varphi}{50000f} \left( \frac{1}{2}e^2x^2\sin^2\varphi - \frac{2eux^3}{3f}sin\varphi\ cos\varphi + \frac{u^2x^4}{4f^2}\cos^2\varphi - C \right).$$

The constant $C$ will be found by setting $x=OC$, for which the integral vanishes. Then, for $OC=k$,

$$C = \frac{1}{2}e^2k^2\sin^2\varphi - \frac{2euk^3}{3f}sin\varphi\ cos\varphi + \frac{u^2k^4}{4f^2}\cos^2\varphi - C.$$

Let us set $x=OD=f$, and the moment of motion (power) over the entire sail will be given by

$$\frac{hu\cos\varphi}{50000f} \left( \begin{array}{l} \frac{1}{2}e^2\left(f^2-k^2\right)\sin^2\varphi - \frac{2eu}{3f}\left(f^3-k^3\right)sin\varphi \\ \cos\varphi + \frac{u^2}{4f^2}\left(f^4-k^4\right)\cos^2\varphi \end{array} \right),$$

and if the windmill is equipped with four of such sails, the moment of motion for the force (power) of the wind will be given by the following:

$$F \propto= \frac{hu\cos\varphi}{12500f} \left[ \begin{array}{l} \frac{1}{2}e^2\left(f^2-k^2\right)\sin^2\varphi - \\ \frac{2eu}{3f}\left(f^3-k^3\right)sin\varphi\ cos\varphi + \\ \frac{u^2}{4f^2}\left(f^4-k^4\right)\cos^2\varphi \end{array} \right]. \tag{19}$$

Upon differentiation of Eq. 19, Euler then found the maximum velocity that the sails should turn at their extremities $D$:

$$u = \frac{ef\tan\varphi}{9\left(f^4-k^4\right)} \left[ 8\left(f^3-k^3\right) \mp \left(f-k\right) \sqrt{\begin{array}{l} 10f^4+20f^3+84f^2k^2 + \\ 20fk^3+10k^4 \end{array}} \right], \tag{20}$$
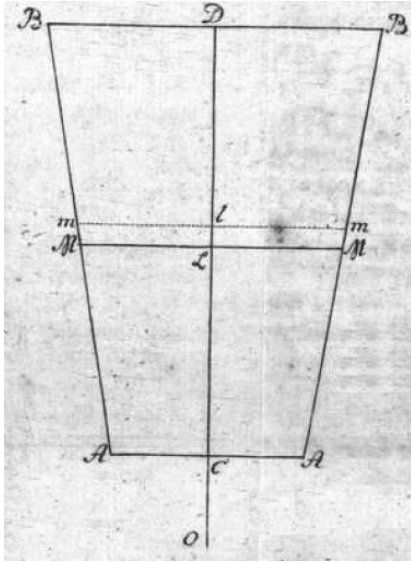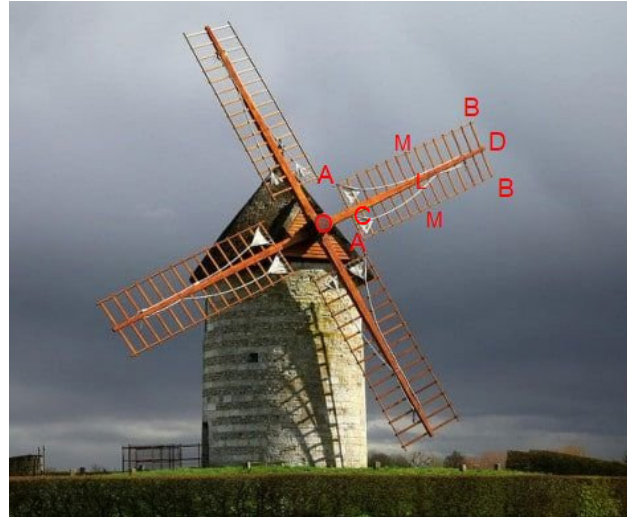
Fig. 8. Frontal view of the sail of a windmill (Euler, 1754)



Fig. 9. Image of a real windmill, showing elements of the sail (without the sail cloth) considered in Fig. 8 (adapted from https://www.conserve-energy-future.com/how-windmills-work.php)

where the minus sign before the radical should be chosen for the maximum motion to be achieved.

Since the distance $OC=k$ can be chosen as small as possible, then it is allowed to consider $k=0$ to obtain $u = \dfrac{e\tan\varphi}{9}\left(8 \mp \sqrt{10}\right)$. By setting $\dfrac{\left(8 \mp \sqrt{10}\right)}{9} = \delta$, such that $u = \delta e \tan\varphi$, from Eqs. 19 and 20, the moment of motion for the total force (total power) of the wind will be given by the following:

$$F \propto = \frac{68 \mp 5\sqrt{10}}{729} \cdot \frac{e^3 fh \sin^3 \varphi}{12500}. \qquad (21)$$

Whereas the maximum motion will be obtained with the minus sign before the radical, giving a tip velocity $u = \delta e \tan\varphi = 0.537525\, e \tan\varphi$, and as Eq. 21 shows, the maximum total power will be obtained, instead, with the plus sign before the radical, which is then given by the following:

$$F \propto = \frac{68 + 5\sqrt{10}}{729} \cdot \frac{e^3 fh \sin^3 \varphi}{12500} = \frac{e^3 fh \sin^3 \varphi}{108726}. \qquad (22)$$

It is seen that the maximum action of the wind would be obtained by setting $\varphi$ as a right angle; however, this would be unfeasible because the force $F$ will be zero, since it varies with $\cos\varphi$, and $\propto$ will go to infinite, since $u$ varies with $\tan\varphi$. Next, Euler provided design formulas for $u$ and $F\propto$ for three values of $\varphi$, 45°, 55°, and 60°.

Finally, Euler considered the case where $\varphi = 54°, 45'$, $\tan\varphi = \sqrt{2}$, giving a tip velocity $u=0.76018$, resulting in one revolution of the sails every $8.2654\dfrac{f}{e} = t$

seconds. In the case where the windmill is driving piston pumps to raise water, and considering that each piston would accomplish $\mu$ cycles per turn of

the sails $\dfrac{2b}{i \propto} = t = \dfrac{8.2654 f}{\mu e}$ , $i = \dfrac{0.24197 \mu be}{\propto f}$ we obtain .

From these, it is possible to write the following:

$$\lambda = \frac{1}{2} + \sqrt{\left(\frac{1}{4} + \frac{0.01972\, \mu eF \propto l}{c^2 g^2}\right)}; \qquad (23)$$

and

$$a = \sqrt{\frac{5.2617 f \cdot F \propto}{\lambda \mu nbeg}}. \qquad (24)$$

Considering that from Eq. 22, $F \propto = \dfrac{e^3 fh}{199743}$, then, from Eqs. 23 and 24 we have the following:

$$\lambda = \frac{1}{2} + \sqrt{\left(\frac{1}{4} + \frac{\mu e^4 hl}{10128960\, c^2 g^2}\right)}; \qquad (25)$$

and

$$a = \frac{ef}{195}\sqrt{\frac{h}{\lambda \mu bg}}. \qquad (26)$$

From these expressions, it is then possible to determine the piston diameter = $a$, the piston excursion = $b$, the diameter of the piping system = $c$, and the number of cycles per turn of the sails $\mu$, such that the value of $\lambda$ becomes as small as possible. Not only the pressure at the exit of the pump, which is = $\lambda g$, will be the smallest, but also the quantity of water that will be raised, which is given by Eq. 2 as

$$M = \frac{3600 F \propto}{\lambda g}\left(ft^3/h\right) = \frac{3600 e^3 fh}{199743 \lambda g}\left(ft^3/h\right)$$, will be the largest. Or else:

$$M = \frac{e^3 fh}{55.5\, \lambda g}\left(\frac{ft^3}{h}\right), \qquad (27)$$

bearing in mind that $e$ is the velocity of wind, $f$ is the span of the sails, and $h$ is their width, and that

the sails should turn one revolution in $8.2654\dfrac{f}{e}$ seconds.

**The Windmill at Sanssouci:** as an example of application of the above formulation for windmills driving piston pumps, let us consider a windmill that, supposedly, was used to raise waters at Sanssouci, which was examined in the paper by Eckert (2002): "… Pumps, driven by a windmill, should raise the water of the Havel River to an elevated reservoir. This proposal was executed; it involved the construction of a water reservoir on top of a hill 150 feet above the river level, with a windmill-driven water pump half-way between the river and the reservoir. The water had to be guided by a canal from the river to the site of the pump station, from where it would be pumped through pipes up the hill and into the reservoir. … Construction began in the summer of 1748. The canal from the Havel River to the pump station was finished by November. The windmill and the pumps were finished by the end of the year. The mechanism used to transmit the motion of the windmill to the pumps was described as clumsy, but it seemed to work. The pumps also were connected to a mechanism that could be set into motion by horses (Göpelwerk) if there were no wind…"

In Euler's publication (Euler, 1754b), there is no description on the characteristics of the pumps, neither on the windmill at Sanssouci, because, as a matter of fact, this particular system was never directly mentioned in this publication, although, as commented above, it was certainly motivated by Euler's involvement with this water park in 1749. However, as far as the characteristics of the pump are concerned, and for the sake of the present exercise, we can consider the pump characteristics given by Euler in an example of application at the end of Euler's publication (Euler, 1754b) itself: the piston pump diameter $a = \dfrac{4}{3}\,ft$ , and the piston excursion $b = 4\,ft$. Then, let us assume that $n = 1$ (one pair of pumps), and that each pump completes four cycles per turn of the sails, then $\mu = 4$.

Some information about the piping system at Sanssouci was also reported by Eckert (2002) as follows: "… at the first system trial, by 1749, the wooden piping system burst at the lower end, … eventually, by 1753, these were replaced by lead tubes with an inner diameter $c = \dfrac{1}{3}\,ft$ …" In this same publication, there are indications that the length of the piping system was (approximately) $l = 8000\,ft$.

No information could be found on the characteristics of the windmills at Sanssouci; just a

brief comment by Eckert (2002) that, by 1753: "… a second windmill was constructed at a different site to raise water to the reservoir independently of the first one, but it never seems to have worked properly…" Nonetheless, to put some reality into this exercise, it is possible to guess some information from the image of the windmill shown in Fig. 9: the span of the sails $f = 50\,ft$, the width of the sails $h = 12\,ft$. Wind speed $e = 25\,ft/s$ (assumed), we obtain one revolution in $8.2654\dfrac{f}{e} = 8.2654\dfrac{50}{25} = 16.53$ seconds, or 3.63 RPM.

Then, from Eq. 25 we have the following:

$$\lambda = \frac{1}{2} + \sqrt{\left(\frac{1}{4} + \frac{\mu e^4 h l}{10128960 c^2 g^2}\right)} =$$

$$\frac{1}{2} + \sqrt{\left(\frac{1}{4} + \frac{4 \cdot 25^4 \cdot 12 \cdot 8000}{10128960 \cdot \left(\dfrac{1}{3}\right)^2 150^2}\right)} = 2.98,$$

giving a system efficiency of $1/\lambda = 33.6\%$.

From Eq. 27, the flow rate is as follows:

$$M = \frac{e^3 f h}{55.5 \lambda g} = \frac{25^3 \cdot 50 \cdot 12}{55.5 \cdot 2.98 \cdot 150} = 378\left(\frac{ft^3}{h}\right).$$

The value of $\lambda = 2.98$ shows that to raise the water to a height of *150 ft*, the pressure that is developed at the lower end of the pipeline (pump exit) $p = \lambda g = 447ft$. However, a common assumption by the fontainiers and hydraulic engineers at the time was to consider that the necessary pressure developed by the pump would be equivalent to the height of the reservoir, which, as pointed out by Euler, was obviously incorrect. The consequence of not recognizing these high pressures was certainly the main cause of failure of the wooden pipelines at Sanssouci, as reported by Eckert (2002).

As far as the performance of the system is concerned, the following remarks by Eckert (2002) speak for themselves: "… By the spring of 1754, an abundance of snow and rain together with the water-raising machine (described as "miserably slow") produced some tangible results. On Good Friday 1754, with a half-filled reservoir, the King was given a demonstration. But that day it was windy and the main fountain rose to only about half the height that the King had expected [100 ft]– and after an hour, the reservoir was empty…" This was not surprising because the output of only 378 (*ft³/ h*) = 10.7 (*m³/h*) as estimated above would not be sufficient for the grandeur of the water park wished by King Frederick[h].

---

[h] A steam-driven water pump was inaugurated in 1842 to supply water from the Havel River to the Sanssouci Palace, which in 2017 was nominated a "Civil Engineering Historical Landmark in Germany".

### Using Natural Sources of Power Today

The natural sources of power considered here are still in much use nowadays (Gasch and Twele, 2016). For instance, the power of running waters, or hydropower as is known today, is widely employed in hydroelectricity, or hydroelectric power, where electricity is produced from hydropower. In 2015, hydropower generated 16.6% of the world's total electricity and 70% of all renewable electricity and was expected to increase by about 3.1% each year for the next 25 years. Hydropower is produced in 150 countries, with the Asia-Pacific region generating 33% of global hydropower in 2013. China is the largest hydroelectricity producer, with 920 TWh of production in 2013, representing 16.9% of domestic electricity use (Atkins, 2003) (Hydroelectricity (n.d.). In: Wikipedia. Accessed March 21, 2021, https://en.wikipedia.org/wiki/Hydroelectricity).

Different classes of hydraulic turbines for hydroelectric power plants can be selected according to the available head and flow rate, and due to the advances in the design of these machineries, they can operate with efficiencies up to 90%.

Wind power, or wind energy, is the use of wind to provide mechanical power through wind turbines to turn electric generators for electrical power. Wind power is a popular sustainable, renewable source of power that has a much smaller impact on the environment compared to burning fossil fuels. Wind farms consist of many individual wind turbines, which are connected to the electric power transmission network (Bennert and Werner, 1989). Onshore wind is an inexpensive source of electric power, competitive with or in many places cheaper than coal or gas plants. Onshore wind farms have a greater visual impact on the landscape than other power stations, as they need to be spread over more land and need to be built away from dense population (von König, 1976). Offshore wind is steadier and stronger than on land, and offshore farms have less visual impact, but construction and maintenance costs are significantly higher. Small onshore wind farms can feed some energy into the grid or provide power to isolated off-grid locations (Wind power (n.d.). In: Wikipedia. Accessed March 22, 2021, https://en.wikipedia.org/wiki/Wind_power).

A wind turbine is a machine that converts kinetic energy from the wind into electricity. The blades of a wind turbine turn between 13 and 20 revolutions per minute, depending on their technology, at a constant or variable velocity, where the velocity of the rotor varies in relation to the velocity of the wind in order to reach a greater efficiency. The wind turbine is automatically oriented to take maximum advantage of the kinetic energy of the wind, from the data registered by the vane and anemometer that are installed at the top. The nacelle turns around a crown located at the end of the tower. The wind makes the blades turn, which start to move with wind speeds of around 3.5 m/s and provide maximum power with a wind speed 11 m/s. With very strong winds (25 m/s), the blades are feathered and the wind turbine slows down in order to prevent excessive voltages. The rotor (unit of three blades set in the hub) turns a slow axis that is connected to a gear box that lifts the turning velocity from 13 to 1,500 revolutions per minute. The gearbox transfers its energy through a fast axis that is connected to the generator, which produces the electricity (accessed March 22, 2021, https://www.acciona.com/renewable-energy/wind-energy/wind-trurbines/).

Besides being unreliable and because of its irregular and much lower power output, man and animal power has not developed in the same pace as hydropower and wind power. Nonetheless, there are still some attempts in the use of these natural sources of power for driving machineries for different purposes (Fuller and Aye, 2012; Phaniraja and Panchasara, 2009).

Fig. 10 shows an image from a patent of invention aiming to provide an animal powered mechanical device for water desalination. The machine is described as follows (US Patent No. US7387728B2, by Pathak et al., date of publication: June 17, 2008): a pair of bulls, capable of exerting more than 100 kg of draft and walking at a rate of 50 meters/minute is coupled to a mechanical link with the help of a rope. The pair of bulls generates a pressure of 300 psi and a discharge of 20 liters/minute, when it completes one rotation of 8 meters diameter circular path.

Fig. 11 shows an image from a patent of invention of a system and method for producing electricity using the biological energy of the muscles of animals like horses. The machine is described as follows (US Patent No. US20050161289A1, by Gomez-Nacer, date of publication: July 28, 2005): "… A system and method for generating electricity by means of increasing the velocity of an animal on a mechanical device directly or indirectly attached to the hoof or other part of the limbs of the animal to use the force of its muscle contraction and the force produced
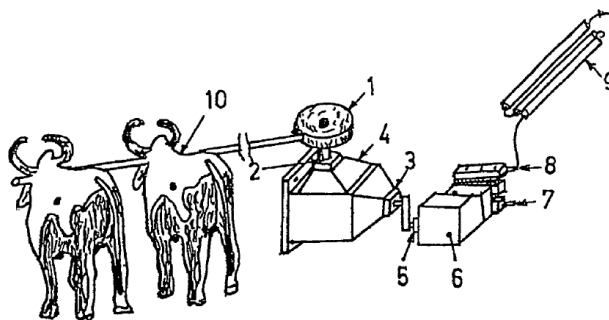


Fig. 10. Image from a patent of invention of an animal powered mechanical device for water desalination. Element # 9 is an osmosis membrane module (source: US Patent No. US7387728B2, by Pathak et al., date of publication: June 17, 2008)

13
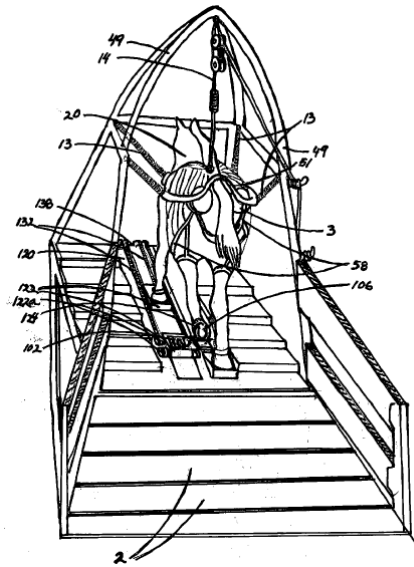
Fig. 11. Image from a patent of invention of a system and method for producing electricity using the biological energy of the muscles of animals like horses (source: US Patent No. US20050161289A1, by Gomez-Nacer, date of publication: July 28, 2005)



Fig. 12. Human muscle power operating a gear reduction system for charging automotive batteries (source: Yadav and Rao, 2015)

by its gravity to make spin multiplying wheels in communication to an electricity generator…"

Fig. 12 shows an image of a gear reduction system operated by human muscle power or animal power to drive a car alternator as a generator to charge a typical 12V 40Ah lead-acid automotive battery (not shown in the figure). In the experiments, human and animal power were used to charge the batteries. It took three hours to fully charge a 50% discharged battery and 1.5 hours to fully charge a 75% discharged battery.

**Conclusions**

Mechanical power as is known today, as a measure of the capacity to perform work, seems to have emerged in the first half of the 18th century in the works of de Belidor, and was extensively used by Euler in his 1754 publication, in which he applied a pioneering approach in providing rational calculations for the power needed to drive different machinery to raise waters with piston pumps, by means of natural sources of power (human power, animal power, water flow power, and wind power). With the advent of the steam engine in the mid-18th century, the horsepower as a measure of mechanical power was proposed, which later found its equivalent in the internationally standardized watt unit. It was shown that the use of hydropower and wind power have evolved considerably, particularly for the generation of electricity, and, despite of its much lower attractiveness, there have been some attempts in the use of human and animal power in particular applications that do not require large and constant amounts of power inputs.

## References

Atkins, W. (2003). Hydroelectric power. *Water: Science and Issues*, Vol. 2, pp. 187–191.

Bennert, W. and Werner, U. J. (1989). *Windenergie*. Berlin: VEB Verlag Technik, 144 p.

de Belidor, B. F. (1819). *Architecture Hydraulique, ou l'art de conduire, d'élever et de ménager les eaux pour différents besoins de la vie. Nouvelle édition, avec des notes et additions par M. Navier, ingénieur du Corps Royal des Ponts -et-Chaussées. Première partie - Tome premier.* Paris: Firmin Didot, 666 p.

Eckert, M. (2002). Euler and the fountains of Sanssouci. *Archive for History of Exact Sciences*, Vol. 56, pp. 451–468. DOI: 10.1007/s004070200054.

Euler, L. (1754a). E206. Sur le mouvement de l'eau par des tuyaux de conduite. Mémoires de l'académie des sciences de Berlin, Vol. 8, pp. 111–148.

Euler, L. (1754b). E207. Discussion plus particulière de diverses manières d'elever de l'eau par le moyen des pompes avec le plus grand avantage. *Mémoires de l'académie des sciences de Berlin*, Vol. 8, pp. 149–184.

Fuller, R. J. and Aye, L. (2012). Human and animal power – The forgotten renewables. *Renewable Energy*, Vol 48, pp. 326–332. DOI: 10.1016/j.renene.2012.04.054.

Gasch, R. and Twele, J. (eds.) (2016) *Windkraftanlagen. Grundlagen, Entwurf, Planung und Betrieb*. 9th edition. Wiesbaden: Springer, 622 p.

Golding, E. W. (1976). *The generation of electricity by wind power*. London: E. & F. N. Spon Ltd., 332 p.

Kahlow, A. (2017*)*. Das Pumpwerk für die Fontänen von Sanssouci. In: *Historische Wahrzeichen der Ingenieurbaukunst, Band 21*. Berlin: Bundesingenieurkammer, 92 p.

Landels, J. G. (1978). *Engineering in the ancient world*. Berkley & Los Angeles: University of California Press, 224 p.

Mariconda, P. R. (2008). As mecânicas de Galileu: as máquinas simples e a perspectiva técnica moderna. *Scientiae Studia*, Vol. 6, No. 4, pp. 565–606. DOI: 10.1590/S1678-31662008000400006.

Phaniraja K.L. and Panchasara H. H. (2009). Indian draught animals power. *Veterinary World*, Vol. 2 (10), pp. 404–407.

von König, F. (1976). *Windenergie in praktischer Nutzung*. Munchen: Udo Pfriemer Verlag, 184 p.

Yadav, D. K. and Rao, P. (2015). Study and analysis of animal and human muscle power for electricity generation. *International Journal of Engineering Research & Technology*, Vol. 3, Issue 20, IJERTCONV3IS20107.

# ANALYSIS OF EFFICIENCY OF THREE-LAYER WALL PANELS WITH A DISCRETE CORE

Vladimir Karpov, Evgeny Kobelev*

Saint Petersburg State University of Architecture and Civil Engineering
Vtoraja Krasnoarmeyskaya st., 4, Saint Petersburg, Russia

*Corresponding author: evgeny.kobelev@gmail.com

**Abstract**

**Introduction:** The paper addresses thin-walled three-layer plates and panels with cutouts, reinforced with an orthogonal grid of stiffeners or rectangular reinforcement plates parallel to the coordinate lines. In this case, the thickness of the entire structure is taken into account analytically using unit column functions. **Purpose of the study:** We aimed to build a mathematical model of deformation and develop a method for the analysis of the stability of thin-walled elastic isotropic three-layer plates and wall panels with a discrete core. **Methods:** Based on the mathematical apparatus of generalized functions using the Bubnov–Galerkin method, an eigenvalue problem is solved to determine the critical parameters of a compressed three-layer wall panel with a discrete core. **Results:** According to the suggested method, we perform a stability analysis of three-layer wall panels with different values of core stiffness and study the impact of the discrete core parameters on the buckling load, consumption of materials, and efficiency of three-layer engineering structures.

**Keywords**

Three-layer plate, wall panel, discrete core, cutout, stiffener.

## Introduction

Currently, to improve the weight and economic efficiency, specific strength, and stiffness of thin-walled structures, especially in construction, shipbuilding, mechanical engineering, and other technical industries, three-layer plates and shells are widely used. The heterogeneous layered structure of such shells provides the necessary strength and stiffness characteristics as well as soundproofing and heat and vibration isolation properties.

The used thin-walled structure analysis principles are common for bending flat three-layer panels, three-layer panels resisting compression and bending, and three-dimensional three-layer structures — shells.

Since three-layer structures have a core (solid or discrete, e.g., ribbed) offering relatively low resistance to shear, the bending strains in these structures are accompanied by mutual skin displacement. It is possible to perform three-layer panel and shell analysis either based on the precise methods of the elasticity theory or through the introduction of certain hypotheses that reflect the specifics of structure behavior and make it possible to significantly simplify the process of problem-solving with no considerable error.

The precise method of core element analysis uses an equation for a three-dimensional problem of the elasticity theory. This method was first used for thick slabs by Galerkin (1931).

In the case of cylindrical bending, Rzhanitsyn's theory of built-up columns (1986) can also be applied effectively for the analysis of three-layer panels. In this case, the panel skins are considered as built-up column laminations while the core is considered as transverse and shear connections evenly distributed along the column length.

Three-layer panels with low section height and, therefore, high flexibility are usually supported on four sides or secured on supports and calculated based on the non-linear theory with account for chain (membrane) forces acting in the middle surface.

The analysis of stiffened three-layer panels has a number of specific features. In three-layer wall panels (especially if there is a solid core), stiffeners are distributed relatively sparsely, therefore, in the analysis, it is necessary to account for the non-uniformity of the distribution of normal stresses in the skins along the width of the panel, caused by shear forces along the lines where the skins and the stiffeners come together (Aleksandrov et al., 1960; Davies, 2001).

The general theory of the analysis of three-layer plates and shells with a structural core was developed by Aleksandrov (1959), Aleksandrov et al. (1960), Bryukker (1965), Grigolyuk and Chulkov (1973), Grigolyuk and Kogan (1972), Levchuk (2008a, 2008b) as well as Dragan and L evchuk (2011).

Numerous researchers (Eremeev and Zubov, 2017; Kipiani, 2014; Kobelev et al., 1984; Kreja, 2011;

Pukhliy and Pukhliy, 2019) dealt with the development of new analytical models for three-layer plates and shells. The wide implementation of new materials that enable making structures with unique properties in engineering and construction has significantly complicated analytical models. Among the studies addressing methods for the analysis of thin-walled structures made of composite materials, we would also like to mention publications by Kaledin et al. (2014), Nguyen et al. (2019), and Solomonov et al. (2014).

Currently, numerical calculations of three-layer panels are usually performed using finite-element modeling packages. The skins are modeled by finite elements of the plates and the core is modeled by solid finite elements. The creation of powerful computing systems based on the finite element method (FEM) opens up opportunities for the development of new analytical models with regard to the analysis of the stress-strain state of multi-layer plates and shells with irregular structures (Baculin, 2018; Golovanov et al., 2006; Grishanov, 2018). Mathematical models for the analysis of modern thin-walled three-layer structures shall meet a lot of requirements. Among other things, they shall allow us to determine with high accuracy the stress-strain state, load-bearing capacity, and critical buckling values of such structures, taking into account the heterogeneity of layers and a wide range of external effects (Karpov, 2010; Karpov et al., 2002).

Despite the fact that current computational resources make it possible to build and analyze complex finite element models in a comparatively short time, the very development of an analytical model that would reliably take into account the stress-strain state of an irregular structure requires the involvement of a highly qualified computing engineer and significant programming efforts. The creation of a method for stability analysis of three-layer panels with a discrete core, based on the mathematical apparatus of generalized functions and variational analysis methods, is quite an important task.

The paper builds a mathematical model and develops an algorithm for the analysis of three-layer wall panels with a discrete core in the form of some inner cutouts, which is equivalent to a core in the form of a system of wide cross stiffeners.

**Mathematical model for the analysis of plates and wall panels**

The paper addresses plates and panels reinforced with an orthogonal grid of stiffeners parallel to the coordinate lines. The height and location of the stiffeners are specified according to Karpov (2010) using unit column functions $\overline{\delta}(x-x_j)$ $\overline{\delta}(y-y_i)$ as follows:

$$H(x,y) = \sum_{j=1}^{m} h^j \overline{\delta}\left(x-x_j\right) +$$
$$\sum_{i=1}^{n} h^i \overline{\delta}\left(y-y_i\right) - \qquad (1)$$
$$\sum_{i=1}^{n}\sum_{j=1}^{m} h^{ij} \overline{\delta}\left(x-x_j\right)\overline{\delta}\left(y-y_i\right),$$

where $h^j$, $h^i$ — the height of the stiffeners parallel to the $y$ and $x$ axes, respectively; $h^{ij} = \min\left\{h^i, h^j\right\}$;

$\overline{\delta}(x-x_j)$, $\overline{\delta}(y-y_i)$ — the unit column functions equal to 1 at points where the stiffeners are located or 0 outside those locations. If $h^j = h^j(y)$ $h^i = h^i(x)$, then $h^{ij} = \min\left\{h^i(x_j); h^j(y_i)\right\}$.

Therefore, the thickness of the entire structure is equal to $h + H$. If $H > 0$, then the plate is reinforced with stiffeners or reinforcement plates. If $H < 0$, then it is weakened by cutouts.

Let us consider a wall panel with thickness $h$ with a rectangular cutout reinforced with eccentric stiffeners in the direction of the $x$ axis.

If a slab, reinforced with stiffeners, the size and location of which are specified by function $H(x,y)$ in the form of Eq. (1), also has cutout holes, the location of which is specified by function $H_2(x,y)$ in the following form:

$$H_2\left(x,y\right) = -h\sum_{j_2=1}^{m_2}\sum_{i_2=1}^{n_2} \overline{\delta}\left(x-x_{j_2}\right)\overline{\delta}\left(y-y_{i_2}\right),$$

then the total thickness of the slab will be $h + H(x,y) + H_2(x,y)$.

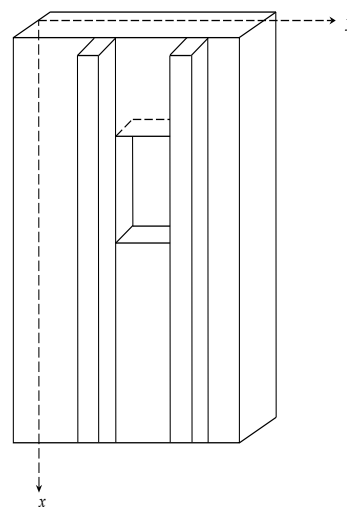The internal forces in the panel can be represented as follows:



Fig. 1. Wall panel with a rectangular cutout reinforced with stiffeners

$$M_x = \frac{E}{1-\mu^2}\left(\frac{h^3}{12}+J_x+\overline{J}\right)(\chi_1+\mu\chi_2),$$

$$M_y = \frac{E}{1-\mu^2}\left(\frac{h^3}{12}+J_y+\overline{J}\right)(\chi_2+\mu\chi_1),$$

$$M_{xy} = \frac{E}{2(1+\mu)}\left(\frac{h^3}{12}+J_y+\overline{J}\right)\chi_{12},$$

$$M_{yx} = \frac{E}{2(1+\mu)}\left(\frac{h^3}{12}+J_x+\overline{J}\right)\chi_{12},$$

$$\tilde{M}_{xy} = \frac{1}{2}\left(M_{xy}+M_{yx}\right),$$

where expressions for the moments of inertia have the following form:

$$\overline{J} = -\frac{h^3}{12}\sum_{j_1=1}^{m_1}\sum_{i_1=1}^{n_1}\overline{\delta}\left(x-x_{j_1}\right)\overline{\delta}\left(y-y_{i_1}\right),$$

$$J_x = \sum_{i=1}^{n}J^i\overline{\delta}(y-y_i)+r_a\sum_{j=1}^{m}J^j\overline{\delta}(x-x_j)-$$

$$r_a\sum_{i=1}^{n}\sum_{j=1}^{m}J^{ij}\overline{\delta}(x-x_j)\overline{\delta}(y-y_i),$$

$$J_y = \sum_{j=1}^{m}J^j\overline{\delta}(x-x_j)+r_b\sum_{i=1}^{n}J^i\overline{\delta}(y-y_i)-$$

$$r_b\sum_{i=1}^{n}\sum_{j=1}^{m}J^{ij}\overline{\delta}(x-x_j)\overline{\delta}(y-y_i),$$

$$r_a = r_j/a, \ r_b = r_i/b.$$

The equilibrium equation for the slab compressed in the direction of the $x$ axis will be as follows:

$$\frac{\partial^2 M_x}{\partial x^2}+\frac{\partial^2 M_y}{\partial y^2}+2\frac{\partial^2 \tilde{M}_{xy}}{\partial x\partial y}-N_x\frac{\partial^2 W}{\partial x^2}=0. \quad (2)$$

Let us consider a wall panel in the form of a three-layer slab with a discrete core. Such a structure can be specified according to Karpov et al. (2002) if a slab of thickness $h$ with internal cutouts of depth $h/3$ is considered. Let us assume that the cutouts have the same size and are rectangular with side $a_1$ along the $x$ axis and side $b_1$ along the $y$ axis. In the direction of the $x$ axis, there will be $m_1$ cutouts, and in the direction of the $y$ axis, there will be $n_1$ cutouts (Fig. 2).

The reduced area of the cutouts will be equal to the following:

$$K_1 = \frac{a_1 m_1 b_1 n_1}{b}.$$

The moment of inertia of such a slab with the zero stiffness of the cutouts "smeared" along the entire plate will be equal to the following:



Fig. 2. Wall panel with inner cutouts

$$\widetilde{J} = J - J_1 K_1,$$

where:

$$J = h^3/12, \ J_1 = \int_{-h/6}^{h/6} z^2 dz = \frac{h^3}{324}=\frac{h^3}{12\cdot 27}.$$

Then the moments in Eq. (2) will be as follows:

$$M_x = \frac{E}{1-\mu^2}\tilde{J}\left(\chi_1+\mu\chi_2\right),$$

$$M_y = \frac{E}{1-\mu^2}\tilde{J}\left(\chi_2+\mu\chi_1\right),$$

$$\tilde{M}_{xy} = \frac{E}{2(1+\mu)}\tilde{J}\chi_{12}.$$

**Analysis of the efficiency of three-layer wall panels with a discrete core**

Let us study the stability of wall panels in the form of three-layer plates with a discrete core compressed in the direction of the *OX* axis with force $N_x$ uniformly distributed along the middle plane of the slab ($N_x = -\,const$). The equilibrium equation for such a slab has the form of Eq. (2).

Let us assume that the edges of the slab have pin support. We need to find such value of $N_x$ where deflection $W(x,y)$ is other than 0. This value of $N_x$ will be critical. Let us present $W(x,y)$ in the following form:

$$W_{mn} = \sum_{j=1}^{m}\sum_{i=1}^{n}A_{ij}\sin\frac{i\pi x}{a}\sin\frac{j\pi y}{b}. \quad (3)$$

To find the $A_{ij}$ coefficients according to the Bubnov–Galerkin method, we will derive a system of homogeneous linear algebraic equations.

$$\int_0^a \int_0^b \left( \frac{\partial^2 M_x(W_{mn})}{\partial x^2} + \frac{\partial^2 M_y(W_{mn})}{\partial y^2} + 2\frac{\partial^2 \tilde{M}_{xy}(W_{mn})}{\partial x \partial y} \right) \sin\frac{i_1 \pi x}{a} \sin\frac{j_1 \pi y}{b} dxdy =$$

$$= N_x \int_0^a \int_0^b \frac{\partial^2 W_{mn}}{\partial x^2} \sin\frac{i_1 \pi x}{a} \sin\frac{j_1 \pi y}{b} dxdy,$$

$$i_1 = 1, 2, ..., m, \ j_1 = 1, 2, ..., n.$$

Having determined the integrals of known functions, we will obtain the following:

$$\sum_{i=1}^m \sum_{j=1}^n C_{iji_1j_1} A_{ij} = N_x \sum_{i=1}^m \sum_{j=1}^n B_{iji_1j_1} A_{ij},$$

$$i_1 = 1, 2, ..., m, \ j_1 = 1, 2, ..., n.$$

As a result, we have an eigenvalue problem. We need to find such values of $N_x$ where this system has a non-zero solution.

If small deflections are considered, the first approximation of the Bubnov–Galerkin method can be considered, i.e., $W(x,y)$ can be adopted in the following form:

$$W_1(x, y) = C_1 \sin\frac{\pi x}{a} \sin\frac{\pi y}{b}.$$

For a slab of constant thickness $h$, we will obtain the following:

$$C_1 \frac{\pi^4}{a^4} \frac{ab}{4}\left(1 + 2\frac{a^2}{b^2} + \frac{a^4}{b^4}\right) = -N_x \frac{C_1}{D} \frac{\pi^2}{a^2} \frac{ab}{4},$$

where:

$$D = \frac{Eh^3}{12(1-\mu^2)}.$$

Therefore:

$$N_x = -\frac{D\pi^2}{a^2}\left(1 + 2\frac{a^2}{b^2} + \frac{a^4}{b^4}\right). \qquad (4)$$

For a rectangular slab at $a=b$, we will obtain the following:

$$N_{xcr} = -3.615\frac{Eh^3}{a^2}.$$

Let us consider a wall panel in the form of a three-layer slab with a discrete core. The thickness of such a structure can be specified if we consider a slab of thickness $h$ with inner cutouts of depth $h/3$ (Fig. 3).

Let us assume that the cutouts have the same size and are rectangular with side $a_1$ along the $x$ axis and side $b_1$ along the $y$ axis. In the direction of the $x$ axis, there will be $m_1$ cutouts, and in the direction of the $y$ axis, there will be $n_1$ cutouts. The reduced area of the cutouts will be equal to the following:

$$K_1 = \frac{a_1 m_1 b_1 n_1}{ab}.$$

The moment of inertia of such a slab will be equal to $J–J_1K_1$ where:

$$J = \int_{-h/2}^{h/2} z^2 dz = \frac{h^3}{12}, \quad J_1 = \int_{-h/6}^{h/6} z^2 dz = \frac{h^3}{324} = \frac{h^3}{12 \cdot 27}.$$

Therefore:

$$D = \frac{Eh^3}{12(1-\mu^2)}\left(1 - \frac{K_1}{27}\right),$$

and the critical load will be as follows:

$$N_x = -\frac{D\pi^2}{a^2}\left(1 + \frac{a^2}{b^2}\right)^2.$$

Let us consider a specific example. Let us assume that the width of a cutout is two times larger than the width of the connection between the cutouts. Then, if there are four cutouts and five connections in the direction of the $x$ axis, then 13 units of length will correspond to the distance $a$ and the distance $a/13$ will correspond to each unit of length.

Since two units of length are required per one cutout, then $8a/13$ will correspond to four cutouts. There will be five cutouts in the direction of the $y$ axis, i.e., $b/16$ per one unit of length, and $10b/16$ per five cutouts. Let us find $K_1$ for this case:
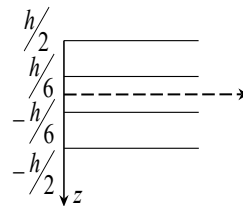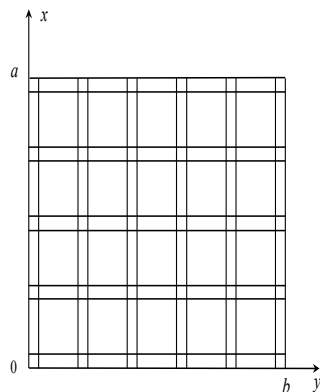


Fig. 3. Slab with inner cutouts

$$K_1 = \frac{ab \cdot \dfrac{8}{13} \cdot \dfrac{10}{16}}{ab} = 0.3846.$$

Therefore, $\left(1 - \dfrac{K_1}{27}\right) = 0.9858.$ The value of the critical load $N_x$ almost has not changed, but the volume of the slab has decreased and become as follows:

$$V = abh - \frac{2a}{13} \cdot 4 \cdot \frac{2b}{16} \cdot 5 \cdot \frac{h}{3} = abh \cdot 0.8718 \, \text{m}^3.$$

Let us increase the area of the cutouts. Let us assume that the width of a cutout is three times larger than the width of the connection between the cutouts. The number of cutouts in the direction of the $x$ axis will remain the same, i.e., four. We assume that in the direction of the $y$ axis, their number is 10. In this case:

$$K_1 = \frac{12}{17} \cdot \frac{30}{41} = 0.5165, \left(1 - \frac{K_1}{27}\right) = 0.981.$$

The volume of the slab will be equal to the following:

$$V = abh \cdot 0.8278 \, \text{m}^3.$$

If a reinforced concrete panel with the dimensions $a = 3m$, $b = 6m$, $h = 0.3m$, ($E = 3.25 \cdot 10^4$ specific density $\rho = 200$ kg/m³) is weakened by the above cutouts, then its dead weight will be as follows:

$$S_b = V \cdot \rho = 8940.24 \, \text{kg}.$$

The dead weight of a solid panel with the same dimensions will be as follows:

$$S_b = abh\rho = 10800 \, \text{kg},$$

i.e., such a panel will be heavier than a panel with cutouts by more than 1 ton.

Therefore, for the panel with cutouts, the critical load has decreased by 1.9%. Meanwhile, its weight has decreased by 17.2%. The example above shows that it is economically efficient to use three-layer panels with a discrete core, providing the required design stability parameters at reduced consumption of materials in construction.

**Conclusion**

We have built a mathematical model for the deformation of thin-walled elastic isotropic three-layer plates and wall panels with a discrete core in the form of a system of cross stiffeners, taking into account their width. The thickness of the entire structure is taken into account analytically by means of unit column functions.

To determine critical parameters of a compressed three-layer wall panel using the Bubnov–Galerkin method, the eigenvalue problem has been solved. According to the method suggested, we have performed stability analysis of three-layer wall panels with different values of core stiffness and studied the impact of the discrete core parameters on the buckling load, consumption of materials, and efficiency of three-layer engineering structures.

The reliable mathematical model and relative simplicity of the analysis algorithm make it possible to recommend the suggested method for the assessment of efficiency of three-layer wall panels with a discrete core.

## References

Aleksandrov, A. Ya. (1959). Filler content analysis for three-layer plates with account for layer separation. In: *Issues of aerostructure analysis. Analysis of three-layer plates and shells*, No. 1. Moscow: Oborongiz, pp. 14–38.

Aleksandrov, A. Ya., Bryukker, L. E., Kurshin, L. M. and Prusakov, A. P. (1960). *Analysis of three-layer panels*. Moscow: Oborongiz, 272 p.

Baculin, V. N. (2018). Block based finite element model for layer analysis of stress strain state of three-layered shells with irregular structure. *Mechanics of Solids*, Vol. 53, Issue 4, pp. 411–417. DOI: 10.3103/S0025654418040064.

Bryukker, L. E. (1965). Some options for the simplification of equations for three-layer plates exposed to bending. In: *Aerostructure analysis*. Moscow: Mashinostroyenie, pp. 29–31.

Davies, L. M. (ed.) (2001). *Lightweight sandwich construction*. Oxford: Blackwell Science, 370 p.

Dragan, V. I. and Levchuk, A. A. (2011). Strength and elasticity of double skinned metal faced panels. *Vestnik of Brest State Technical University*, No. 1, pp. 53–58.

Eremeev, V. V. and Zubov, L. M. (2017). On instability of a three-layered nonlinear elastic rectangular plate with prestressed middle layer. In: Pietraszkiewicz, W. and Witkowski, W. (eds.), *Shell Structures: Theory and Applications*, Vol. 4. London: CRC Press, pp. 215–218. DOI: 10.1201/9781315166605-46.

Galerkin, B. G. (1931). Elastic rectangular and triangular freely supported thick slabs exposed to bending. *Papers of the USSR Academy of Sciences. A Series*, pp. 273–280.

Golovanov, A. I., Tyuleneva, O. N. and Shigabutdinov, A.F. (2006). *Finite element method in statics and dynamics of thin-walled structures*. Moscow: Fizmatlit, 392 p.

Grigolyuk, E. I. and Chulkov, P. P. (1973). *Stability and vibrations of three-layer shells*. Moscow: Mashinostroyenie, 172 p.

Grigolyuk, E. I. and Kogan, F. A. (1972). State of the art of the theory of multilayer shells. *Soviet Applied Mechanics*, Issue 6, pp. 583–595. DOI: 10.1007/BF00892606.

Grishanov, A. N. (2018). An efficient method of building approximate solutions using multigrid finite elements. *Proceedings of the Russian Higher School Academy of Sciences*, Issue 3 (40), pp. 47–57. DOI: 10.17212/1727-2769-2018-3-47-57.

Kaledin, V. O., Aulchenko, S. M., Mitkevich, A. B., Reshetnikova, Ye. V., Sedova, Ye. A. and Shpakova, Yu. V. (2014). *Modeling statics and dynamics of shell structures made of composite materials*. Moscow: Fizmatlit, 196 p.

Karpov, V. V. (2010). *Strength and stability of stiffened shells of revolution. In 2 parts. Part 1. Models and algorithms for the analysis of strength and stability of stiffened shells of revolution*. Moscow: Fizmatlit, 288 p.

Karpov, V. V., Ignatyev, O. V. and Salnikov, A. Yu. (2002). *Non-linear mathematical models for the deformation of shells of variable thickness and algorithms of their study*. Moscow, Saint Petersburg: ASV Publishing House, Saint Petersburg State University of Architecture and Civil Engineering, 424 p.

Kipiani, G. (2014). Definition of critical loading on three-layered plate with cuts by transition from static problem to stability problem. *Advanced Materials Research*, Vol. 1020, pp. 143–150. DOI: 10.4028/www.scientific.net/AMR.1020.143.

Kobelev, V. N., Kovarsky, L. M. and Timofeyev, S. I. (1984). *Analysis of three-layer structures*. Moscow: Mashinostroyenie, 304 p.

Kreja, I. (2011). A literature review on computational models for laminated composite and sandwich panels. *Open Engineering*, Vol. 1, Issue 1, pp. 59–80. DOI: 10.2478/s13531-011-0005-x.

Levchuk, A. A. (2008a). Computation model of double skin metal faced panels. *Vestnik of Brest State Technical University*, No. 1, pp. 97–102.

Levchuk, A. A. (2008b). Static calculation of double skin metal faced panels with rock wool or foam plastic core. *Bulletin of Belarusian-Russian University*, No. 2, pp. 151–156.

Nguyen, H.-N., Nguyen, T.-Y., Tran, K. V., Tran, T. T., Nguyen, T.-T., Phan, V.-D. and Do, T. V. (2019). A finite element model for dynamic analysis of triple-layer composite plates with layers connected by shear connectors subjected to moving load. *Materials*, Vol. 12, Issue 4, 598. DOI: 10.3390/ma12040598.

Pukhliy, V. A. and Pukhliy, K. V. (2019). Application of the theory of three-layer structurally orthotropic shells for the analysis of the stress-strain state of blades in gas turbine and combined installations. *Theory of Mechanisms and Machines*, Vol. 17, No. 3 (43), pp. 86–96.

Rzhanitsyn, A. R. (1986). *Built-up columns and plates*. Moscow: Stroyizdat, 316 p.

Solomonov, Yu. S., Georgievsky, V. P., Nedbay, A. Ya. and Andryushin, V. A. (2014). *Applied problems of mechanics of composite cylindrical shells*. Moscow: Fizmatlit, 408 p.

# АНАЛИЗ ЭФФЕКТИВНОСТИ ТРЕХСЛОЙНЫХ СТЕНОВЫХ ПАНЕЛЕЙ С ДИСКРЕТНЫМ ВНУТРЕННИМ СЛОЕМ

Владимир Васильевич Карпов, Евгений Анатольевич Кобелев*

Санкт-Петербургский государственный архитектурно-строительный университет
2-ая Красноармейская ул., 4, Санкт-Петербург, Россия

*E-mail: evgeny.kobelev@gmail.com

**Аннотация**
Рассматриваются тонкостенные трехслойные пластины и панели с вырезами, подкрепленные ортогональной сеткой ребер или прямоугольных накладок параллельных координатным линиям. Толщина всей конструкции при этом учитывается аналитически с помощью единичных столбчатых функций. **Целью работы** было построение математической модели деформирования и создание методики расчета на устойчивость тонкостенных упругих изотропных трехслойных пластин и стеновых панелей с дискретным внутренним слоем. **Методы:** На основе применения математического аппарата обобщенных функций методом Бубнова – Галеркина решена задача на собственные значения для определения критических параметров сжатой трехслойной стеновой панели с дискретным внутренним слоем. **Результаты:** По предложенной методике проведены расчеты трехслойных стеновых панелей на устойчивость при различной жесткости внутреннего слоя и исследовано влияние параметров дискретного внутреннего слоя на величину критической нагрузки, материалоемкость и эффективность трехслойных строительных конструкций.

**Ключевые слова**
Трехслойная пластина, стеновая панель, дискретный внутренний слой, вырез, ребро жесткости.

# RESEARCH ON MECHANICAL PROPERTIES AND GROUTABILITIES OF GROUTED MORTISE-TENON JOINTS FOR PREFABRICATED STRUCTURES

Huang Mingli[1], Shen Qiaofeng[2]*, Zhang Zhancheng[3]

[1]Beijing Jiaotong University
Haidian District, Beijing, 100044, China
[2]Emperor Alexander I St. Petersburg State Transport University
Moskovsky pr., 9, St. Petersburg, Russia
[3]China Overseas Engineering Group
Haidian District, Zizhuyuan Road No. 1, Beijing, China

*Corresponding author: 18813094515@163.com

## Abstract

**Introduction:** The paper addresses grouted tenon-and-groove joints in the prefabricated structure of Changchun subway station. For the first time, grouting of prefabricated structure joints with organic epoxy grouting material is analyzed. **Purpose of the study:** We aimed to make sure that an organic epoxy grouting material can be injected into the joints uniformly and in full and conducted its experimental study. To establish the applicability of the epoxy grouting material in the prefabricated structures, we studied the mechanical properties of the epoxy grout and its adhesive properties in relation to concrete. **Methods:** In the course of the study, we used a set of test equipment and an independently developed method. **Results:** High-quality grouting can be guaranteed at an injection pressure of 0.4 MPa and a temperature of 5–10°C. The relationship between the slurry flow rate and time was fit according to the experimental data at 5 and 10°C. The optimal quartz powder ratio was determined at the level of 1:0.6–1:0.8, and the optimal quartz powder particle size (D50) was determined at the level of 18–25 μm. The results of the study can provide references for similar projects in the future.

## Keywords

Prefabricated structure, grouted tenon-and-groove joints, epoxy grouting material, groutability, mechanical properties, experiment.

## Introduction

Prefabrication is a construction technology that makes it possible to switch from traditional cast-in-situ concrete structures to prefabrication of components in a factory and on-site assembly. Due to its advantages, which include civilized construction, guaranteed construction quality, and reduced construction time, prefabrication will see broad application prospects in the coming decades with the rise of construction industrialization (Yan et al., 2004).

In China, Changchun Subway Line 2 encountered several problems: a tight construction schedule, high impact of construction on the surrounding environment, and low temperatures during the construction process. A number of open-cut subway stations were constructed using prefabrication and assembly technology. One of the stations has a single-arch, large-span structure assembled from seven prefabricated components with a ring width of 2 m. Fig. 1 shows a sectional diagram of the prefabricated structure. Fig. 2 shows ring and longitudinal connections between the members, made with a new type of grouted tenon-and-groove joint using concrete of grade C50 (Yang and Huang, 2018; Yang et al., 2019a).

Both domestic and foreign researchers have studied prefabricated assembled structures. Scandinavian countries and Russia have rich experience in the construction of prefabricated assembled subway stations (Li, 1995; Vlasov et al., 2002; Yurkevich, 1995). Li et al. (2019) analyzed the mechanical properties of two kinds of subway station structures (arched and rectangular) and concluded that the arched structure is characterized by better performance as well as lower stresses and deformations under the same load. Li and Liu (2016) analyzed factors affecting the bending stiffness of single tenon-and-groove joints in prefabricated subway stations and concluded that the bending moment of the joints is the most important factor leading to the reduction of their bending stiffness. An increase in the axial load and grouting of the joints significantly improves the bending stiffness of the
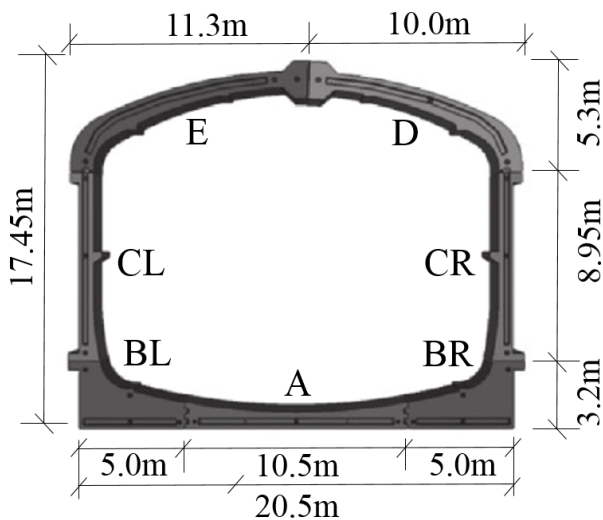
Fig. 1. Sectional diagram of the prefabricated structure



Fig. 2. Tenon-and-groove joints

joints. The degree of influence from changes in the dimensional parameters of the joint on its bending stiffness is related to the axial load applied to the joint. Su et al. (2016) conducted destructive tests on different combinations of axial and bending loads acting on different types of tenon-and-groove joints of fully assembled subway station structures to determine the flexural load-bearing capacity of the joints with account for five stages of flexural load bearing. Yang et al. (2019b, 2019c, 2020a, 2020b) performed a number of experiments to study the bending stiffness of grouted tenon-and-groove joints in prefabricated subway station structures and proposed a general formula for its calculation. Li et al. (2015a, 2015b, 2017, 2018) and Xu et al. (2017) systematically investigated the mechanical properties of tenon-and-groove joints in prefabricated structures using numerical simulations and structural loading tests, with the Yuanjiadian station of Changchun Metro Line 2 as the research background. Ding et al. (2018) and Tao et al. (2019) experimentally studied the seismic response characteristics of prefabricated subway station structures. Du et al. (2019) investigated the seismic performance of beam-slab-column joints in the cross-section of prefabricated assembled subway stations. Zhou et al. (2017) studied the tenon-and-groove grouting technology for prefabricated components.

Structural joints are still characterized by a design that is not very reliable. Bolted connections, pre-stressed rod connections, and cylindrical connections do not guarantee structural integrity. Water tightness cannot be guaranteed either. Although structural integrity and water tightness are guaranteed in weld and tenon-and-groove connections, the joined seams are filled with inorganic materials. The solidification and hardening of these materials are limited by temperature. Therefore, they are not suitable for use in low-temperature areas and low in adhesive strength (Wang et al., 2009).
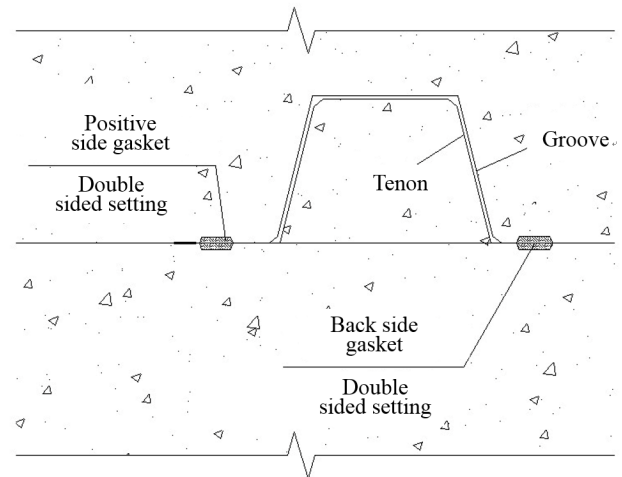
Epoxy resin adhesives have a number of advantages. They are characterized by low shrinkage and strong adhesion to a variety of materials, easy to prepare and use. Besides, they ensure the high hardness of cured products and can be easily modified (Peng, 2004). To promote the further development of prefabricated assembled structures and solve issues with previous versions, epoxy resin was proposed as a potting material for joints. Inorganic rigid-particle quartz powder was used to modify it (Zhao and Yun, 1999). The influence of quartz powder introduction and the particle size on the mechanical properties of the epoxy grout and bonded concrete was studied experimentally. Researchers determined the optimal amount of quartz powder to be introduced and the particle size to develop the optimal epoxy grout formulation and conducted a full-scale test. To ensure successful grouting completion, Yang et al. (1997) studied epoxy grout injectability using unique test equipment and test methods that they developed, and analyzed the mechanical properties of the epoxy grout and bonded concrete.

**Methods**

1. Mechanical performance test model

The base fluid used for the test was epoxy resin with quartz powder particle sizes D50 of 16.71, 18.49, 21, 26.26, and 34.24 µm, and the test temperature was 13–14°C.

Compression strength and compression modulus were tested using GB 1041-79 plastic compression test method (State Standard of China, 1993). Shear bond strength was determined using three 100 × 100 mm C50 concrete test blocks bonded in triangles with epoxy grout as shown in Fig. 3. The test load was force-controlled with a loading rate of 0.2 KN/s. Tensile bond strength was determined by bonding two 100 × 100 mm C50 concrete specimens as shown in Fig. 4. The test load was displacement-controlled with a loading rate of 2 mm/min.

(a) Design drawing

(b) Physical implementation
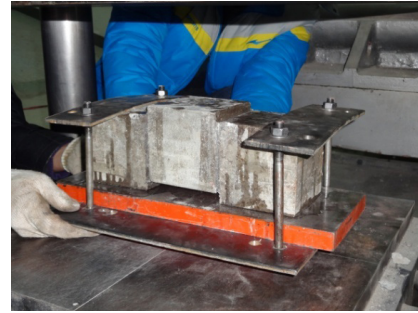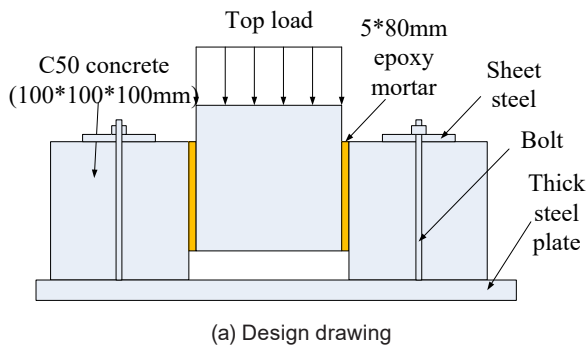
Fig. 3. Shear bond strength test system



(a) Design drawing

(b) Physical implementation
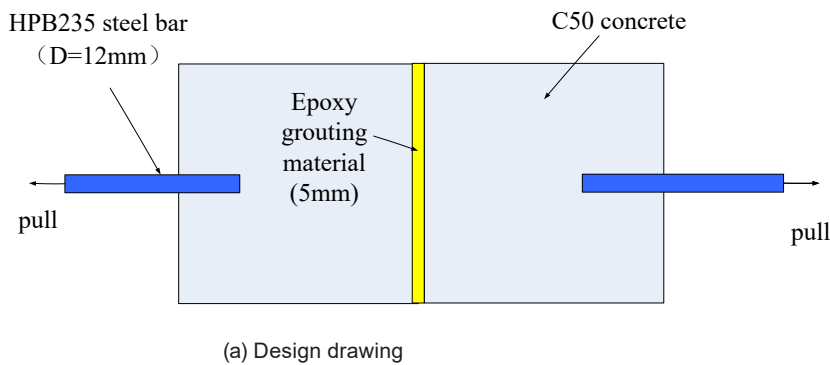
Fig. 4. Tensile bond strength test system

To study the load-bearing capacity of tenon-and-groove joints under different overburden loads, a full-scale test of tenon-and-groove joints was conducted. Due to the complex shape of the original structure, the test was simplified and the test specimen consisted of two rectangular reinforced concrete blocks with tenons and grooves, with 5 mm of epoxy grout in the middle of the tenon and groove. The concrete grade, reinforcement grade, and reinforcement rate of the specimens were the same as in the original structure. The test was performed by applying an axial load to one end of the specimen by a jack to simulate the overburden load, and the bending moment at the tenon and groove was applied by two forces of equal size at equal distance from the tenon and groove. The test load was force-controlled. Fig. 5 shows a schematic diagram of full-scale test loading.

2. Injectability test model

Due to the complex shape and large size of the original structure, the original structure was simplified for the test without changing the thickness of the joints. Fig. 6 shows an injection test device used in the test. Its cross-section is given in Fig. 7, and the longitudinal section is given in Fig. 8. The main design parameters of the injection test device were the following: the seam spacing was 100 mm (1/6 of the original structure), the seam thickness was 5 mm, the total length of the grouting section was $1.6 \times 3 + 1.65 \times 2 + 0.1 \times 4 = 8.5$ m, and the internal

diameter of the grouting pipe was of the original structure.

The test system consisted of a grouting pump, grouting tank, injection test device, and slurry collecting bucket, with all components connected by a grouting pipe. Fig. 9 shows its design diagram, and Fig. 10 shows its physical implementation.

The test process was as follows:

(1) Connect the grouting pump, grouting tank, injection test device, and slurry collecting bucket with the grouting pipe, ensure firm and dense connection. Open the valve and ventilate to test the tightness of the test device.

(2) Calculate the required amount of slurry to be injected (mass = density x volume) and multiply by a factor of 1.2 to prevent the air from being injected into the test device and causing damage to it. Prepare slurry and take measures to maintain the slurry and chamber temperature at the test temperature, test viscosity at that temperature. Close the valve at the bottom of the grouting tank, open the tank, slowly pour in epoxy resin slurry, and then close the tank.

(3) Add a relatively small pressure to the air pump, open the valve at the bottom of the grouting tank, close the valve at the bottom of the grouting tank after slurry flows out from the grouting port, increase air pump pressure to the design value, then open the valve at the bottom of the grouting tank, and record the level of slurry with a marker every 5 s.
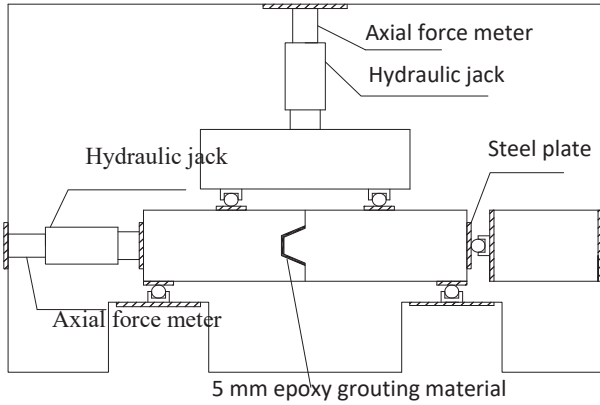
Fig. 5. Schematic diagram of full-scale test loading
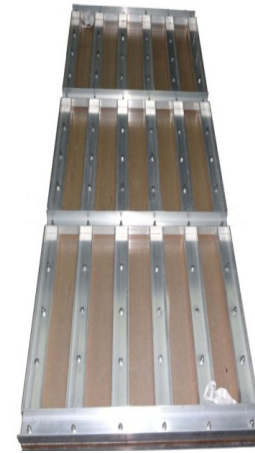


Fig. 6. Injection test device
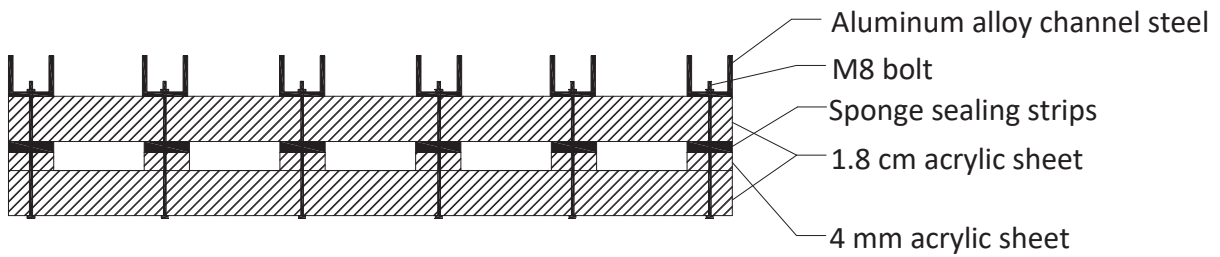


Fig. 7. Diagram of the cross-section



Fig. 8. Diagram of the longitudinal section
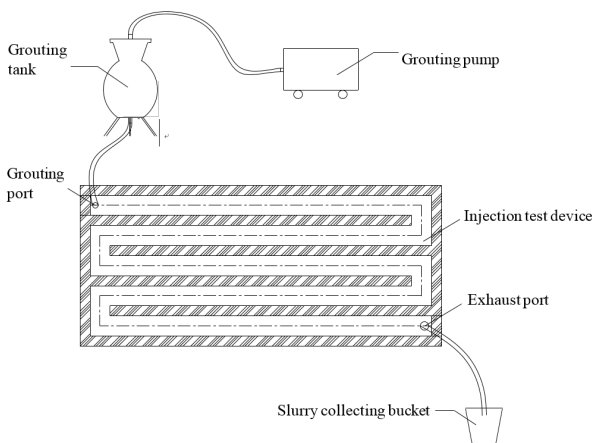


Fig. 9. Design diagram of the injection test system



Fig. 10. Injection test system

(4) After slurry injection, close the valve of the grouting tank and grouting pump.

**Results**

1. Mechanical performance test results

Fig. 11 shows the compressive strength of the epoxy grout vs. the amount of quartz powder, and Fig. 12 shows the elastic modulus of the epoxy grout vs. the amount of quartz powder.

Cao et al. (2005) studied the effect of adding ultrafine $SiO_2$ to epoxy resin on its mechanical properties and found that with small filler amounts, it is possible to reduce the shrinkage of epoxy resin,
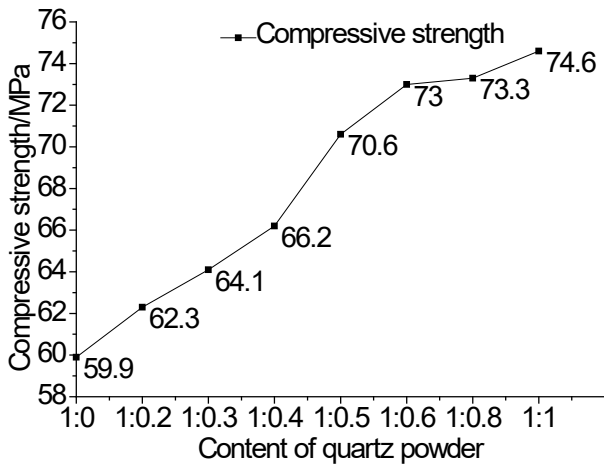
Fig. 11. Compressive strength of the epoxy
grout vs. quartz powder amount
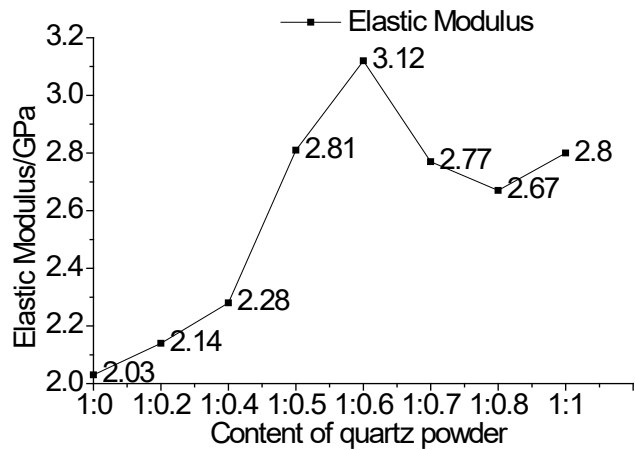


Fig. 12. Elastic modulus of the epoxy
grout vs. quartz powder amount
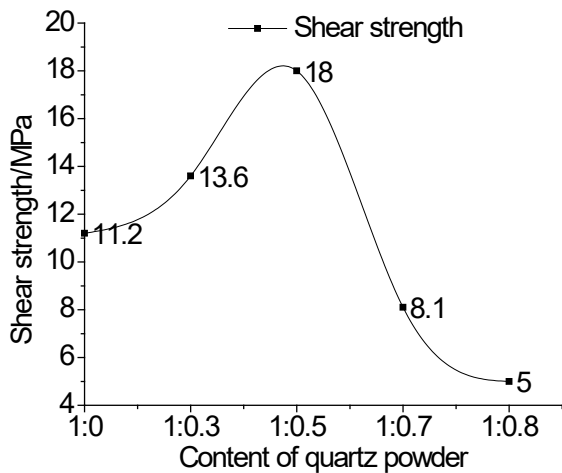


Fig. 13. Shear strength of epoxy grout bonded
concrete vs. quartz powder amount
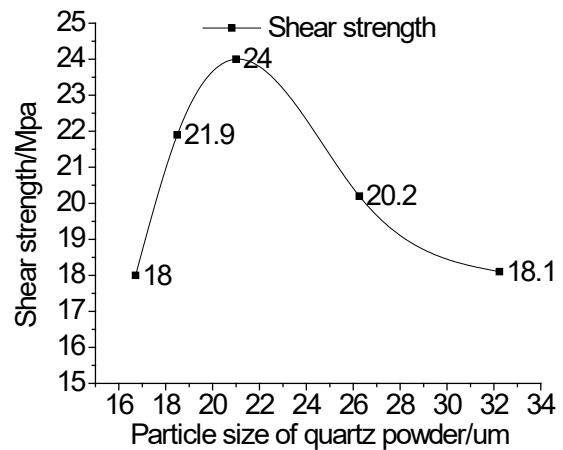


Fig. 14. Shear strength of epoxy grout bonded
concrete vs. quartz powder particle size

absorb energy, and terminate the silver pattern, thus reducing residual stress during epoxy resin curing and uniforming the process. Therefore, with an increase in the filler ratio, the compressive strength will increase as well. However, when the filler amount exceeds a certain value, the stress fields generated by the filler overlap and dominate, and the compressive strength of epoxy resin decreases.

It can be seen from Fig. 11 that the compressive strength of epoxy mortar can exceed the compressive strength of C50 concrete. The compressive strength grows slowly when the quartz powder ratio is from 1:0.6 to 1:0.8 and is close to the maximum value.

As can be seen from Fig. 12, the elastic modulus of epoxy mortar first gradually increases with the addition of quartz powder, and then gradually decreases; it is close to the maximum value in the interval from 1:0.5 to 1:1. The introduction of quartz powder can improve the elastic modulus of epoxy resin since the elastic modulus of quartz powder is much larger than that of epoxy resin. Within a certain

range of addition, quartz powder interacts better with the epoxy resin interface and resists the expansion of cracks, and beyond that range, the effect of quartz powder becomes smaller (You et al., 2006).

Fig. 13 shows the shear strength of epoxy grout bonded concrete vs. the amount of quartz powder. Fig. 14 shows the shear strength of epoxy grout bonded concrete vs. the size of quartz powder particles.

As can be seen from Fig. 13, with an increase in the amount of quartz powder when the ratio is less than 1:0.5, shear strength increases. It reaches the maximum value of 18 MPa when the ratio is 1:0.5, which is 60.7% higher than the shear strength of pure epoxy resin (11.2 MPa). When the ratio is greater than 1:0.5, shear strength gradually decreases. The reason is that when the amount of filler added is small, the filler particles do not interfere with each other and are uniformly dispersed in the epoxy resin matrix, and the filler makes it possible to reduce the shrinkage of the adhesive system, thus reducing residual stress during adhesive curing and uniforming the process. Therefore, with an increase in the

filler amount, the shear mechanical properties will improve. However, when the filler amount exceeds a certain value, the stress fields generated by the filler overlap, and the adhesive bonding performance and adhesive shear resistance decrease.

As can be seen from Fig. 14, with an increase in the quartz powder particle size (D50), the shear strength of epoxy grout bonded concrete first gradually increases and then gradually decreases, reaching a maximum value of 24 MPa when the quartz powder particle size (D50) is 21 μm. The reason is that when the quartz powder particle size (D50) increases but does not exceed 21 μm, the total area of quartz powder contact with concrete decreases after the epoxy grout is filled into the

specimen, thus more epoxy resin can penetrate concrete and increase shear strength, while an increase in the area of epoxy resin contact with concrete will also increase shear strength. When the quartz powder particle size (D50) exceeds 21 μm, quartz powder deposition occurs during epoxy grout curing, thus, a part of the contact area between epoxy grout and concrete loses shear strength and the total shear strength decreases. Therefore, the quartz powder particle size (D50) shall be in the range from 18 to 25 μm, and this range can provide a better formulation.

The tensile strength of epoxy grout bonded concrete depending on the amount of quartz powder is shown in Table 1.

Table 1. Tensile strength (MPa)

| Amount of quartz powder | Group 1 | Group 2 | Group 3 | Group 4 |
|---|---|---|---|---|
| 1:0 | 2.53 | 2.88 | 2.96 | 2.79 |
| 1:0.5 | 2.52 | 2.79 | 2.84 | 2.72 |
| 1:0.8 | 2.66 | 2.73 | 2.81 | 2.73 |

The measurements and specimen damage diagram show that the tensile strength of the bonding surface of the epoxy grout bonded concrete specimens is much greater than the tensile strength of concrete. The specimens were damaged due to concrete failure. The value of tensile strength depends on the value of concrete tensile strength and has a weak relationship with the amount of quartz powder and particle size.

Fig. 15 shows the general damage pattern of full-scale test specimens. It can be seen that damage is distributed not along the tenon-and-groove joints but along the contact surface of reinforcement and concrete, and concrete on the joints peeled off at the time of damage, which indicates that the

epoxy grout is safe for gluing tenon-and-groove joints.

To determine the flexural load-bearing capacity of the full-scale test specimens under different axial loads, three points of specimen damage were established: joint side opening of 3 mm when the corresponding bending moment is $M_1$; the end of the crack stable development stage when the corresponding bending moment is $M_2$; reinforcement stress reduction at the tenon-and-groove joint at the same time when the corresponding bending moment is $M_3$. In all three cases, the load-bearing capacity was taken as the smallest value among the bending moment values under the same axial load. The results are shown in Table 2.
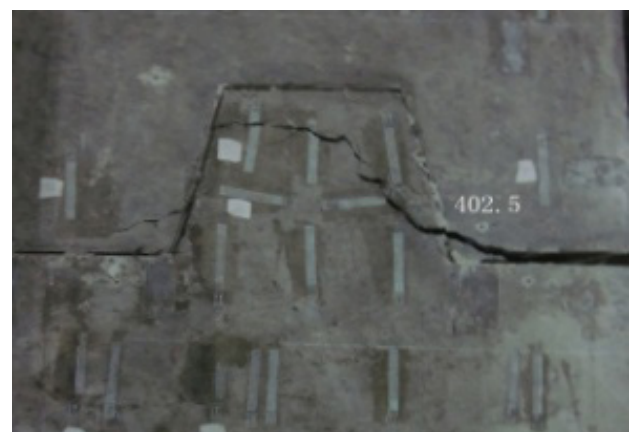


Fig. 15. Failure mode in the full-scale test
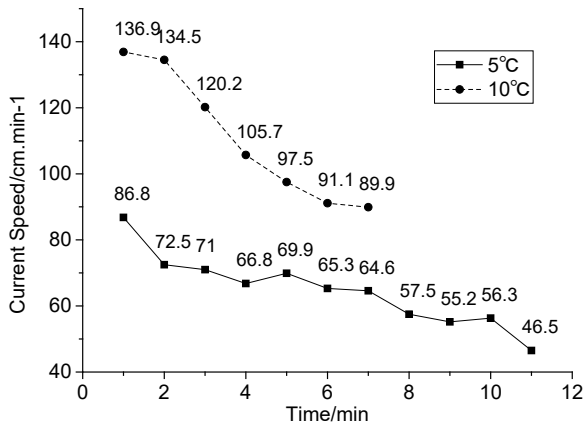
Fig. 16. Current speed vs. time
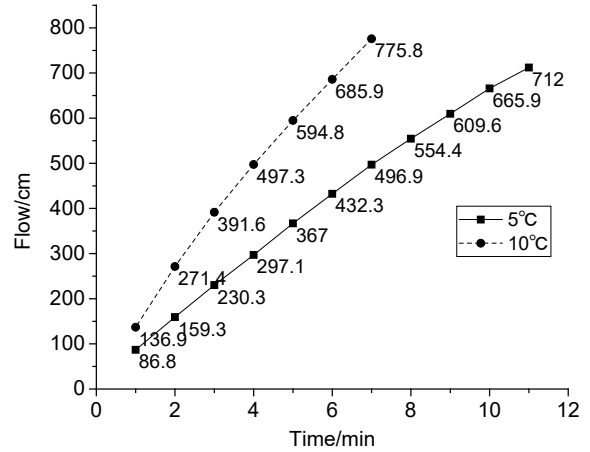


Fig. 17. Flow vs. time

Table 2. Flexural load-bearing capacity under different axial loads

| Axial load | $M_1$ | $M_2$ | $M_3$ | Load-bearing capacity |
|---|---|---|---|---|
| 0 | — | 87.5 | — | 87.5 |
| 500 | 230 | 250 | — | 230 |
| 1000 | 335 | 326 | 330 | 326 |
| 1600 | 471 | 470 | 480 | 470 |
| 2000 | 593 | 500 | 550 | 500 |

2. Injectability test results

During the tests, we used a modified epoxy grout developed by Beijing Jiaotong University. The test pressure was 0.4 MPa. Fig. 16 shows a relationship between the flow rate and time, and Fig. 17 shows a relationship between the flow and time.

With an increase in the grouting distance, the flow rate gradually becomes slower, which is caused by the internal friction between the layers. In other words, viscosity plays an important role. To study the relationship between the grouting volume and time, the measured data were fit; the fitting results are shown in Fig. 18.

The fitting results show that the correlation between the fit curve and the measured data curve is as high as 0.999, indicating that the function obtained by fitting is in good agreement with the actual results. They also show that the slurry volume and time are approximately parabolic, and the relationship between the flow rate and time can be obtained by the derivation of the function of the flow rate vs. time:
- Flow rate vs. time at 5°C: V = –2.5822t + 78.556.
- Flow rate vs. time at 10°C: V = –9.1642t + 141.97.
The function shows that, with an increase in time, the flow rate decreases gradually. The flow rate at the beginning of grouting at 5°C is 78.556 cm/min, and it decreases at a rate of 2.5822 cm/min. The time of epoxy grout injection at 5°C is 30.4 min, and the longest injection distance is 12.02 m. The flow rate at the beginning of grouting at 10°Cis 141.97 cm/min, and it decreases at a rate of 9.1642 cm/min. According to these calculations, the time of epoxy grout injection at 10°C is 15.5 min, and the longest injection distance is 11.02 m. The theoretical time of grouting for the next joint at 5and 10°C calculated by the fitting formula is shown in Table 3.

Table 3. Theoretical time of joint grouting (min)

| Joints | | A | B | C | D, E |
|---|---|---|---|---|---|
| Grouting time | 5°C | 15.6 | 6.1 | 13.1 | 16.3 |
| | 10°C | 9.2 | 3.5 | 7.6 | 9.6 |

The above test results do not consider the effect of concrete surface friction on injectability. To consider it, we performed two sets of comparative tests, one with the use of Plexiglas plates with grit 60 emery cloth on the inner surface and another without emery cloth. Fig. 19 shows a relationship between the flow rate and time.

**Conclusion**

(1) The results of the mechanical properties test for the epoxy grout and bonded concrete were obtained.

Considering the effect of quartz powder introduction on the compressive strength and elastic modulus of the epoxy grout as well as the effect on the shear strength of low-temperature epoxy grout bonded concrete and the project cost, while ensuring the best use of the tenon-and-groove joint, the optimal ratio of quartz powder was determined at the level of 1:0.6–1:0.8.

Considering the effect of the quartz powder particle size on the shear strength of low-temperature epoxy grout bonded concrete, the optimal quartz powder particle size (D50) was determined at the level of 18–25 μm.

The tensile strength of epoxy grout bonded concrete depends on the tensile strength of concrete

and does not depend on the quartz powder amount and particle size in epoxy grout.

The full-scale test showed that it is possible to ensure that the mechanical properties of joints meet the engineering needs by bonding tenon-and-groove joints with epoxy grout.

(2) The results of the epoxy grout injectability test demonstrate the following:

With a construction temperature of 5°C or higher and a grouting pressure of 0.4 MPa, the grouting quality of all joints in the project can be guaranteed.

The flow rate decreases with grouting time, the epoxy grout injection time at 5°C is 30.4 min, and the longest injection distance is 12.02 m. The epoxy grout injection time at 10°C is 15.5 min, and the longest injection distance is 11.02 m. The relationship between the slurry flow rate and time was fit according to the experimental data at 5 and 10°C.

Friction has a relatively small effect on injectability.

The application of prefabricated structures in underground engineering has broad prospects. The design of joints is the key to the success or failure of prefabricated structures application. The results of the research on the grouting material ratio and grouting technical parameters in this paper can provide references for practical engineering.
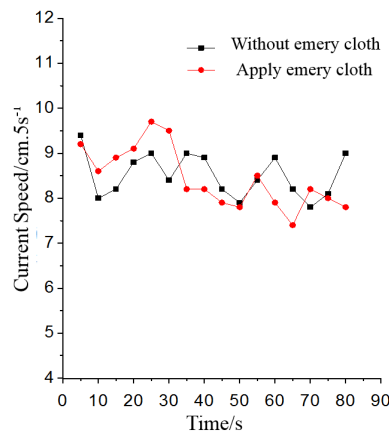


Fig. 18. Fitting results for the relationship between the flow and time
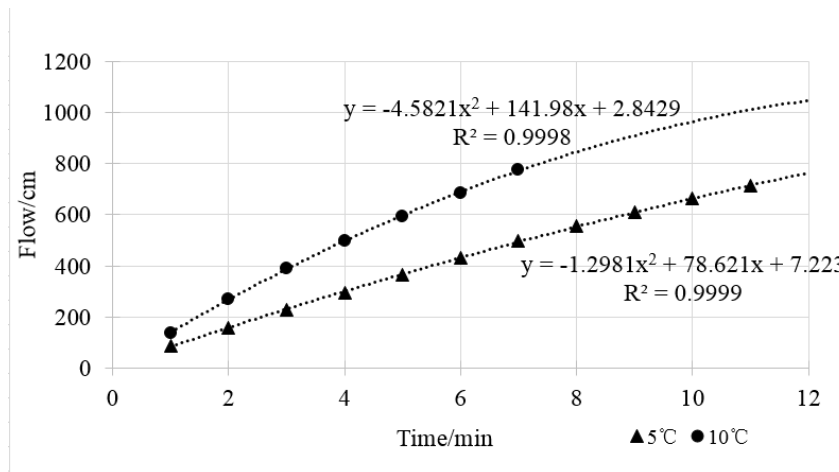


Fig. 19. Friction effect test diagram

**References**

Cao, P., You, M., Liu, G. and Cai, J. (2005). Effect of SiO2 on the strength of epoxy adhesives. *China Adhesives*, Vol. 14, Issue 4, pp. 15–17.

Ding, P., Tao, L., Yang, X., Zhao, J. and Shi, C. (2018). Three-dimensional dynamic response analysis of a single-ring structure in a prefabricated subway station. *Sustainable Cities and Society*, Vol. 45, pp. 271–286. DOI: 10.1016/j.scs.2018.11.010.

Du, X.-L., Liu, H.-T. and Xu, C.-S. (2019). Study on seismic performance of beam-column-slab interior joints in cross section of assembled monolithic subway station. *Journal of Building Structures*, Vol. 40, Issue 8, pp. 51–60.

Li, T.-H. (1995). Design and construction experience of Minsk single arch metro station. *Metro and Light Rail*, Vol. 2, pp. 44–48.

Li, Z.-P., Li, K.-X., L(u), S.-Q., Su, H.-F. and Wang, C. (2018). Experimental study on stress evolution rule of double tenon-groove joints for prefabricated metro station structure. *China Railway Science*, Vol. 39, Issue 5, pp. 15–21. DOI: 10.3969/j.issn.1001-4632.2018.05.03.

Li, X.-W. and Liu, Q. (2016). Influencing factor analysis of bending stiffness of single tenon groove joint of subway station constructed with prefabricated element. *Railway Standard Design*, Vol. 60, Issue 8, pp. 113–117. DOI: 10.13238/j.issn.1004-2954.2016.08.024.

Li, X.-H., Liu, C.-Y. and Zhang, Q. (2019). Comparative analysis of mechanical properties of arched and rectangular subway stations. *Construction Technology*, Vol. 48, Issue 16, pp. 1–4.

Li, Z.-P., Su, H.-F., Lu, S.-Q., Wang, C., and Xu, X.-Z. (2017). Experimental study on flexural mechanical properties of the double tenon groove joints of prefabricated subway station. *China Civil Engineering Journal*, Vol. 50, Issue S2, pp. 28–32.

Li, Z.-P., Wang, C., Su, H.-F., Shi, S.-F. (2015a). An experiment study on the evolution law of concrete structure crack and joint seam deformation for tenon groove joints in the prefabricated metro station. *China Civil Engineering Journal*, Vol. 48, Issue S1, pp. 409–413.

Li, Z.-P., Wang, C., Su, H.-F., Shi, S.-F. and Wang, P. (2015b). Mechanical property of tenon-groove joints for metro station constructed by prefabricated structure. *China Railway Science*, Vol. 36, Issue 5, pp. 7–11. DOI: 10.3969/j.issn.1001-4632.2015.05.02.

Peng, L.-G. (2004). *Study on epoxy resin adhesive for architecture structure*. Master's thesis. Xi'An: Xi'an University of Architecture and Technology.

State Standard of China (1993). GB/T 1041-92. *Test method for compressive properties of plastics*. Beijing: State Bureau of Quality and Technical Supervision.

Su, H.-F., Li, X.-W. and Wang, C. (2016). Experimental study on flexural capacity of joints of structure of metro station with prefabricated concrete structure. *Journal of the China Railway Society*, Vol. 38, Issue 9, pp. 118–123. DOI: 10.3969/j.issn.1001-8360.2016.09.017.

Tao, L., Ding, P., Shi, C., Wu, X., Wu, S. and Li, S. (2019). Shaking table test on seismic response characteristics of prefabricated subway station structure. *Tunnelling and Underground Space Technology*, Vol. 91, 102994. DOI: 10.1016/j.tust.2019.102994.

Vlasov, S. N., Alexandrov, V. N. and Kurakin, N. I. (2002). *Essentials of Russian underground railway construction*. Beijing: China Railway Press.

Wang, M.-N., Li, Z.-Y. and Wei, L.-H. (2009). *Prefabrication technology of tunnel and underground railway*. Chengdu: Southwest Jiaotong University Press.

Xu, X.-Z., Li, Z.-P., Zhu, Y.-C. and Su, H.-F. (2017). Study on shear property of tenon groove joint of prefabricated subway station. *China Civil Engineering Journal*, Vol. 50, Issue S2, pp. 141–146.

Yan, W., Cao, Y.-H. and Li, G.-R. (2004). Development of assembly-type RC structure and building industrialization. *Journal of Chongqing Jianzhu University*, Vol. 26, Issue 5, pp. 131–136.

Yang, X.-R. and Huang, M.-Q. (2018). Research strategies on new prefabricated technology of underground subway station. *Urban Rapid Rail Transit*, Vol. 31, Issue 1, pp. 78–85.

Yang, X.-R., Huang, M.-Q. and Lin, F. (2019a). Research strategies on new prefabricated technology for underground metro stations. *Urban Rail Transit*, Vol. 5, Issue 3, pp. 145–154. DOI: 10.1007/s40864-019-0106-z.

Yang, X.-R., Huang, M.-Q., Lin, F., Wang, C. and Su, H.-F. (2019b). Experimental method of grouted mortise-tenon joint for prefabricated metro station structure. *Urban Rapid Rail Transit*, Vol. 32, Issue 5, pp. 83–90.

Yang, X.-R., Huang, M.-Q. and Lin, F. (2020a). Research on bending resistance characteristics of grouted mortise-tenon joints for prefabricated metro station structures. China Civil Engineering Journal, Vol. 53, Issue 2, pp. 33–40.

Yang, X.-R., Lin, F. and Huang, M.-Q. (2020b). Experimental research on flexural rigidity of grouted single mortise-tenon joints for prefabricated metro station structures. *China Civil Engineering Journal*, Vol. 53, Issue 3, pp. 38–43.

Yang, X.-N., Lu, S.-L. and Ge, J.-L. (1997). Bolt-grouting support and its application in weak rock roadway. *Chinese Journal of Rock Mechanics and Engineering*, Vol. 16, Issue 2, pp. 171–177.

Yang, X.-R., Shi, Z.-H. and Lin, F. (2019c). Influence of geometrical parameters on performance of grouted mortise and tenon joints for application in prefabricated underground structures. *Advances in Civil Engineering*, Vol. 2019, 3747982. DOI: 10.1155/2019/3747982.

You, M., Cao, P., Wei, X.-H. and Yu, H.-Z. (2006). Effect of SiO2 filler on the elastic modulus and Poisson's ratio of epoxy layer. *China Adhesives*, Vol. 15, Issue 3, pp. 12–14.

Yurkevich, P. (1995). Developments in segmental concrete linings for subway tunnels in Belarus. *Tunnelling and Underground Space Technology*, Vol. 10, No. 3, pp. 353–365. DOI: 10.1016/0886-7798(95)00015-Q.

Zhao, S.-Q. and Yun, H.-M. (1999). Study on rigid particle toughened epoxy resin. *China Plastics*, Vol. 13, Issue 9, pp. 35–39.

Zhou, S., Zhang, X., Dong, J.-L., Li, S.-L. and Wang, Q.-B. (2017). Grouting technology of prefabricated groove for prefabricated metro station. *Building Technique Development*, Vol. 44, Issue 18, pp. 70–71.

# INTERCHANGEABILITY AND STANDARDIZATION OF THE PARAMETERS OF COMBUSTIBLE GASES WHEN USING HYDROGEN

Alexander Shkarovskiy[1,2]*, Anatolii Koliienko[3], Vitalii Turchenko[3]

[1]Saint Petersburg State University of Architecture and Civil Engineering
2-nd Krasnoarmeiskaya St. 4, St. Petersburg, Russia
[2]Koszalin University of Technology
Sniadeckich St. 2, 75-453 Koszalin, Poland
[3]National University "Yuri Kondratyuk Poltava Polytechnic"
Piershotravnevyj Ave. 24, Poltava, 36011 Ukraine

*Corresponding author: szkarowski@mail.ru

## Abstract

**Introduction and purpose of the study:** The paper presents results of studies aimed to provide a rationale for the possibility of a gradual transition to hydrogen combustion in gas supply to domestic and commercial consumers without changes in the design and operation of burners. For this purpose, we have considered tasks of determining the indicators of interchangeability for natural gas and its mixtures with hydrogen. The main characteristics of combustible gases with various hydrogen content in a mixture have been studied. We have established the impact of the hydrogen content on the heat rate, emissions of harmful substances, as well as light back and flame lift phenomena. We have also analyzed the available interchangeability criteria and their applicability when using natural gas/hydrogen mixtures. The impact of the hydrogen content on the radiation heat transfer in the furnaces of gas equipment is described in the paper for the first time. **Methods**: The methodology of the paper is based on a critical analysis of available literature data on combustible gases interchangeability as well as theoretical and experimental studies performed by the authors. We have derived dependencies that allow us to determine the possibility of gas equipment transition to the combustion of natural gas/ hydrogen mixtures. We have also developed recommendations on the permissible hydrogen content in a natural gas/ hydrogen mixture that would ensure the efficient, safe, and green use of such fuel in domestic and commercial heating units. **Results**: Scientific findings and practical results of the study make it possible to implement partial gradual cost-effective decarbonization in the area of gas fuel utilization as an intermediate stage of transition to more extended hydrogen combustion.

## Keywords

Gas supply, decarbonization, natural gas, hydrogen, mixtures, interchangeability, permissible content.

## Introduction

Currently, studies and pilot projects related to the use of hydrogen as a fuel are of the most immediate interest. The reason for such interest is the possibility of decarbonization of the atmosphere through reaching zero $CO_2$ emissions with combustion products and reducing the impact on global climate changes (European Commission, 2020).

However, as often happens, the road from the idea to its technical implementation is long and difficult. First of all, it is worth mentioning numerous technical and economic issues of hydrogen production, storage, transportation, and use, which are nowadays contradictory. This is especially when we refer to great and almost global plans for transition to this type of fuel (Grib, 2019). The so-called catalytic steam reforming of hydrocarbons is a quite simple and well-mastered method. However,

the process is accompanied by such quantities of $CO_2$ emissions that the thesis on the green nature of hydrogen fuel does not make sense. Well-known hydrous pyrolysis does not have this drawback, but it is 1.8–3 times more expensive than reforming. Electric power required for electrolysis can be of green origin only so as not to bump into the issue of $CO_2$ plume (Konoplyanik, 2020). In our opinion, the necessary investment and functional-cost analysis of many related issues is still far from completion.

Despite this, the idea has already won recognition. In 2019, the EU presented a hydrogen strategy as part of the European Green Deal (European Commission, 2019). It is planned that hydrogen will be able to replace carbon energy sources, and by 2050 it will transform Europe into the first climate-neutral continent where greenhouse gas emissions into the atmosphere will not exceed

the volume consumed by the ecosystem. The EU states are willing to invest 180 to 470 bn EUR into this project by 2050. Within the framework of this strategy, there is a project to provide the EU with hydrogen with a hydrogen production capacity of 80 GW.

Decisions concerning hydrogen economy development, including in the Russian Federation, are made at the governmental level (Government of the Russian Federation, 2020). The largest energy providers negotiate the use of entire territories for the construction of hydrogen production enterprises (RBC, 2021c). This trend is also observed in cooperation at the international level (RBC, 2021a).

However, the issues of hydrogen use are not limited to the matters of its production, storage, and transportation. The thing is that hydrogen and hydrocarbon fuels, such as natural gas, are combustible gases disparate in terms of their main indicators. Calorific value and density, air consumption and volume of combustion products, flame speed and flammability limits — all these most important characteristics differ several times (Staskevich et al., 1990). Therefore, full replacement of gas burners rather than their adjustment is required. New devices can be developed for dozens and hundreds of units, as is the case with power turbines (RBC, 2021b). However, for hundreds of thousands and even millions of low-power devices, such replacement in one go is impossible. In this situation, the idea to use hydrogen in mixtures with natural gas seems most reasonable (European Commission, 2020). It is not a case of zero $CO_2$ emissions, but each 10% of hydrogen in such a mixture make it possible to proportionately reduce carbon dioxide emissions into the atmosphere (Szkarowski, 2020).

**Analysis of the current state of the issue**

When studying if it is possible to use such mixtures in practice, the issue of permissible hydrogen content is the key factor. The solution to this problem is a typical trade-off. On the one hand, there is a wish to increase the share of hydrogen and its environmental effect. On the other hand, it is required to ensure compliance with the fuel utilization efficiency and safety principles and minimize the volume of investments necessary for the transition of gas burner and furnace units from pure natural gas they were designed for to natural gas/hydrogen mixtures (Flórez-Orrego, 2011).

The matters of interchangeability of combustible gases are not new for the theory and practice of fuel consumption (Knoy, 1941, 1953). In many countries, the issue of transition from synthetic gases to natural gas was handled at different times (Gilbert and Prigg, 1956). Nowadays, it can be biogas, generator gas, refinery gas, propane-butane gas, liquefied natural gas (LNG), or their mixtures with each other and air (Jones, 2005).

Hydrogen or its mixtures with other gases may be a similar alternative. For example, refinery gas with high hydrogen content in a mixture with natural gas is used at refineries as a fuel for oil refinery furnaces and oil refinery units (Kolienko and Kolienko, 2011).

For the majority of EU countries that receive natural gas via gas trunk lines from the Russian Federation, it is the main type of fuel. However, it does not rule out the possibility of using other types of gas fuel. Therefore, the standardization of interchangeability of various gases in such countries is reflected at the appropriate level (Delbourg and Lafon, 1971).

**Subject, tasks, and methods**

Interchangeability can be defined as the ability of combustible gas to be substituted by another without the need to adjust gas burner units (GBUs) or other equipment of gas devices, change the operation mode or settings of such equipment. The units will continue to operate safely and satisfactorily (International Organization for Standardization, 2013; Honus et al., 2016)

Therefore, the possibility of a seamless transition from one type of gas fuel to another while preserving (or with permissible changes to) equipment characteristics exists only for interchangeable gases. These characteristics are as follows:

– heat rate $N$, kW;

– energy conversion efficiency $\eta$, %;

– steady operation of GBUs without light back or flame lift;

– complete combustion (permissible concentration of incomplete chemical combustion products in combustion products), $mg/m^3$ or vol.%;

– absence of yellow tipping indicating pyrolytic processes and sooting related to the insufficient air intake for combustion (total or primary air).

**Therefore, the subject of the study is the effective and safe utilization of various gases in commercial and domestic sectors in terms of the increasingly widespread use of hydrogen and its mixtures**.

It is known from the practice of combustible gas combustion that steady and efficient gas combustion in the flow significantly depends on the operating parameters of this process. Such parameters include the following: air and gas consumption, including primary air (for burners with two-stage air supply); ratio between actual and theoretical air consumption (air excess factor $\alpha$); gas and air velocity, etc. (Halchuk-Harrington and Wilson, 2006).

The stable position of the flame front in space and absence of light back and flame lift are ensured by the equality of the flame speed and the gas-air mixture speed at each point of the front. In turn, this equality depends on the properties of the fuel, efficiency of mixing processes, flame holding methods, and burner heat output. That is why the composition as well as physical and chemical properties of the gas

are crucial for the interchangeability of combustible gases and fuel utilization efficiency.

The region of efficient and steady combustion is limited to the regions of loss of flame stability (light back and flame lift) and incomplete combustion with preceding yellow tipping indicating sooting. The diagram in Fig. 1 (Halchuk-Harrington and Wilson, 2006) shows these regions in the "burner heat output" – "primary air excess factor" coordinates.

The diagram is somewhat conditional since it uses only concepts, without any numerical values. From this perspective, the diagram given in Fig. 2 (Staskevich et al., 1990) is more conclusive. It presents a steady and efficient combustion region in the "gas/air mixture velocity" – "primary air excess factor $\alpha_1$" coordinates. Please note that the gas/air mixture velocity is associated with the gas flow rate and burner heat rate.

Therefore, when resolving the issue of gas interchangeability, it is required to ensure steady and efficient operation not only without changes to the GBU design while complying with the rated capacity but also within the whole range of the output control.

According to the effective standards (Euro-Asian Council for Standardization, Metrology and Certification, 2012; European Committee for Standardization, 2021), all types of combustible gases are classified first by gas family and then by group and subgroup. For example, natural gases are in Family 2 where high-methane gases are in Group E. Gases of the same group have the same combustion characteristics and are clustered by the value of one of the interchangeability indicators — the (superior) Wobbe index $W_s$, MJ/m$^3$:

$$W_s = \frac{H_s}{\sqrt{\overline{\rho}}} = \frac{H_s}{\sqrt{\dfrac{\rho_g}{\rho_a}}}, \qquad (1)$$

where $H_s$ — the superior calorific value, MJ/m$^3$; $\overline{\rho}$ — the relative gas density; $\rho_g$, $\rho_a$ — the gas density and air density, respectively, all other factors being equal, kg/m$^3$.

For the matter at hand, the following is important: the fact that the Wobbe index of other gases differs by not more than 5% means that the design and operating parameters of GBUs used for burning gases of this group do not require any changes and the unit heat rate will be preserved.

Natural gas of groups L and E is mainly supplied to Europe from Russia via gas trunk lines. According to the above requirements, the superior Wobbe index for group L gases shall be 39.1–44.8 MJ/m$^3$ (the volume is given for a temperature of 15°C and a pressure of 1013.25 mbar). Based on Eq. (1), the calorific value of such gas shall be 29.3–34.5 MJ/m$^3$. For group E, these limits are as follows: $W_s$ = 40.9–54.7 MJ/m$^3$; $H_s$ = 31.3–44.4 MJ/m$^3$.

However, according to the same standard (European Committee for Standardization, 2021), to ensure safe and efficient GBU operation, the unit shall be tested by burning not the gas of this group but so-called test gases, each of which, in terms of composition, is critical for certain equipment performance characteristics. Table 1 provides characteristics of test gases for group L and E gases.

Therefore, the Wobbe index is no longer the only interchangeability criterion. The equality of the Wobbe index for different gases is a necessary but not sufficient condition of their full interchangeability. **The purpose of this study** was to determine principles for the reliable standardization of combustible gas interchangeability parameters.

As for the **methods**, we chose a comparative critical analysis of regulatory documents and available experimental data as well as performed theoretical and experimental studies in this field.

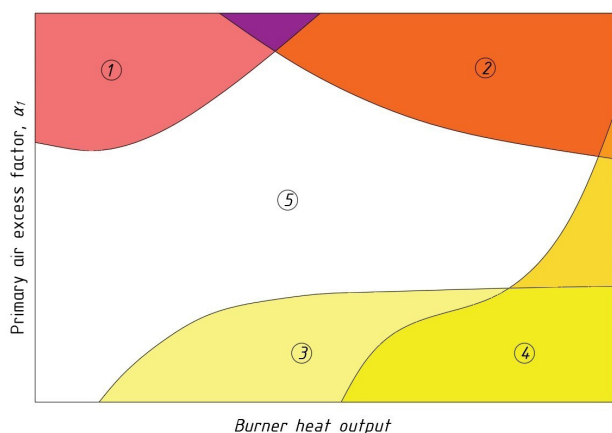

Fig. 1. Gas combustion diagram of the American Gas Association (AGA): 1 — the light back region, 2 — the flame lift region; 3 — the yellow tipping region, 4 — the incomplete combustion products region, 5 — the steady and efficient gas combustion region
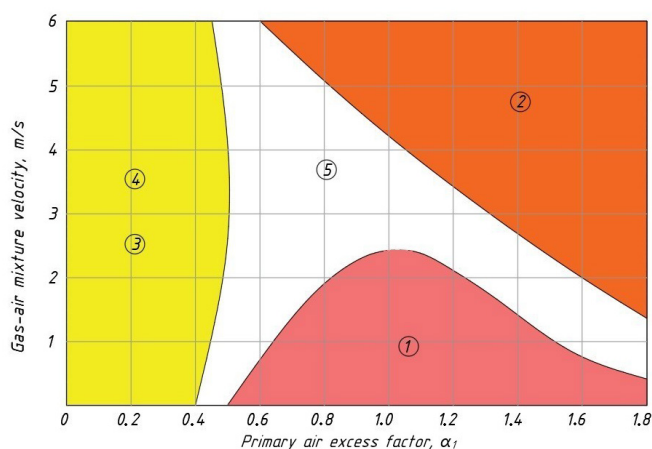


Fig. 2. Diagram of steady and efficient operation of an injection gas burner. The designations of the regions are the same as in Fig. 1

35

Table 1. Test gas characteristics

| Combustible gas | Test No., test gas composition and characteristics for the following critical equipment operation modes: | | |
|---|---|---|---|
| | Light back | Flame lift | Incomplete combustion and yellow tipping |
| Family 2, Group L | G25<br><br>$CH_4$ = 86 vol.%<br>$N_2$ = 14 vol.%<br>$W_s$ = 41.52 MJ/m³<br>$H_s$ = 32.49 MJ/m³ | G27<br><br>$CH_4$ = 82 vol.%<br>$N_2$ = 18 vol.%<br>$W_s$ = 39.06 MJ/m³<br>$H_s$ = 30.98 MJ/m³ | G26<br>$CH_4$ = 80 vol.%<br>$C_3H_8$ = 7 vol.%<br>$N_2$ = 13 vol.%<br>$W_s$ = 44.83 MJ/m³<br>$H_s$ = 36.91 MJ/m³ |
| Family 2, Group E | G222<br>$CH_4$ = 77 vol.%<br>$H_2$ = 23 vol.%<br>$W_s$ = 47.87 MJ/m³<br>$H_s$ = 31.86 MJ/m³ | G231<br>$CH_4$ = 85 vol.%<br>$N_2$ = 15 vol.%<br>$W_s$ = 40.90 MJ/m³<br>$H_s$ = 32.11 MJ/m³ | G21<br>$CH_4$ = 87 vol.%<br>$C_3H_8$ = 13 vol.%<br>$W_s$ = 54.76 MJ/m³<br>$H_s$ = 45.28 MJ/m³ |

**Results and discussion**
**1. Preliminary analysis**

As follows from Table 1, to check equipment for light back, test gas with a hydrogen content of **up to 23%** is used (G222 test gas). Such hydrogen content in a mixture with natural gas is already critical in terms of loss of flame stability. It is very important for the subsequent analysis.

It should be noted that State Standard GOST EN 437:2012 (Euro-Asian Council for Standardization, Metrology and Certification, 2012) did not become in Russia (as a natural gas exporter) the main document to determine gas quality and gas interchangeability criteria. When formulating gas quality requirements, the exporter uses State Standard GOST 5542-2014 (Interstate Council for Standardization, Metrology and Certification, 2015).

According to this document, the (superior) Wobbe index is the only indicator of gas interchangeability. Its value for natural gas shall be 41.2–54.5 MJ/m³

(at a temperature of 20°C) and permissible deviation **from the nominal value** shall not exceed ±5%. This ensures the constant heat rate of the unit upon combustible gas substitution. There are no other gas interchangeability requirements in this document. Besides, the concept of the "nominal value" is not explained in any way. In practice, it is usually the value established in a gas supply agreement. However, the range of possible Wobbe index values according to the GOST (41.2–54.5 MJ/m³) is no less than 32% relative to the lower limit for group E gases.

When the issue of interchangeability of natural gas and its mixture with hydrogen is analyzed more deeply, it should be noted that hydrogen and natural gas have drastically different characteristics. Table 2 compares the physical and chemical properties of methane (as the primary combustible component of natural gas) and hydrogen (Staskevich et al., 1990; Szkarowski, 2020).

Table 2. Some characteristics of methane and hydrogen ($t$ = 20°C)

| Combustion characteristic | Unit of measurement | $CH_4$ | $H_2$ |
|---|---|---|---|
| Superior calorific value $H_s$ | MJ/m³ | 39.82 | 12.75 |
| Superior Wobbe index $W_s$ | MJ/m³ | 53.55 | 48.47 |
| Inferior calorific value $H_i$ | MJ/m³ | 35.88 | 10.79 |
| Inferior Wobbe index $W_i$ | MJ/m³ | 48.22 | 41.02 |
| Flammability limits in a mixture with air:<br>lower limit $c_l$<br>upper limit $c_u$ | vol.% | 5.0<br>15.0 | 4.0<br>75 |
| Stoichiometric air volume for complete combustion | m³/m³(gas) | 9.52 | 2.38 |
| Maximum combustion temperature | °C | 2043 | 2235 |
| Stoichiometric volume of combustion products | m³/m³(gas) | 10.52 | 2.88 |
| Maximum flame speed | m/s | 0.37 | 2.67 |
| Air excess factor at the flammability limits:<br>at the lower limit<br>at the upper limit | – | 1.8<br>0.65 | 9.8<br>0.15 |
| Gas density | kg/m³ | 0.71 | 0.089 |

Evidently, the differences in the combustion characteristics of methane and hydrogen are drastic. The stoichiometric air volume for complete combustion, the volume of combustion products, and the upper flammability limit that guarantees combustion without light back differ by 4 times, and the flame speed — by 7 times. It is extremely important to compare the Wobbe index for methane and hydrogen. It differs almost by 10%, which means that it is impossible to convert burners to hydrogen use without changing their design.

This confirms the relevance of the matter related to the use of not pure hydrogen but its mixture with natural gas, which has already been noted in the introduction. Here, the issue of permissible hydrogen content in such a mixture, ensuring a seamless transition to a new type of gas fuel, is pivotal. We calculated the main characteristics of the mixture with various hydrogen content. The calculation data are given in Table 3 and Figs. 3–5.

Table 3. Some characteristics of the natural gas/hydrogen mixture ($t$ = 20°C)

| Characteristic | Unit of measurement | $H_2$ content in the mixture, vol.% | | |
|---|---|---|---|---|
| | | 10 | 30 | 50 |
| Density | kg/m³ | 0.65 | 0.53 | 0.40 |
| Superior calorific value $H_s$ | MJ/m³ | 37.10 | 28.36 | 23.33 |
| Superior Wobbe index $W_s$ | MJ/m³ | 52.18 | 49.58 | 47.08 |
| Difference in the superior Wobbe index for the mixture and natural gas ($W_s$ = 53.6 MJ/m³) | % | 2.6 | 7.5 | 12.2 |
| Inferior calorific value $H_i$ | MJ/m³ | 33.38 | 28.36 | 23.33 |
| Inferior Wobbe index $W_i$ | MJ/m³ | 46.95 | 44.37 | 41.81 |
| Difference in the inferior Wobbe index for the mixture and natural gas ($W_i$ = 48.22 MJ/m³) | % | 2.6 | 8.0 | 13.2 |
| Flammability limits in the mixture with air: lower limit upper limit | vol.% | 4.9 16.3 | 4.6 19.7 | 4.4 25.0 |
| Air excess factor at the flammability limits: at the lower limit at the upper limit | | 2.2 0.58 | 2.70 0.55 | 3.62 0.5 |
| Maximum mixture velocity at light back | m/s | 0.19 | 0.26 | 0.37 |
| Primary air excess factor at the boundary of yellow tipping | – | 0.21 | 0.19 | 0.17 |
| Stoichiometric air volume required for complete combustion | m³/m³(gas) | 8.8 | 7.4 | 5.9 |
| Volume of combustion products ($\alpha$ = 1.15) | m³/m³(gas) | 11.1 | 9.3 | 7.6 |
| Stoichiometric composition of combustion products: - water vapor $H_2O$ - nitrogen $N_2$ - oxygen $O_2$ - carbon dioxide $CO_2$ | vol.% | 17.1 72.3 2.5 8.1 | 18.2 71.8 2.4 7.5 | 19.8 71.2 2.4 6.6 |
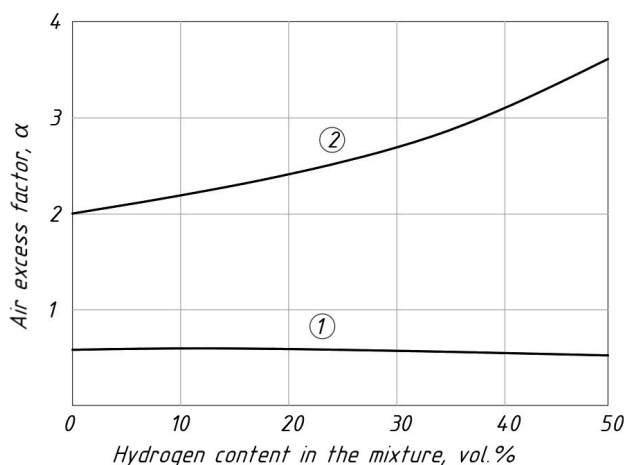


Fig. 3. Air excess factor at the lower (2)
and upper (1) flammability limits
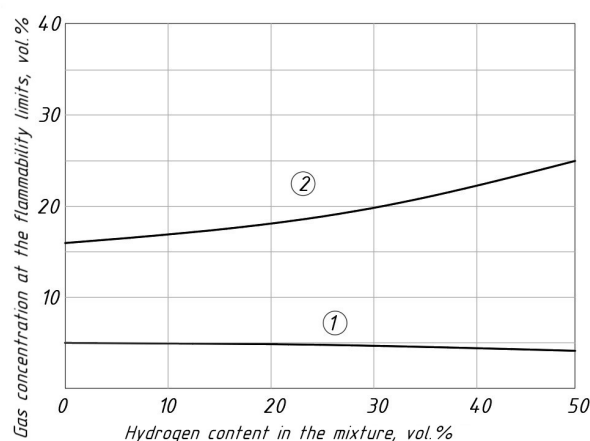


Fig. 4. Gas concentration at the lower (1)
and upper (2) flammability limits

Comparison by the Wobbe index has a principal meaning for the analysis. It is not accidental that the comparison was also made by the inferior index value. The superior index value uses the concept of the superior calorific value that can be achieved only at the condensation of water vapors forming during combustion, which is achievable in a limited group of condensing equipment. Moreover, it is fundamentally impossible in household gas stoves.

The comparison shows that the permissible Wobbe index variation (5%) for the natural gas/hydrogen mixture is not met already at a hydrogen content of 20%. Therefore, it is impossible to ensure a transition from natural gas to a combustible mixture with a hydrogen content of more than 20% without changing the burner design and operating parameters when trying to preserve the burner heat rate. As for forced-draught gas burners, changes in the design and operating parameters of the draught equipment would also be needed.

In a gas mixture, hydrogen expands the range between the lower and upper flammability limits. This increases the danger of light back. In terms of operation, a mixture with hydrogen becomes explosion hazardous in a wider range of concentrations.

The comparison indicates strongly that the conclusion about the possibility of using natural gas/hydrogen mixtures based on the Wobbe index alone is not sufficient. The issues of gas fuel utilization efficiency, environmental performance, and safety require analysis of a wider range of interchangeability indicators.

## 2. Analysis of interchangeability criteria

The issue of interchangeability of natural gas and its mixture with hydrogen was additionally studied with account for the requirements adopted in the international standard ISO 13686:2013 (International Organization for Standardization, 2013). A list of interchangeability indicators is given in Table 4. Each of them enables analysis of certain adverse effects that may occur at fuel substitution.

Table 4. Interchangeability methods and criteria according to ISO 13686:2013

| Method or index | Country | Controlled parameters |
| --- | --- | --- |
| Knoy factor | EU | Unit heat rate |
| Dutton's criteria | Great Britain, Australia | Flame lift<br>Yellow tipping<br>(sooting)<br>Complete combustion |
| Weaver method | USA | Complete combustion<br>Flame lift<br>Light back<br>Yellow tipping<br>Unit heat rate<br>Required air excess factor (blasting air consumption) |
| AGA method | USA | Flame lift<br>Light back<br>Yellow tipping |
| Delbourg method | France | Yellow tipping. Sooting |
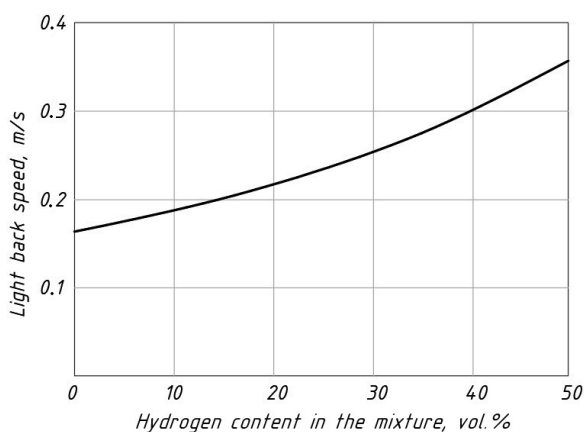


Fig. 5. Maximum gas/air mixture speed at the burner exit when light back is possible

### 2.1. Knoy factor

The $J_{(K)}$ factor is one of the early interchangeability indices and a variation of the Wobbe index (Briggs, 2014; Knoy, 1953):

$$J_{(K)} = \frac{H_s - 0.65 \cdot 10^7}{\sqrt{\bar{\rho}}},$$ (2)

where $H_s$ — the superior calorific value, J/m³; $\bar{\rho}$ – the relative gas density.

If the Knoy factor for the substitute gas differs by more than 5%, the gases are not interchangeable. The calculation data show that, in case of natural gas/hydrogen mixtures, it happens with a hydrogen content of more than 20%. With the hydrogen share in the mixture increasing, the unit heat rate will decrease. Therefore, in terms of the Knoy factor, gases with higher hydrogen content are not

interchangeable with natural gas.

### 2.2. Dutton's criteria

Dutton's criteria include the following (Dutton, 1984; Dutton and Wood, 1984; Lander, 2002): $J_{ICF(D)}$ — the incomplete combustion factor, $J_{LI(D)}$ — the lift index, $J_{SI(D)}$ — the soot index.

The **incomplete combustion factor** determines the probability of incomplete combustion products formation when the base gas is replaced with a substitute gas:

$$J_{ICF(D)} = \frac{W_i - 50.73 + 0.03E_{PN}}{1.56} - \frac{\Omega_{H_2}}{100}, \quad (3)$$

$W_i$ — the Wobbe index, MJ/m³;

$E_{PN}$ — the volume fraction of nitrogen and propane in the stoichiometric mixture, vol.%;

$\Omega_{H_2}$ — the volume fraction of hydrogen in the stoichiometric mixture, vol.%.

The Gas Safety Regulations effective in Great Britain require that the value of $J_{ICF(D)}$ be less than 0.48 to prevent incomplete gas combustion. The extreme value of this factor for a substitute gas shall not exceed 1.48. When gases with a higher factor are burned, incomplete combustion products will form and the unit efficiency factor will decrease.

Fig. 6 shows the results of calculations under Eq. (3) for natural gas mixtures with different $H_2$ content.

According to the calculation data, an increase in hydrogen content does not deteriorate the incomplete combustion factor and is not critical for the mixture, as it is accompanied by a decrease in the hydrocarbon concentration in the mixture. Therefore, in terms of the incomplete combustion factor, natural gas and its mixtures with hydrogen are interchangeable at any hydrogen content.

The **lift index** assesses the possibility of combustible gases interchangeability by the combustion stability criterion — the danger of flame lift and light back phenomena (International Gas Union, BP Gas Marketing Ltd., GL Industrial Services UK Ltd., 2011):

$$J_{LI(D)} = 3.25 - 2.41\arctan\left\{ \begin{array}{l} \left(0.122 + 0.0009\Omega_{H_2}\right) \cdot \\ \left[\left(W_i - 36.8 - 0.0019E_{PN}\right) + \\ \left(0.755 - 0.118E_{PN}^{0.33}\right)\Omega_{H_2}\right] \end{array} \right\}, \quad (4)$$

when $J_{LI(D)} = 0$, there is no visible detachment of the flame base from the burner ports in multi-flame burners. When $J_{LI(D)} = 6$, this means the complete detachment of 50–100% of the flames.

We also analyzed the shift of the index to the region of negative values, not referred to in the publication (International Gas, BP Gas Marketing Ltd., GL Industrial Services UK Ltd., 2011). This would mean the possibility of another critical phenomenon — flame lift with a range of adverse and hazardous consequences.

Fig. 7 shows the results of index calculations for natural gas/hydrogen mixtures under Eq. (4). Evidently, this indicator is not critical for natural gas/hydrogen mixtures within the whole range of hydrogen content under consideration. The deviation of the index value from zero is insignificant.

Dutton's **soot index** assesses the risk of transition from one type of gas to another in terms of danger related to pyrolytic processes of hydrocarbon degradation and formation of soot particles that color the flame yellow (International Gas, BP Gas Marketing Ltd., GL Industrial Services UK Ltd., 2011):

$$J_{SI(D)} = 0.896\arctan\left( \begin{array}{l} 0.0255E_{PN} - \\ 0.009\Omega_{H_2} + 0.617 \end{array} \right). \quad (5)$$

The limit value of this index is 0.6. A higher value of $J_{SI(D)}$ for a substitute gas means the danger of sooting and limited interchangeability.



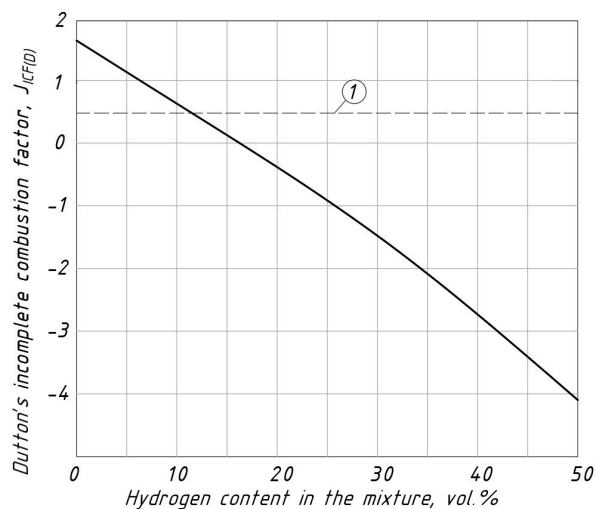Fig. 6. Dutton's incomplete combustion factor for a natural gas/ hydrogen mixture (1 — the normalized value of $J_{ICF(D)}$) = 0.48)
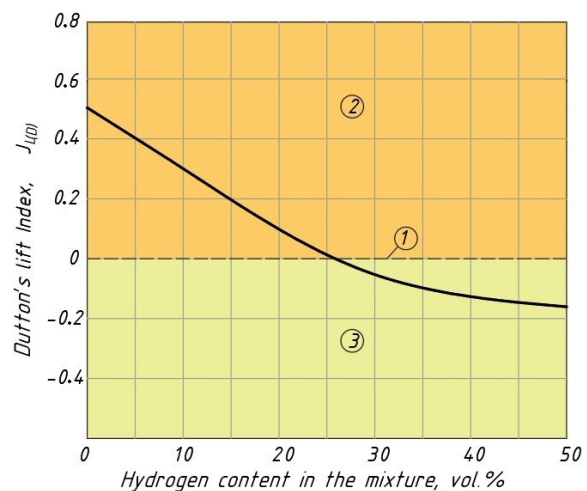


Fig. 7. Dutton's lift index for natural gas/hydrogen mixtures (1 — the limit value; 2 — the flame lift region; 3 — the light back region)

Fig. 8 shows the results of Dutton's soot index calculation for natural gas/hydrogen mixtures. They indicate that the introduction of hydrogen into the mixture does not lead to sooting. Therefore, in terms of this index, natural gas/hydrogen mixtures are interchangeable.

Therefore, according to Dutton's criteria, the substitution of natural gas with its mixture with hydrogen is impossible already at a hydrogen concentration of 20–25 vol.% due to light back and flame out.

### 2.3. Weaver method

This multi-index method was first published in 1946 and has been continuously revised and updated (American Gas Association, 2002; Weaver, 1951). The method assesses the possibility of gas interchangeability in a wider and complex context. It is based on dozens of thousands of experiments with 500 different gases (Ortíz, 2014). During these experiments, the possibility of low-pressure burners transition to another gas without loss of combustion stability and efficiency was studied.

The method aims to determine a set of gas and combustion process characteristics for the base gas and substitute gas as well as compare indicators with the required values. If the requirement is met, the gases are considered interchangeable by this criterion.

The first three indices have a limit of 1.0.

The **heat rate ratio** is the ratio between the Wobbe index for the substitute gas $W_{ss}$ and the Wobbe index for the adjustment gas $W_{sa}$:

$$J_{i\,(W)} = \frac{W_{ss}}{W_{sa}}. \qquad (6)$$

The condition $J_{H(W)}$ = 1.0 (±5%) is a condition of interchangeability of two gases (Ortíz, 2014). A
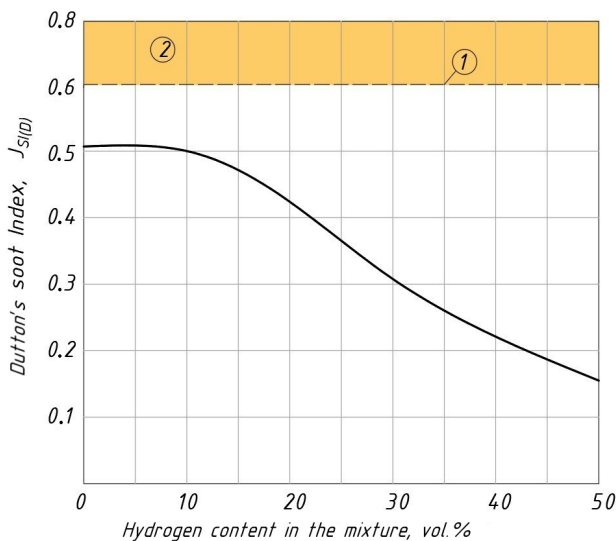
Fig. 8. Dutton's soot index for natural gas/hydrogen mixtures (1 — the limit value; 2 — the sooting region)

higher deviation is considered impermissible by the conditions of changes in the heat rate. Besides, this makes for incomplete combustion, increase in heat losses, efficiency reduction, and loss of combustion stability. Evidently, this condition has been preserved in the majority of the effective standards.

The **primary air ratio** includes theoretical required air for combustion of the adjustment gas $V_{ta}$ and substitute gas $V_{ts}$, and their relative density, $\overline{\rho}_a$ and $\overline{\rho}_s$, respectively:

$$J_{A(W)} = \frac{V_{ts}\sqrt{\overline{\rho}_a}}{V_{ta}\sqrt{\overline{\rho}_s}}. \qquad (7)$$

The value of 0.95 < $J_{A(W)}$ < 1.05 is a condition of seamless transition of burners to another gas (Ferguson, 2007). An increase in the upper limit means air shortage, which leads to incomplete combustion, increased emissions of harmful substances, and reduced efficiency of the unit. When the value is less than 0.95, air excess is too high and danger of flame lift occurs, heat losses with exhaust gases increase, the efficiency of the unit decreases, and emissions of toxic nitrogen oxides grow.

The **lifting index** includes the flame speed for the adjustment gas $S_a$ and substitute gas $S_s$, as well as the volume fraction of oxygen in them, $\Omega_{O_2a}$ and $\Omega_{O_2s}$, respectively (Ferguson, 2007):

$$J_{L(W)} = J_{A(W)}\frac{S_s}{S_a}\frac{100-\Omega_{O_2s}}{100-\Omega_{O_2a}}. \qquad (8)$$

Substitute gases with a value of $J_{L(W)}$ more than 1 are prone to flame lift.

The next three indices are compared by the zero value.

The **flash back index** is calculated by the equation below using the characteristics described above:

$$J_{F(W)} = \frac{S_s}{S_a} - 1.4J_{A(W)} + 0.4. \qquad (9)$$

If $J_{F(W)}$ > 0 for the substitute gas, unit operation can be accompanied by light (flash) back, which causes the danger of an emergency (Lander, 2002).

The **yellow tipping index** is calculated using the total content of hydrogen atoms in a molecule of the adjustment gas and substitute gas, $N_{Ca}$ and $N_{Cs}$, respectively (Halchuk-Harrington and Wilson, 2006):

$$J_{Y(W)} = J_{A(W)} + \frac{N_{Cs} - N_{Ca}}{110} - 1. \qquad (10)$$

If $J_{Y(W)}$ > 0 for the substitute gas, it means the possibility of local air shortage, yellow tipping and subsequent sooting.

The **incomplete combustion index** is calculated using the ratio of the number of hydrogen and carbon atoms in molecules of the compared gases, $R_{H/Ca}$ and $R_{H/Cs}$, respectively (Halchuk-Harrington and Wilson, 2006):

$$J_{I(W)} = J_{A(W)} - 0{,}366\frac{R_{H/Cs}}{R_{H/C\alpha}} - 0.634. \qquad (11)$$

If the calculated data for the substitute gas show that $J_{I(W)} > 0$, it means that gas combustion will be accompanied by incomplete combustion and, therefore, reduced unit efficiency and increased

emissions of harmful substances. Evidently, this phenomenon can occur both due to a shortage of air for combustion and an increase in the hydrogen content in the substitute gas.

Table 5 shows the results of indices calculations for a natural gas/hydrogen mixture.

Table 5. Comparison of interchangeability indices for natural gas and its mixtures with hydrogen according to the Weaver method

| Interchangeability index | Designation | Nominal value (requirement) | Hydrogen concentration in a mixture with natural gas, vol.% | | | |
|---|---|---|---|---|---|---|
| | | | 0 | 10 | 30 | 50 |
| Heat rate ratio | $J_{H(W)}$ | 1 (±5%) | 1.0 | 0.95 | 0.92 | 0.87 |
| Primary air ratio | $J_{A(W)}$ | 1 (±5%) | 1.0 | 0.96 | 0.90 | 0.83 |
| Lifting index | $J_{L(W)}$ | 1 (±5%) | 1.0 | 1.12 | 1.44 | 1.83 |
| Flash back index | $J_{F(W)}$ | ≤ 0.0 | 0.0 | 0.22 | 0.73 | 1.46 |
| Yellow tipping index | $J_{Y(W)}$ | ≤ 0.0 | 0.0 | −0.04 | −0.01 | −0.18 |
| Incomplete combustion index | $J_{I(W)}$ | ≤ 0.0 | 0.0 | −1.2 | −1.5 | −1.9 |

The analysis using the Weaver interchangeability method makes it possible to draw the following conclusions concerning the **transition from natural gas to natural gas/hydrogen mixtures** in commercial and domestic gas units. The first four indices give a negative result:

– **in terms of the heat rate ratio**, interchangeability is not achieved when the hydrogen content in the mixture is more than 10 vol.%;

– **in terms of the primary air ratio**, combustion of mixtures, in any case, occurs with increased air excess factors, which will be accompanied by the reduced unit efficiency and danger of flame lift (especially when the hydrogen content in the mixture is more than 20 vol.%);

– **in terms of the lifting index**, any hydrogen content increases the probability of this adverse effect;

– **in terms of the flash back index**, any hydrogen content is also accompanied by the danger of an adverse effect on burners.

It should be noted that the lifting and flash back indices, which are the most negative, were obtained for burners with partial preliminary mixing of gas with air, i.e., for injection burners. Therefore, e.g., for household gas stoves, the result of the analysis using the Weaver method is actually critical. It means that the transition of gas burners from natural gas to natural gas/hydrogen mixtures shall be accompanied by changes in the design of burners, forced-draught equipment, and combustion stabilization devices, as well as changes in burner operation.

As for forced-draught gas burners, flame lift and light back phenomena are not typical for them. The same goes for modern low-power gas boilers with additional flame stabilization, e.g., grid stabilization.

The last two Weaver interchangeability criteria, i.e., the **incomplete combustion index** and the

**yellow tipping index**, show that any hydrogen content in a mixture with natural gas does not lead to any phenomena that would deteriorate the combustion process or unit safety.

**3. Analysis of interchangeability by heat transfer conditions**

All existing interchangeability criteria are related directly to gas burners. However, there is another interchangeability issue that has not been studied yet. It is changes in the nature of heat transfer in boiler furnaces and industrial furnaces during the transition to substitute gases with hydrogen content.

The volume and composition of combustion products change if there is hydrogen in the mixture (Table 3). When the hydrogen content is 30%, the combustion products volume decreases from 11.95 to 7.59 m³/m³ with a simultaneous decrease in the content of $CO_2$ in their composition. Both these factors deteriorate heat transfer in the furnaces of thermal generating units. The first one — due to the reduced rate of combustion products, and the second one — due to the reduced intensity of the radiation heat transfer component.

We studied the combustion of refinery gas with hydrogen content, and the results of the studies indicate that the combustion of gases with a hydrogen content of more than 20% significantly reduces flame radiation and the intensity of convection heat transfer on heating surfaces.

Fig. 9 presents changes in the relative amount of heat received by the water walls of a boiler depending on the hydrogen content in the mixture. Reduction of the radiation heat transfer component in the furnace transfers its significant amount to a less efficient convective section of the boiler. This inevitably increases the temperature of exhaust gases and reduces boiler efficiency.
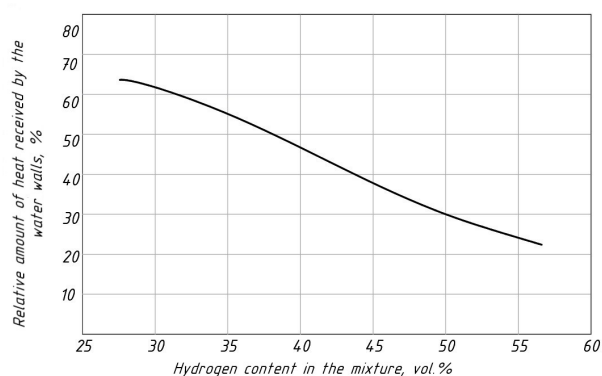
Fig. 9. Impact of the gas composition
on heat emission in a furnace

The reason for such a situation is changes in the above ratio of the carbon and hydrogen content in the elemental gas composition, C/H (Mochan et al., 1998). A shift in the C/H ratio to a higher hydrogen fraction reduces the so-called flame "luminosity", i.e., reduces the yellow (carbon) spectrum component and, therefore, the furnace emissivity.

It should also be noted that the reduction in the stability of injection gas burners operation was confirmed during the studies. With a significant hydrogen content, uncontrolled light back was often observed. It requires immediate intervention of equipment operators in order to avoid an emergency.

Therefore, the use of substitute gases in the form of natural gas/hydrogen mixtures requires an adjustment of the existing method of thermal and aerodynamic analysis of boilers and other heat recovery equipment.

**Conclusions**

1. The use of natural gas/hydrogen mixtures, including in the domestic sector, is an effective intermediate step in the decarbonization of human activities. This decision makes it possible to ensure the proportionate reduction of $CO_2$ emissions without changes in the design of gas burners and gas equipment. The main issue in such a transition is permissible hydrogen content in the mixture that would not change the parameters of gas fuel utilization efficiency, environmental performance, and safety.

2. Numerous gas interchangeability criteria are used in different countries. It should be noted that all of them were derived for specific test conditions that are not necessarily applicable to current conditions.

For example, the well-known Weaver criteria were derived for the test gas with a superior calorific value of 800 BTU/ft^{3} (approx. 29.8 MJ/m^{3}). Suffice it to say that group E natural gas is characterized by a value of this parameter of more than 1000 BTU/ft^{3}. Besides, tests are always conducted using certain burners. However, burners of the same type (e.g., injection burners) can have a variety of differences, which leads to different light back and flame lift indicators. The same can be observed in seemingly identical devices. The design accuracy of nozzles and burner ports, their depth and angle, differences in the distance between them — all of this matters. Even slight differences in the material of the device can result in a catalytic or, on the contrary, inhibiting effect on the combustion process.

3. The above requires very careful and responsible application of the interchangeability criteria on a case-by-case basis. Based on the analysis and studies performed, it is safe to say that the use of a natural gas/hydrogen mixture with a hydrogen content of 10 vol.% is permissible for injection burners of household gas stoves and low-power equipment without changes in their design and operation. In a number of cases, a higher hydrogen content (up to 15–20 vol.%) is possible, which, however, requires additional testing.

4. The forced-draught burners of industrial and heating boilers are not prone to light back and flame lift due to the nature of combustion organization. In this case, it is possible to recommend the safe operation of devices using a mixture with a hydrogen content of up to 20–25 vol.%. The same goes for low-power boilers with modern methods of combustion stabilization. However, we should consider accompanying heat rate reduction (up to 15–20%) and assess in advance the technical capability of this phenomenon compensation, e.g., by increasing fuel consumption.

5. The studies performed also allowed us to establish a significant negative impact of adding hydrogen to the mixture on the radiation characteristics of the flame. This should be taken into account (along with heat rate reduction) in heating equipment where radiation heat transfer in the furnace is an important technological component. They, first of all, include boiler units with water-walled furnaces.

## References

American Gas Association (2002). *Interchangeability of other fuel gases with natural gas. Research Bulletin 36. AGA XH0203*. AGA, 86 p.

Briggs, T. (2014). The combustion and interchangeability of natural gas on domestic burners. *Industrial Engineering Letters*, Vol. 4, No. 3, pp. 67–87.

Delbourg, P. and Lafon, J. (1971). *Interchangeabilité des gaz*. Paris: Association technique de l'industrie du gaz en France, 200 p.

Dutton, B. C. (1984). A new dimension to gas interchangeability. communication 1246. *The Institute of Gas Engineers, 50th Autumn Meeting*.

Dutton, B. C. and Wood, S. W. (1984). Gas interchangeability: prediction of soot deposition on domestic gas appliances with aerated burners. *Journal of the Institute of Energy*, September 1984, p. 381.

Euro-Asian Council for Standardization, Metrology and Certification (2012). EN 437: 2012. Test gases. Test pressures. Appliance categories. Minsk: Euro-Asian Council for Standardization, Metrology and Certification, 40 p.

European Commission (2020). *Communication from the Commission to the European Parliament, the Council, the European Economic and Social Committee, and the Committee of the Regions. A hydrogen strategy for a climate-neutral Europe*. Brussels: European Commission, 23 p.

European Committee for Standardization (2021). *BS EN 437:2021. Test gases — Test pressures — Appliance categories*. Brussels: European Committee for Standardization.

Ferguson, D.H. (2007). Fuel interchangeability considerations for gas turbine combustion. *Fall 2007 Eastern States Section Meeting of the Combustion Institute, October 21–24, 2007, Charlottesville, VA*.

Flórez-Orrego, D. A. (2011). *Métodos para el estudio de la intercambiabilidad de una mezcla de Gas Natural y Gas Natural-Syngas en quemadores de premezcla de régimen laminar:* Un artículo de revisión, 34 p. DOI: 10.13140/RG.2.2.32284.03202.

Gilbert, M. G. and Prigg, J. A. (1956). *The prediction of the combustion characteristics of town gas. Vol. 35 of Research Communication*. London: Gas Council, 47 p.

Government of the Russian Federation (2020). *Order No. 2634-r dated October 12, 2021.* [online] Official website for legal information. Available at: http://publication.pravo.gov.ru/Document/View/0001202010220027 [Date accessed December 20, 2020].

Grib, N. (2019). Hydrogen economy: myths and reality. *Oil and Gas Vertical*, No. 19. pp. 61–69.

Halchuk-Harrington, R. and Wilson R. D. (2006). AGA bulletin #36 and weaver interchangeability methods: yesterday's research and today's challenges. In: *Operating Section Proceedings*, May 2–4, 2006, Boston, MA, USA. Washington, DC: American Gas Association (AGA), pp. 802–823.

Honus, S., Kumagai, Sh. and Yoshioka, T. (2016). Replacing conventional fuels in USA, Europe, and UK with plastic pyrolysis gases – Part II: Multi-index interchangeability methods. *Energy Conversion and Management*, Vol. 126, pp. 1128–1145. DOI: 10.1016/j.enconman.2016.08.054.

International Gas Union, BP Gas Marketing Ltd., GL Industrial Services UK Ltd. (2011). *Guidebook to gas interchangeability and gas quality*, 155 p.

International Organization for Standardization (2013). *ISO 13686:2013. Natural gas — Quality designation*. Geneva: ISO, 48 p.

Interstate Council for Standardization, Metrology and Certification (2015). *State Standard GOST 5542-2014. Natural fuel gases for commercial and domestic use. Specifications*. Moscow: Standartinform, 9 p.

Jones, H. R. N. (2005). *The application of combustion principles to domestic gas burner design*. London, New York: Taylor & Francis, 205 p.

Knoy, F. (1941). Combustion experiments with liquefied petroleum gases. *Gas*, Vol. 17, pp. 14–19.

Knoy, M. F. (1953). Graphic approach to the problem of interchangeability. *A.G.A. Proceedings*, pp. 938–947.

Kolienko, V. and Kolienko, A. (2011). Generation and use of synthesis gas from low grade types of fuel. *Rocznik Ochrona Środowiska*, Vol. 13, pp. 471–483.

Konoplyanik, A. (2020). *Decarbonising European gas: a new EU-Russia partnership?* [online] Natural Gas World. Available at: https://www.naturalgasworld.com/gas-decarbonisation-in-europe-80282 [Date accessed July 7, 2020].

Lander, D. (2002). UK situation regarding gas quality. Presentation to Marcogaz Gas Quality WG, June 28, 2002.

Mochan, S. I, Abryutin, A. A., Kagan, G. M. and Nazarenko, V. S. (eds.) (1998). *Thermal design of boilers (standard method).* 3rd edition. Saint Petersburg: RAO UES, All-Russia Thermal Engineering Institute, I. I. Polzunov Scientific and

Development Association on the Research and Design of Power Equipment, 258 p.

Ortíz, J. M. (2014). Fundamentos de la intercambiabilidad del gas natural. *Met&Flu,* No. 9*, pp. 6–15.*

RBC (2021a). *Japanese Ambassador speaks about interest in cooperation with Russia on hydrogen.* [online] Available at: https://www.rbc.ru/politics/27/12/2021/61bb348b9a794712c3360e0e?from=from_main_10 [Date accessed December 27, 2021].

RBC (2021b). *Manturov announces the term of creation of hydrogen turbines in Russia.* [online] Available at: https://www.rbc.ru/rbcfreenews/61ae161f9a794767a3285327 [Date accessed December 6, 2021].

RBC (2021c). *Trutnev invites Korean investors to the Kurils*. [online] Available at: https://www.rbc.ru/rbcfreenews/61a-fad469a7947fd75dcf0bf [Date accessed December 07, 2021].

Staskevich, N. L., Severinets, G. N. and Vidgorchik, D. Ya. (1990). *Handbook on gas supply and use.* Leningrad: Nedra, 762 p.

Szkarowski, A. (2020). *Paliwa gazowe. Podstawy efektywnego i ekologicznego wykorzystania*. Warsaw: Wydawnictwo Naukowe PWN SA, 152 p.

Weaver, E. R. (1951). Formulas and graphs for representing the interchangeability of fuel gases. *Journal of Research of the National Bureau of Standards*, Vol. 46, No. 3, pp. 213–245.

# ВЗАИМОЗАМЕНЯЕМОСТЬ И НОРМИРОВАНИЕ ПАРАМЕТРОВ ГОРЮЧИХ ГАЗОВ ПРИ ИСПОЛЬЗОВАНИИ ВОДОРОДА

Александр Леонидович Шкаровский[1,2]*, Анатолий Григорьевич Колиенко[3], Виталий Сергеевич Турченко[3]

[1]Санкт-Петербургский государственный архитектурно-строительный университет
2-ая Красноармейская ул., 4, Санкт-Петербург, Россия
[2]Кошалинский Технологический университет,
ул. Снядецких, 2, Кошалин, Польша
[3]Национальный университет «Полтавская политехника имени Юрия Кондратюка»
Першотравневий проспект, 24, Полтава, Украина

*E-mail: szkarowski@mail.ru

**Аннотация**
В статье представлены результаты исследований, **целью которых является** обоснование возможности постепенного перехода на сжигание водорода в газоснабжении коммунально-бытовых и промышленных потребителей без необходимости изменения конструкции горелок и режима их работы. Для этого комплексно **рассмотрены задачи** определения показателей взаимозаменяемости природного газа и его смесей с водородом. Исследованы основные характеристики горючего газа при различном содержании водорода в смеси. Определено влияние содержания водорода на показатели тепловой мощности, выход вредных веществ, а также явления проскока и отрыва пламени. Проанализированы известные критерии взаимозаменяемости и их применимость в рассматриваемой задаче использования смесей природного газа с водородом. Впервые рассмотрено влияние содержания водорода на показатели лучистого теплообмена в топках газоиспользующего оборудования. **В основу методологии работы** положен критический анализ имеющихся литературных данных по вопросу взаимозаменяемости горючих газов, а также собственные теоретические и экспериментальные исследования. **Получены зависимости,** которые дают возможность определить возможность перевода имеющегося газового оборудования на сжигание смесей природного газа с водородом. **Разработаны рекомендации** по допустимому содержанию водорода в смеси с природным газом, обеспечивающим эффективное, безопасное и экологичное использование такого топлива в бытовых и промышленно-отопительных устройствах. **Научные и практические результаты работы** дают возможность осуществить малозатратную частичную и постепенную декарбонизацию в области использования газового топлива в качестве промежуточного этапа при переходе к более широкому сжиганию водорода.

**Ключевые слова**
Газоснабжение, декарбонизация, природный газ, водород, смеси, взаимозаменяемость, допустимое содержание.

# METHOD OF CALCULATION FOR WALLS OF VERTICAL SQUARED TIMBER

Olga Tretiakova[1,2]

[1]Perm National Research Polytechnic University
Komsomolsky prospekt, 29, Perm, Russia
[2]Perm State Agro-Technological University named after Academician D.N. Pryanishnikov
Petropavlovskaia St., 23, Perm, Russia

E-mail: olga_wsw@mail.ru

**Abstract**

**Introduction:** In recent years, houses out of vertical squared timber have become widespread. Vertical bars make it possible to use the effective wood behavior in compression and ensure maximum strength of the material along the fibers. Vertical bars are subject to compression with bending, which can result in loss of strength and buckling in building structures. In the available research papers and technical literature, the issue of the stress-strain state of such walls has not been analyzed. **The purpose of this study** was to formulate a calculation method for walls out of vertical squared timber, based on the available traditional approaches to wooden structures. We propose a calculation **method** for walls out of vertical squared timber as a set of elements resisting compression with bending, including a check for limiting slenderness. **Results:** Permissible heights of walls for buildings with bays of 10 and 12 m were obtained. The results can be used in the design of low-rise residential and public buildings, mansard superstructures of multi-story buildings.

**Keywords**

Vertical squared timber, stress-strain state, compression, bending.

## Introduction

Wood is becoming increasingly widespread in construction due to its positive mechanical and physical properties (Mayo, 2015; Zmijewki and Wojtowicz-Jankowska, 2017). They include low density, low thermal conductivity, low coefficient of linear expansion, and biological compatibility with humans. In addition, wooden structures are characterized by high acoustic performance and architectural expression. Nowadays, much attention is paid to resource-saving and environmentally friendly materials that have a minimal environmental impact. Whole-section timber meets these requirements in full (Müller et al., 2021; Skullestad et al., 2016). According to the results of studies on wood materials, solid wood has the least impact on the human habitat (Cabral and Blanchet, 2021; Dias et al., 2020). It is no doubt that wooden houses are energy-efficient. Wood, as a structural material, has been scrutinized by researchers, housebuilders, and building users.

Design concepts of wooden buildings and structures come in a great variety. Recent studies show that a significant share of wooden houses is built out of solid, whole-section timber (Cohen and Gaston, 2003; Janakieska et al., 2021). Comprehensive design systems for such houses are being developed (Chaggaris et al., 2021). They include tests for strength, serviceability, fire safety, and cost.

Modern researchers and practitioners discuss various options of wall structures made out of solid wood. The method of connection plays a significant role in the operation of wooden walls.

Resch (1999) as well as Piao and Shupe (2016) suggested using composite vertical elements out of small-diameter timber (3.6–12.8 cm). Each element consists of several bars joined with tenons and glue.

Tsai and Wonodihardjo (2018) described a method of house construction out of waste wood using nails and screws as connectors. Bedon and Fragiacomo (2019) conducted a numerical analysis of timber-to-timber joints with inclined self-tapping screws. The studies showed that the strength properties of walls made out of composite members with metal fittings are lower than those of walls made out of whole-section members.

Sandhaas (2016) developed wooden walls out of laminated elements consisting of lamellae arranged side-by-side and connected with dowels. The wall structure is built without the use of glue. Miyata (2020) noted sufficient stiffness characteristics of such walls. However, walls made out of laminated elements have shear strains exceeding those in walls made out of whole-section timber.

Schiro et al. (2018) conducted experimental studies on timber-to-timber screw-connections. Iraola et al. showed that, in connections of timber elements, made with metal fittings, the geometry of the contact

area has a substantial significance.

The elements of wooden walls are connected not only with metal but also with wooden fasteners. Thermo-mechanically compressed wood dowels were suggested as a joint element as an alternative to glue and metal fasteners (El Houjeyri et al., 2021).

Structures out of solid wood with contact joints are of interest. Wooden wall elements with dovetail contact joints are manufactured by means of digital milling (Cokcan et al., 2016). Squared and round timber processed using CNC machines (Bucklin et al., 2021; Colella, 2020) are used for walls of arbitrary curvilinear shapes. Digitally produced mortise and tenon joints are currently under investigation (Gamerro et al., 2020). Such inventions are not yet widely used in wooden buildings due to the complexity of the manufacturing process and the low number of wooden buildings of curvilinear configurations.

The efficiency of mortise and tenon joints largely depends on the quality of squared timber milling. Violations of the manufacturing procedure lead to gaps and the weakening of structures (He et al., 2021). Theoretical and experimental studies on such joints were conducted (Feio et al., 2014; Yu et al., 2021). New timber processing techniques (Pinkowski et al., 2019) and milling methods (Starikov et al., 2020) were implemented.

The tenon joint performance also depends on the wood species and strength. Lara-Bocanegra et al. (2020) pointed out that by choosing the material properly, it is possible to ensure the high strength of items with tenon joints.

Therefore, the subject of this paper, addressing walls out of solid wood, is highly relevant and under debate.

Based on the cited studies, it should be noted that shear strains of walls out of laminated and composite members with metal fittings exceed those of walls out of whole-section timber. Therefore, in a number of cases, composite timber members with metal fittings are characterized by lower strength than whole-section timber elements with timber-to-timber contact joints. Joints with metal fittings are less practical to manufacture than timber mortise and tenon joints. Therefore, based on the performed studies, it is possible to consider contact tenon joints of wooden members to be the most efficient. Besides, contact joints are less sensitive to changes in temperature and humidity in the room since they allow for some freedom of strains in wooden members. To be used in practice, items shall be easy to manufacture. Pavlenin and Shutova (2020) as well as other researchers noted that the Naturi technology meets the above parameters in many respects.

This paper addresses wall structures for low-rise houses, made out of vertical squared timber using the Naturi technology.

Houses built out of vertical squared timber using the Naturi technology are gaining popularity in modern low-rise construction since the technology provides positive structural and operational performance of walls. Such a solution makes it possible to use the type of wood compression along fibers advantageous for wood, and reduce settlement of walls while they are in use as compared to walls made out of horizontal squared timber. Walls are made out of whole-section timber without the use of metal fittings and glue. This simplifies the manufacturing process and makes it possible to avoid the influence of the ductility of joints. Besides, the use of whole-section timber rules out the delamination of items along the glue lines.

The history of construction out of vertical squared timber started as early as in the 20th century. We are aware of historic buildings where walls were made of squared and round timber installed vertically. However, such a structure has a disadvantage, which was noted by Russian architect Krasovsky (2002): gaps between the bars, occurring during operation.

Austrian researcher Georg Ganaus (2009) patented the Naturi technology for the construction of houses out of vertical squared timber. Based on this technology, squared timber is milled and drilled to make cutouts to connect the bars with each other. Thus, it is possible to avoid open gaps between the bars in the wall structure. Afterward, this technology was improved by Ganaus together with Russian experts Lazarev, Stepanishchev, and Yelchugin (Ganaus et al., 2018).

The growing interest in structures out of vertical squared timber results in the design of not only residential but also public buildings, including for rural infrastructure. Public buildings have increased bays and floor height in comparison to residential buildings. As a result, the load on the walls and their effective length increase. For practical design, data on strength and stability of walls out of vertical squared timber for various building bays as well as thermal characteristics are required.

To this date, a number of studies on such walls have been performed. Höckner (2019) specified their positive thermal properties.

Among studies on the stress-strain state of wooden walls and methods of their analysis, papers addressing wall panels out of solid wood can be distinguished. Researchers studied the static structural behavior of CLT (cross laminated timber) (Meloni et al., 2018) and DLT (dowel laminated timber) panels (Miyata, 2020). Meloni et al. (2018) used the finite element method to analyze the shear strains of CLT wall panels (Meloni et al., 2018). Thiel and Schickhofer (2010) described software to determine the bending stresses and deformations of CLT panels for two limit states and a number of design situations.

Miyata et al. (2018) considered a numerical analysis model of walls with pillars stacked with nails or screws. The strength of the walls was estimated by

the performance of nail or screw joints.

Inayama et al. (2011) proposed a calculation method for rigidity and ultimate strength of inserted wooden siding walls.

Despite many studies, the issues of the stress-strain state of walls out of vertical squared timber with contact joints have not been covered in contemporary technical and academic literature.

The given finite-element models are a convenient tool for the analysis of wooden wall structures since they make it possible to determine a number of options with minimal labor input. It is needless to say that numerical methods are needed for practical calculations. However, there were cases when the elastic response of wood was overestimated in numerical calculations (Iraola et al., 2021). It is a good practice to compare a numerical method with an analytical model.

The purpose of this paper was to formulate an analytical calculation method for walls out of vertical squared timber, made using the Naturi technology based on the available traditional common methods for the analysis of wooden structures. To achieve the purpose, we needed to address the following tasks: to study the wall behavior in compression with bending under the action of the wind load along and across the building; to study the wall buckling strain.

**Methods**

According to the Naturi technology, a wall of a building is made out of vertical milled bars. Such connections do not ensure a monolithic structure but develop composite action due to contact tenon joints. This paper proposes a calculation method for a wall made out of vertical squared timber as a set of conventional posts with wooden joints (hereinafter — conventional posts). Each conventional post consists of two bars connected with mortise and tenon joints and using wooden dowels. A diagram of the post section is given in Fig. 1.

In a general case, vertical and horizontal loads act on a building. Horizontal loads include the action of wind. We evaluated the static structural behavior of conventional posts for two design cases: under the action of wind along and across the building. In terms of the stress-strain state, we analyzed the behavior of conventional posts in compression with bending and buckling strain.

*Calculation for compression with bending*

*Design case: under the action of the wind load across the building*

We considered a wooden wall of a building, made out of vertical squared timber and represented as a set of conventional posts consisting of two bars (Fig. 1). It is accepted that the wind load across the building is distributed between individual conventional posts of the longitudinal wall, as shown in Fig. 2a. The calculation for a wall under the action of the wind load across the building comes down to the calculation for a conventional post in compression with bending.

The calculation was based on a deformation scheme for the combined action of three factors: the longitudinal force of vertical loads, the bending moment from the wind load, and the additional moment from the longitudinal force applied to the deformed post bent due to the moment.

The edge compressive stresses were checked and compared to the design compressive strength of wood along the fibers by Eq. (1).

$$\frac{N}{F_{calc}} + \frac{M_d}{W_{calc}} < R_c, \qquad (1)$$

where $N$ — the longitudinal force;

$M_d$ — the bending moment determined using the deformation scheme;

$R_c$ — the design compressive strength of wood along the fibers.

$$M_d = \frac{M}{\xi}, \qquad (2)$$

where $\xi$ — the coefficient that takes into account the action of the longitudinal force applied to the deformed element.

$$\xi = 1 - \frac{N}{\phi R_c F_{gross}}, \qquad (3)$$

where $\varphi$ — the buckling coefficient.
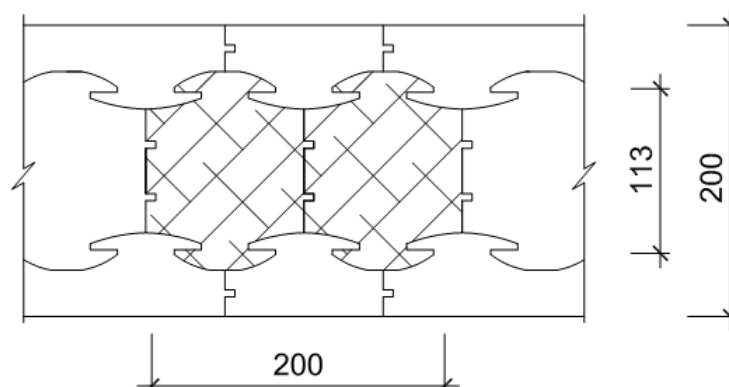


Fig. 1. A diagram of the conventional post section in a wall fragment
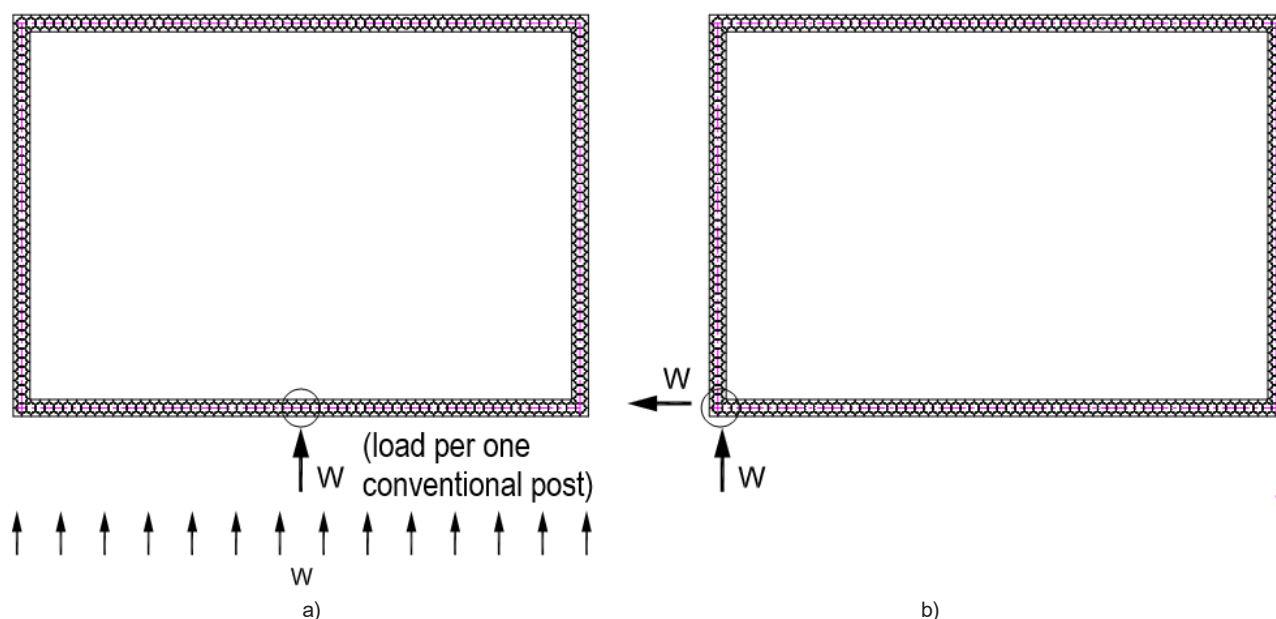
Fig. 2. A diagram of the wind load across the building: a) acting on a conventional post in a row;
b) acting on a conventional post in a corner

$$\phi = \frac{3000}{\lambda^2}, \qquad (4)$$

where $\lambda$ — the element slenderness.

The plane strain buckling, if necessary, can be checked using Eq. (5).

$$\frac{N}{\phi \, R_c F_{gross}} + \left(\frac{M_d}{\phi_f \, R_b W_{gross}}\right)^n < 1, \qquad (5)$$

where $\varphi_f$ — the buckling stability coefficient;

$n$ — the power exponent characterizing the restraint of the strained edge of the element out of the strain plane;

$R_b$ — the design bending strength.

As an example, we performed calculations for a wall out of vertical squared timber. The wall thickness was 20.0 cm with account for the finishing layer of wood. The calculations were performed for a wall element — a conventional post with a design section of 20.0 x 11.3 cm ($h$) shown in Fig. 1. Weakening in the design section was taken into account approximately with the 0.8 coefficient to the sectional area and the section modulus. In the calculations, we used permanent and temporary loads from two stories and roofing as well as the wind load across the building for the first wind area, as shown in Fig. 2a. The section slenderness of the post out of the longitudinal wall plane was adopted equal to the slenderness of an individual branch, i.e., an individual bar. Table 1 shows the obtained indicators for the behavior of a conventional post. The plane strain buckling was not checked due to low values of normal stresses.

Table 1. Geometric parameters, forces, and stresses in conventional posts under
the action of wind across the building

| Wall height, m | Building bay, m | Slenderness of a conventional post (branch) | Buckling coefficient | Bending moment (Eq. (2)), kN·m | Longitudinal force, kN | Normal stresses check, (Eq. (1)), kN/cm² |
|---|---|---|---|---|---|---|
| 3 | 10 | 91.55 < 120* | 0.358 | 0.37 | 11.59 | 0.18 < 1.38** |
| | 12 | 91.55 < 120* | 0.358 | 0.38 | 13.85 | 0.19 < 1.38** |
| 3.5 | 10 | 106.8 < 120* | 0.26 | 0.53 | 11.65 | 0.22 < 1.38** |
| | 12 | 106.8 < 120* | 0.26 | 0.56 | 13.91 | 0.24 < 1.38** |
| 4 | 10 | 122 > 120* | 0.2 | 0.72 | 11.72 | 0.26 < 1.38** |
| | 12 | 122 > 120* | 0.2 | 0.8 | 13.98 | 0.31 < 1.38** |

120* — limiting slenderness (Regulations SP 64 13330.2017 "Timber structures")

1.38** — the design compressive strength of second-grade wood along the fibers (Regulations SP 64 13330.2017 "Timber structures")

Therefore, based on Table 1, we obtain satisfactory results concerning the strength and limiting slenderness of a conventional post at a floor height of up to 3.5 m and building bays of 10 and 12 m. The slenderness of a conventional post with a height of 4 m with the same bays exceeds the limiting one.

*Calculation for compression with bending*

*Design case: under the action of the wind load along the building*

In case of the wind load along the building, there are two options. As for the first option, the wind load is distributed among individual conventional posts of a side wall. This option is similar to the case of the wind load across the building described above. As for the second option, the wind load along the building can be taken up by the entire side wall and distributed equally between the longitudinal walls (Fig. 3a).

Since a longitudinal wall is not monolithic, this load will mostly be received by the outermost conventional posts of the longitudinal walls. The posts will undergo compression with bending in the wall plane according to the same scheme as in the case of the action of the wind load across the building. If the outermost posts cannot take up vertical loads and the wind action from the building side wall, they will affect the neighboring ones. This may cause a deflection in the wall, instability of its geometrical shape. The second option of load distribution is described in the following example.

We performed calculations for a wall out of vertical squared timber with a thickness of 20.0 cm with the finishing layer of wood. The calculations were carried out using Eqs. (1)–(5) for a wall element — a conventional post with a design section of 11.3 x 20.0 cm ($h$) described above (Fig. 1). Fig. 3a shows a diagram for the distribution of the wind load along the building. To take into account the ductility of the post joints in the wall plane, the section slenderness was adopted equal to the slenderness of an individual branch, i.e., an individual bar. Table 2 shows the specified geometric parameters of the conventional posts as well as the obtained forces and stresses in the posts.

In addition, it should be noted that the wall, floor slabs, and roofing form the longitudinal frame of the building and develop composite action to take up the loads along the building. Due to pivot joints and possible shrinkage of wood during operation, the behavior of the floor slabs and roofing is not included in the calculations as some strength margin.

Table 2. Geometric parameters, forces, and stresses in conventional posts under the action of the wind along the building

| Wall height, m | Building bay, m | Slenderness of a conventional post (branch) | Buckling coefficient | Bending moment (Eq. (2)), kN·m | Longitudinal force, kN | Normal stresses check, (Eq. (1)), kN/cm² | Buckling check (Eq. (5)) |
|---|---|---|---|---|---|---|---|
| 3 | 10 | 91.6 < 120* | 0.358 | 7.83 | 11.59 | 1.36 < 1.38** | 0.41 < 1 |
| | 12 | 91.6 < 120* | 0.358 | 9.74 | 13.85 | 1.69 > 1.38** | 0.5 < 1 |
| 3.5 | 10 | 106.8 < 120* | 0.26 | 11.56 | 11.65 | 1.98 > 1.38** | 0.65 < 1 |
| | 12 | 106.8 < 120* | 0.26 | 14.76 | 13.91 | 2.52 > 1.38** | 0.83 < 1 |
| 4 | 10 | 122 > 120* | 0.2 | 16.7 | 11.72 | 2.64 > 1.38** | 1.03 ~ 1 |
| | 12 | 122 > 120* | 0.2 | 22.0 | 13.98 | 3.7 > 1.48** | 1.32 > 1 |

120* — limiting slenderness (Regulations SP 64 13330.2017 "Timber structures")

1.38** — the design compressive strength of second-grade wood along the fibers (Regulations SP 64 13330.2017 "Timber structures")
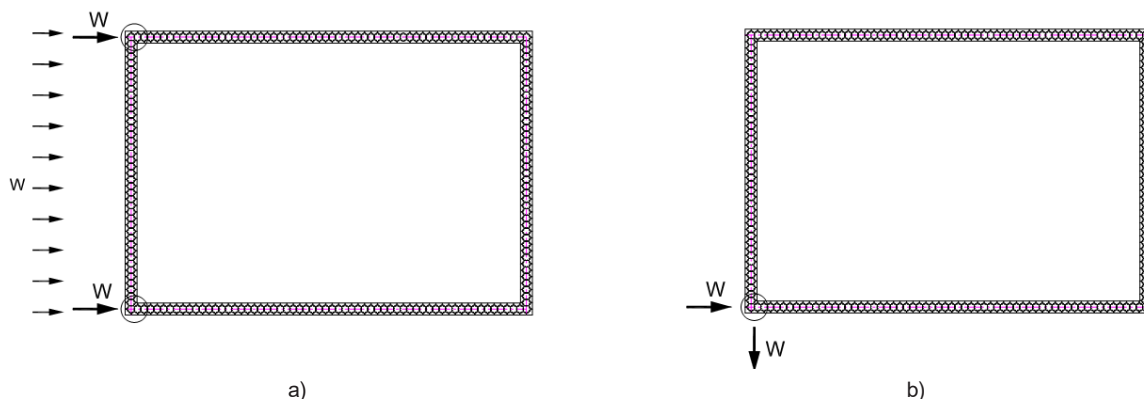


Fig. 3. A diagram of the wind load along the building: a) redistribution of the wind load from the side wall to the conventional posts in the corners; b) positive and negative wind pressure on the post in the corner

Thus, we considered two options for the distribution of the wind load along the building. The first option implies the uniform distribution of the wind load among the conventional posts of the side wall similar to the case of the wind load across the building described above. The second option implies the transfer of the wind load by the side wall to the longitudinal walls through the conventional posts in the corners. Table 2 shows the calculated data for the second case. As shown in the table, the conventional post with a height of 3 m and a building bay of 10 m demonstrates satisfactory performance in terms of strength, plane strain buckling, and limiting slenderness. The conventional post with a height of 3 m and a building bay of 12 m, the posts with a height of 3.5 m and bays of 10 and 12 m demonstrate satisfactory performance in terms of limiting slenderness and plane strain buckling but have high normal stresses exceeding the design wood resistance. The conventional post with a height of 4 m does not demonstrate satisfactory performance in terms of strength, plane strain buckling, and limiting slenderness.

*Calculation for buckling*

If in Eq. (1), the bending stress component is less than 10% of the compression stress component, the design section of the wall (conventional post) is calculated for buckling.

According to the proposed method, a check of wall stability comes down to a check of a conventional post in the plane and out of the plane of the wall depending on the direction of the horizontal wind load causing the bending moment.

The stability of a conventional post is checked based on the following condition:

$$\frac{N}{\phi \, F_{calc}} < R_c. \qquad (6)$$

The slenderness of a conventional post is adopted equal to the slenderness of an individual bar. The buckling coefficient is calculated in the same manner as for axially loaded elements depending on the value of the post slenderness. The design length of a post is adopted equal to the floor height.

**Results and discussion**

A wall out of vertical squared timber is represented by a set of conventional posts, each consisting of two bars. A check of a wall for strength and limiting slenderness comes down to a check of a conventional post. Table 3 summarizes the results of calculations for conventional posts. The following conclusions can be drawn:

At wind loads across the building, a conventional post resists compression with bending out of the longitudinal wall plane. The calculations for the action of specified vertical loads and horizontal wind loads across the building show that the conventional post under consideration has sufficient strength and slenderness not exceeding the limiting one, at a height of up to 3.5 m and bays of 10 and 12 m.

At wind loads along the building, an outermost conventional post resists compression with bending in the longitudinal wall plane. The calculations for the action of specified vertical loads and horizontal wind loads along the building show that, when the wind loads are transferred from the side wall to the longitudinal walls, the outermost conventional posts of the section under consideration can take up wind pressure at a height of max. 3.5 m and bay of max. 10 m.

The buckling strain of conventional posts is taken into account if stresses from the moment are less than 10% of the compression stresses.

The outermost conventional posts are actually corner posts. The corner posts are characterized by a combined stress state under the action of the wind load both along and across the building. In both cases, the posts are exposed to positive and negative wind pressure, as shown in Figs. 2b and 3b. This leads to the bending and torsional buckling mode.

Table 3. Results of the calculations for a conventional post under the action
of the wind load along and across the building

| Wall height, m | Building bay, m | Wind load direction | Condition of strength at normal compression and bending stresses (Eq. (1)), kN/m² | Condition of limiting slenderness | Condition of stability (Eq. (5)) |
|---|---|---|---|---|---|
| 3 | 10 | Across the building | 0.18 < 1.48** | 91.55 < 120* | |
| | | Along the building | 1.36 < 1.48** | | 0.41 < 1 |
| | 12 | Across the building | 0.19 < 1.48** | | |
| | | Along the building | 1.69 > 1.48** | | 0.5 < 1 |

| | | | | | |
|---|---|---|---|---|---|
| 3.5 | 10 | Across the building | 0.22 < 1.48** | 106.8 < 120* | 0.65 < 1 |
| | | Along the building | 1.98 > 1.48** | | |
| | 12 | Across the building | 0.24 < 1.48** | | 0.83 < 1 |
| | | Along the building | 2.52 > 1.48** | | |
| 4 | 10 | Across the building | 0.26 < 1.48** | 122 > 120* | 1.03 ~ 1 |
| | | Along the building | 2.64 > 1.48** | | |
| | 12 | Across the building | 0.31 < 1.48** | | 1.32 > 1 |
| | | Along the building | 3.7 > 1.48** | | |

120* — limiting slenderness (Regulations SP 64 13330.2017 "Timber structures")

1.48** — the design compressive strength of second-grade wood along the fibers (Regulations SP 64 13330.2017 "Timber structures")

Based on the above, the following recommendations can be formulated. The conventional posts to be placed in the corners shall be manufactured out of whole-section rectangular timber in order to rule out the impact of ductility from the contact joints of the bars. Besides, options with a laminated section or a section made by means of a special welding technique are possible (Župčić et al., 2021). To improve the strength characteristics of corner conventional posts, laminated veneer lumber (LVL) can be used with account for the relevant restrictions on the size of sections according to State Standard GOST 33124 "Laminated veneer lumber. Specifications". Compressed wood is distinguished by its good mechanical properties and the possibility to obtain any size of section (Namari et al., 2021). Such type of wood can be used to manufacture corner conventional posts. The strength of walls out of vertical squared timber depends on the quality of bar joints. Their high quality can be achieved by improving milling methods. Automatic robotic assembly of wooden members is also promising (Leung et al., 2021).

**Conclusion**

We formulated an analytical calculation method for walls out of vertical squared timber, made using the Naturi technology. According to the proposed method, a wall is considered a set of conventional posts with contact joints. The stress-strain state of conventional posts is considered under the action of vertical and horizontal loads directed along and across the building. Each conventional post is checked for strength and stability in compression with bending or buckling as well as for limiting slenderness. The method is based on the existing traditional provisions for calculations concerning wooden structures.

Several examples of wall element calculations were provided. Permissible heights of walls for buildings with bays of 10 and 12 m were obtained.

Recommendations on the structure of corner wall sections were provided based on the calculation esults.

These results can be used in the construction of residential and public buildings given the corresponding justification of structure fire resistance.

## References

Bedon, C. and Fragiacomo, M. (2019). Numerical analysis of timber-to-timber joints and composite beams with inclined self-tapping screws. *Composite Structures*, Vol. 207, pp. 13–28. DOI: 10.1016/j.compstruct.2018.09.008.

Bucklin, O., Menges, A., Krieg, O., Drexler, H., Rohr, A. and Amtsberg, F. (2021). Mono-material wood wall : digital fabrication of performative wood envelopes. *Journal of Facade Design and Engineering*, Vol. 9, No. 1, pp. 1–16. DOI: 10.7480/jfde.2021.1.5398.

Cabral, M. R. and Blanchet, P. (2021). A state of the art of the overall energy efficiency of wood buildings—an overview and future possibilities. *Materials*, Vol. 14, Issue 8, 1848. DOI: 10.3390/ma14081848.

Chaggaris, R., Pei, S., Kingsley, G. and Kinder, E. (2021). Cost-effectiveness of mass timber beam–column gravity systems. *Journal of Architectural Engineering*, Vol. 27, Issue 3, 04021028. DOI: 10.1061/(ASCE)AE.1943-5568.0000494.

Cohen, D. H. and Gaston, C. (2003). The use of engineered wood products in traditional Japanese wood house construction. *Wood and Fiber Science*, Vol. 35, No. 1, pp. 102–109.

Cokcan, B., Braumann, J., Winter,W. and Trautz, M. (2016). Robotic production of individualised wood joints: Fabricating an info point structure for the WCTE. In: Chien, S., Choo, S., Schnabel, M. A., Nakapan, W., Kim, M. J. and Roudavski, S. (eds.), *Living Systems and Micro-Utopias: Towards Continuous Designing, Proceedings of the 21st International Conference of the Association for Computer-Aided Architectural Design Research in Asia CAADRIA 2016.* Hong Kong: Association for Computer-Aided Architectural Design Research in Asia (CAADRIA), pp. 559–568.

Colella, M. (2020). The dome as minimal housing unit: "Ghibli" and "D-Home" prototypes. In: Viana, V., Murtinho, V. and Xavier, J. P. (eds.), *Thinking, Drawing, Modelling. Springer Proceedings in Mathematics and Statistics*, Vol. 326, pp. 29–40. DOI: 10.1007/978-3-030-46804-0_3.

Dias, A. M. A., Dias, A. M. P. G., Silvestre, J. D. and de Brito, J. (2020). Comparison of the environmental and structural performance of solid and glued laminated timber products based on EPDs. *Structures*, Vol. 26, pp. 128–138. DOI: 10.1016/j.istruc.2020.04.015.

El Houjeyri, I., Thi, V. D., Oudjene, M., Ottenhaus, L.-M., Khelifa, M. and Rogaume, Y. (2021). Coupled nonlinear-damage finite element analysis and design of novel engineered wood products made of oak hardwood. *European Journal of Wood and Wood Products*, Vol. 79, No. 1, pp. 29–47. DOI: 10.1007/s00107-020-01617-7.

Feio, A. O., Lourenço, P. B. and Machado, J. S. (2014). Testing and modeling of a traditional timber mortise and tenon joint. *Materials and Structures*, Vol. 47, Issue 1–2, pp. 213–225. DOI: 10.1617/s11527-013-0056-y.

Gamerro, J., Bocquet, J. F. and Weinand, Y. (2020). Experimental investigations on the load-carrying capacity of digitally produced wood-wood connections. *Engineering Structures*, Vol. 213, 110576. DOI: 10.1016/j.engstruct.2020.110576.

Ganaus, G. (2009). *Wooden wall of ceiling element (options). Patent No. RU866115U1.*

Ganaus, G., Stepanishchev, A. V., Lazarev, D. B. and Yelchugin, A. V. (2018). *Wooden wall design. Patent No. RU2663854C1.*

He, J.-X., Yu, P., Wang, J., Yang, Q.-S., Han, M. and Xie, L.-L. (2021). Theoretical model of bending moment for the penetrated mortise-tenon joint involving gaps in traditional timber structure. *Journal of Building Engineering*, Vol. 42, 103102. DOI: 10.1016/j.jobe.2021.103102.

Höckner, V. (2019). *Hygrothermische Gebäudesimulation eines Massivholz-Systems im Vergleich zum Monats-Bilanzverfahren. Diploma thesis.* Vienna: Technical University Wien, 151 p.

Inayama, M., Aoyama, S. and Murakami, M. (2011). In-plane shear test and analysis of mechanical behavior of inserted wooden siding wall. *Journal of Structural and Construction Engineering*, Vol. 76, No. 659, pp. 97–104. DOI: 10.3130/aijs.76.97.

Iraola, B., Cabrero, J. M., Basterrechea-Arévalo, M., Gracia, J. (2021). A geometrically defined stiffness contact for finite element models of wood joints. *Engineering Structures*, Vol. 235, 112062. DOI: 10.1016/j.engstruct.2021.112062.

Janakieska, M. M., Ayrilmis, N. and Kuzman, M. K. (2021). The engineered wood products application in vernacular and contemporary architecture in Macedonia. *14th International Scientific Conference of International Association for Economics and Management in Wood Processing and Furniture Manufacturing (WoodEMA) on The Response of the Forest-Based Sector to Changes in the Global Economy, Koper, Slovenya, June 16–18, 2021*, pp. 387–392.

Krasovsky, M. V. (2002) *Encyclopedia of Russian architecture. Wooden architecture*. Saint Petersburg: Satis, 382 p.

Leung, P. Y. V., Apolinarska, A. A., Tanadini, D., Gramazio, F. and Kohler, M. (2021). Automatic assembly of jointed timber structure using distributed robotic clamps. In: Globa, A., van Ameijde, J., Fingrut, A., Kim, N. and Lo, T. T. S. (eds.), Projections – *Proceedings of the 26th International Conference of the Association for Computer-Aided Architectural Design Research in Asia, CAADRIA 2021*, Vol. 1. Hong Kong: Association for Computer-Aided Architectural  esign Research in Asia (CAADRIA), pp. 583–592. DOI: 10.3929/ethz-b-000481928.

Mayo, J. (2015). *Solid wood: case studies in mass timber architecture, technology and design.* London: Routledge, 358 p. DOI: 10.4324/9781315742892.

Meloni, D., Giaccu, G. F., Concu, G. and Valdés, M. (2018). FEM models for elastic parameters identifications of cross laminated marittime pine panels. *WCTE 2018, World Conference on Timber Engineering*, *Seoul, Korea, August 20–23, 2018*.

Miyata, Y. (2020). Lateral loading test of dowel laminated timber and verification of mechanical properties. *AIJ Journal of Technology and Design*, Vol. 26, Issue 64, pp. 940–945. DOI: 10.3130/aijt.26.940.

Miyata, Y., Ochiai, Y., Aoki, K. and Inayama, M. (2018). Development of non-glued massive holz shear wall and proposal of calculation method of allowable strength. *AIJ Journal of Technology and Design*, Vol. 24, Issue 56, pp. 129–134. DOI: 10.3130/aijt.24.129.

Müller, T., Flemming, D., Janowsky, I., Di Bari, R., Harder, N. and Leistner, P. (2021). Bauphysikalische und ökologische Potenziale von Gebäuden in Holzbauweise. *Bauphysik*, Vol. 43, Issue 3, pp. 174–185. DOI: 10.1002/bapi.202100011.

Namari, S., Drosky, L., Pudlitz, B., Haller, P., Sotayo, A., Bradley, D., Mehra, S., O'Ceallaigh, C., Harte, A. M., El-Houjeyri, I., Oudjene, M. and Guan, Z. (2021). Mechanical properties of compressed wood. *Construction and Building Materials*, Vol. 301, 124269. DOI: 10.1016/j.conbuildmat.2021.124269.

Pavlenin, M. V and Shutova, O. A. (2020). Economic feasibility of building houses from a vertical timber. *Modern Technologies in Construction. Theory and Practice*, Vol. 2, pp. 132–136.

Piao, C. and Shupe, T. F. (2016). Mechanical properties of finger-jointed wood from composite utility poles made of small diameter timber *Drvna Industrija*, Vol. 67, Issue 1, pp. 73–78. DOI: 10.5552/drind.2016.1436.

Pinkowski, G., Szymański, W., Krauss, A. and Stefanowski, S. (2019). Effect of sharpness angle and feeding speed on the surface roughness during milling of various wood species. *BioResources*, Vol. 13, Issue 3, pp. 6952–6962. DOI: 10.15376/biores.13.3.6952-6962.

Resch, H. (1999). Massivwände aus behauenem rundholz. *Holzforschung und Holzverwertung*, Vol. 51, Issue 5, pp. 82–84.

Sandhaas, C. (2016). Buildings made of dowel-laminated timber: joint and shear wall properties. In: Eberhardsteiner, J., Winter, W., Fadai, A. and Pöll, M. (eds.), *WCTE 2016 e-book: containing all full papers submitted to the World Conference on Timber Engineering (WCTE 2016), August 22–25, 2016, Vienna, Austria.* Vienna: TU Verlag Wien, pp. 4589–4596.

Schiro, G., Giongo, I., Sebastian, W., Riccadonna, D. and Piazza, M. (2018). Testing of timber-to-timber screw-connections in hybrid configurations. *Construction and Building Materials*, Vol. 171, pp. 170–186. DOI: 10.1016/j.conbuildmat.2018.03.078.

Skullestad, J. L., Bohne, R. A. and Lohne, J. (2016). High-rise timber buildings as a climate change mitigation measure – a comparative LCA of structural system alternatives. *Energy Procedia*, Vol. 96, pp. 112–123. DOI: 10.1016/j.egypro.2016.09.112.

Starikov, A., Gribanov, A., Lapshina, M. and Mohammed, H. (2020). Adaptive milling of solid wood furniture workpieces: analysis of the extended approach capabilities. *IOP Conference Series: Earth and Environmental Science*, Vol. 595, 012026. DOI: 10.1088/1755-1315/595/1/012026.

Thiel, A. and Schickhofer, G. (2010). CLTdesigner – a software tool for designing cross laminated timber elements: 1D-plate-design. In: Ceccotti, A. (ed.), *11th World Conference on Timber Engineering 2010, WCTE 2010*, June 20–24, 2010, Trentino, Italy. Red Hook, NY: Curran Associates, Inc., pp. 1742–1747.

Tsai, M.-T. and Wonodihardjo, A. S. (2018). Achieving sustainability of traditional wooden houses in Indonesia by utilization of cost-efficient waste-wood composite. *Sustainability*, Vol. 10, Issue 6, 1718. DOI: 10.3390/su10061718.

Yu, P., Yang, Q. and Law, S.-S. (2021). Lateral behavior of heritage timber frames with loose nonlinear mortise-tenon connections. *Structures*, Vol. 33, pp. 581–592. DOI: 10.1016/j.istruc.2021.04.061.

Zmijewki, T. and Wojtowicz-Jankowska, D. (2017). Timber - Material of the future - Examples of small wooden architectural structures. *IOP Conference Series: Materials Science and Engineering*, Vol. 245, Issue 8, 082019. DOI: 10.1088/1757-899X/245/8/082019.

Župčić, I., Mihulja, G., Bogner, A., Grbac, I. and Hrovat, B. (2021). Zavarivanje masivnog drva. *Drvna Industrija*, Vol. 59, No. 3, pp. 113–119.

# МЕТОД РАСЧЕТА СТЕНЫ ИЗ ДЕРЕВЯННОГО ВЕРТИКАЛЬНОГО БРУСА

55

Ольга Викторовна Третьякова[1,2]

[1]Пермский национальный исследовательский политехнический университет
пр. Комсомольский, 29, Пермь, Россия
[2]Пермский государственный аграрно-технологический университет имени академика Д.Н. Прянишникова
ул. Петропавловская, 23, Пермь, Россия

E-mail: olga_wsw@mail.ru

**Аннотация**
В последние годы получили распространение дома из деревянного профилированного бруса, установленного вертикально. Такое расположение стенового бруса позволяет использовать эффективный вид работы древесины на сжатие и реализовать максимальную прочность материала вдоль волокон. Вместе с тем брус, установленный в вертикальном положении, работает в условиях сжатия с изгибом, что может привести к потере прочности и устойчивости конструкций здания. В существующих научных публикациях и технической литературе не анализировался вопрос напряженно-деформированного состояния таких стен. **Целью данного исследования** является формулировка метода расчета стен из вертикального бруса на основе известных традиционных подходов к деревянным конструкциям. Предложен **метод** расчета стены из вертикального бруса как совокупности элементов, работающих на сжатие с изгибом, включающий проверку по предельной гибкости. **Результаты:** Получены допускаемые высоты стены при пролетах здания 10м и 12м. Результаты могут быть использованы при проектировании малоэтажных зданий жилого и общественного назначения, мансардных надстроек многоэтажных зданий.

**Ключевые слова**
Деревянный профилированный вертикальный брус, напряженно-деформированное состояние, сжатие, изгиб.

# ADOPTION OF BUILDING INFORMATION MODELING IN THE CONSTRUCTION PROJECT LIFE CYCLE: BENEFITS FOR STAKEHOLDERS

Nguyen Quoc Toan*, Nguyen Van Tam, Tran Ngoc Diep, Pham Xuan Anh

Faculty of Construction Economics and Management, Hanoi University of Civil Engineering
55 Giai Phong Road, Hai Ba Trung Dist., Hanoi, Vietnam

*Corresponding author: toannq@nuce.edu.vn

**Abstract**

**Introduction:** Building Information Modeling (BIM) is characterized by potential benefits at many phases of the construction project life cycle. However, no comprehensive study has been conducted to evaluate the benefits of BIM adoption and implementation for project stakeholders in the Vietnamese construction industry context. **Methods:** This study aimed to identify and evaluate the benefits of BIM adoption and implementation in construction projects based on the perception of project stakeholders through data collection from 159 valid construction practitioners. The reliability and validity tests were performed to analyze collected data by SPSS 22 software. **Results:** The results demonstrated that four primary clusters of the project stakeholders received benefits when BIM was adopted in construction projects: architectural and structural design units (10 benefits), facility management units (8 benefits), contractors (6 benefits), and owners (6 benefits). These clusters accounted for 58.954%, 5.975%, 4.682%, and 3.736%, respectively, of the variance that characterized the benefits of BIM adoption. The findings indicated that 'improve the quality of design drawings', and 'minimize conflicts/changes' were the most significant BIM benefits for architectural and structural design units, whereas 'convenient for managing project data' and 'easy planning and resource mobilization' were the top benefits for facility management units. For contractors, 'minimize construction errors' and 'construction cost saving' were the most prominent benefits. Besides, BIM brought owners such striking benefits as 'maximize project performance' and 'easier to choose investment options'.

**Keywords**

BIM, benefits, project stakeholders, construction industry, life cycle.

## Introduction

Building Information Modeling (BIM) has been recognized as one of the most efficient technological initiatives in response to the challenges within the construction industry (Azhar, 2011). BIM technology makes it possible to create a digitally constructed accurate virtual model of a building. This technology can be used for facility planning, design, construction, and operation. BIM assists architects, engineers, and builders in visualizing what will be built in a simulated environment so that they could identify potential design, construction, or operational issues. BIM represents a new paradigm within the architecture, engineering, and construction (AEC) industry, one that encourages integration of the roles of all stakeholders on a project (Azhar, 2011). A BIM model characterizes the geometry, spatial relationships, geographic information, quantities and properties of building elements, cost estimates, material inventories, and project schedule (Azhar, 2011; Chan et al., 2018). This allows project stakeholders to efficiently collaborate throughout the project lifecycle (Oesterreich and Teuteberg, 2019; Saka and Chan, 2019). BIM can be viewed as a virtual process that encompasses all aspects, disciplines, and systems of a facility within a single, virtual model; it enables all construction project stakeholders to collaborate more precisely and efficiently than using traditional processes (Azhar, 2011). Team members are constantly refining and adjusting their portions in response to project specifications and design changes to ensure the model is as accurate as possible before the project physically begins (Carmona and Irwin, 2007). One of the primary reasons for BIM adoption is to achieve a proper balance between the project management triangle of scope (features & quality), cost and time (Olawumi and Chan, 2019a; Olawumi et al., 2018), which is one of the most important concerns in the (AEC) industry (Chan et al., 2019b).

Stakeholders can maximize benefits in terms of time, cost, and quality by implementing BIM in construction projects (Wong et al., 2009). However, it is not easy to achieve a right balance between these three factors for the construction projects, since so many strategies and solutions are needed

to accomplish it, and innovation can be one of the possible solutions to strike a balance between these three factors (Chan et al., 2019b). Hence, BIM is a new technology in the construction industry, which is expected to deliver numerous benefits to the industry, such as initial conflict control in the designing (Azhar, 2011), project performance and quality enhancement (Succar, 2009), enhance collaboration among construction stakeholders (Kerosuo et al., 2015; Succar, 2009), effective construction process (Abd Hamid et al., 2018), operation and maintenance of buildings (Hoang et al., 2020), improve visualization of project execution (Haron et al., 2015), decision-making process enhancement (Azhar, 2011), effective construction cost (Abbasnejad and Moud, 2013).

Even though BIM has been used in the construction industry in Vietnam since the early 2000s, it is still not widely applied (Van Tam et al., 2021a). This is especially true for construction projects funded with state-managed capital, which makes up the majority of Vietnamese construction projects (Dao et al., 2020). Being aware of BIM benefits, Vietnam has set 2021 as the target year for adopting BIM for all governmental and large construction projects (Dao et al., 2021). Investors and construction firms initially recognized the benefits of adopting BIM after observing the trends of BIM technology adoption. Numerous design firms and contractors have gradually integrated BIM tools into practical projects ranging from concept design to construction management. However, in the Vietnamese construction industry, BIM implementation is very slow. Its slow adoption and implementation are caused by numerous barriers, of which lack of perceived benefits of BIM adoption is considered to have a key role in this regard (Van Tam et al., 2021b). Moreover, there has been no in-depth research in Vietnam to assess the benefits gained by construction project stakeholders when adopting and implementing BIM. Therefore, this study aims to identify and evaluate BIM implementation benefits in construction projects through data collection from construction practitioners who implemented BIM in Vietnam. Benefits have always been achieved through effective implementation, and vice versa. Hence, BIM benefits should influence construction industry practitioners to foster BIM implementation (Al-Ashmori et al., 2020).

### Literature review

BIM has great potential for useful adoption at all stages of the project life cycle. This technology can be used by the owners to understand project needs, by the design team to analyze, design, and develop the project, by the contractors to manage the construction of the project and by the facility managers during operation and decommissioning phases (Bryde et al., 2013; Grilo and Jardim-Goncalves, 2010). BIM has been proved as a very beneficial approach in reducing uncertainties and improving the efficiency of the construction process (Van Tam et al., 2021b). BIM will provide potential beneficial project outcomes by enabling the rapid analysis of different scenarios related to the life cycle performance of a building (Schade et al., 2011). The study of Fallon and Palmer (Fallon and Palmer, 2007) explained that BIM is very useful in increasing the speed and utility of activities by enhancing the quality of scheduling and cost information throughout the project lifecycle; one of the most frequently observed benefits is increased utility and speed (Memon et al., 2014). Several significant BIM benefits were identified by Al-Ashmori et al. (2020) in Malaysia such as (1) increasing productivity and efficiency; (2) assessing time and cost associated with design change; (3) eliminating clashes in design; (4) improving multi-party communication and maintain synchronized communication; (5) integrating construction scheduling and planning, (6) identifying time-based clashes; and (7) tracking progress during construction. In Hong Kong, Chan et al. (2019b) identified 12 benefits of BIM implementation. They found that the most significant benefits are (1) better cost estimates and control; (2) a better understanding of design; (3) reduce construction cost; (4) better construction planning and monitoring; (5) improve project quality. In Vietnam, the study of (Hoang et al., 2020) assessed 12 BIM benefits; the top five significant benefits were determined as follows: (1) collaboration improvement; (2) more accurate information from a data-rich asset; (3) automatically updated model; (4) improved interoperability; (5) increased employees' productivity and efficiency. In Turkey, 41 benefits of BIM adoption were identified by Seyis (2019). The top benefits include (1) planning the tasks and responsibilities in a timely manner; (2) promoting collaboration and coordination in the early design phase; (3) automatic implementation of design changes into 3D CAD model; (4) decreasing uncertainties in the processes by clarifying risks; (5) reducing time variances in the processes.

The introduction and adoption of any new technological advancement, such as BIM, usually necessitates identifying and addressing the factors that may affect the adoption by project stakeholders in order for the innovations to be successfully implemented and the benefits to be derived from them (Abubakar et al., 2014). In order to foster BIM adoption, identifying its benefits in construction projects is necessary. Therefore, various BIM implementation benefits in construction projects have been identified and classified by numerous researchers from various countries. Table 1 provides the most significant benefits of BIM adoption in construction projects from prior studies.

Table 1. Summary on benefits of BIM adoption from prior studies

| Country | Study | Total benefits identified | Benefits of BIM adoption |
|---|---|---|---|
| Australia | (Hong et al., 2019) | 7 | (1) cost saving; (2) time saving; (3) improved team work; (4) improved data management; (5) improved understanding of project. |
| | (Newton and Chileshe, 2012a) | 9 | (1) improved constructability; (2) improved visualization; (3) improved productivity; (4) reduced clashes; (5) improved quality and accuracy. |
| Malaysia | (Enegbuma and Ali, 2011b) | 7 | (1) faster and more effective processes; (2) better design; (3) controlled whole-life costs and environmental data; (4) better production quality; (5) automated assembly. |
| | (Mohd Noor et al., 2018) | 12 | (1) more realistic start and finish dates of project activities; (2) rapid consideration of many alternatives schedule; (3) helps managing the schedule changes when and as they occur; (4) helps evaluating overall project performance; (5) helps to ensure that the quality-related activities are being performed effectively. |
| | (Ibrahim et al., 2019) | 56 | (1) concepts become clearer and project conceptualization easier; (2) earlier and more accurate visualizations of a design to the owner; (3) support decision making regarding the design; (4) improve feasibility studies; (5) improve simulations and coordination |
| | (Memon et al., 2014) | 8 | (1) improved scheduling; (2) improved drawing coordinates; (3) improved work quality; (4) single detailed model; (5) control time and cost. |
| | (Al-Ashmori et al., 2020) | 7 | (1) increase productivity and efficiency; (2) assess time and cost associated with design change; (3) eliminate clashes in design; (4) improve multi-party communication and maintain synchronized communication; (5) integrate construction scheduling & planning. |
| Indonesia | (Sholeh et al., 2020) | 6 | (1) BIM makes flexibility in design and construction; (2) BIM facilitates supply chain integration between stakeholders; (3) BIM facilitates supply chain integration between project phases; (4) flexible work; (5) better risk-sharing between stakeholders. |
| Korea | (Ashcraft, 2008) | 12 | (1) single data entry, multiple uses; (2) design efficiency; (3) consistent design bases; (4) 3D modeling and conflict resolution; (5) conflict identification and resolution. |
| Hong Kong | (Chan et al., 2019b) | 12 | (1) better cost estimates and control; (2) a better understanding of design; (3) reduce construction cost; (4) better construction planning and monitoring; (5) improve project quality. |
| | (Tse et al., 2005) | 5 | (1) creating views and schedules dynamically and automatically; (2) reflecting changes instantly in all drawings and schedules; (3) single project file; (4) toolbars oriented; (5) compatibility with data exchange standards. |
| Jordan | (Matarneh and Hamed, 2017) | 13 | (1) reduce rework during construction; (2) maximizing productivity; (3) reduce conflict/changes; (4) clash detection; (5) enhance collaboration & communication. |
| Nigeria | (Saka et al., 2019) | 15 | (1) facilities management; (2) health and safety; (3) energy management; (4) time saving; (5) better coordination. |
| Vietnam | (Hoang et al., 2020) | 14 | (1) collaboration improvement; (2) more accurate information from a data-rich asset; (3) automatically updated model; (4) improved interoperability; (5) increased employees' productivity and efficiency. |
| New Zealand | (Diaz, 2016) | 6 | (1) better performance and quality of the project; (2) improved productivity; (3) reduction of wastages; (4) faster delivery; (5) new opportunities for revenue and business. |
| | (Stanley and Thurnell, 2014) | 8 | (1) the visualization of projects is increased; (2) collaboration on projects is enhanced; (3) the quality level of the finished projects is improved; (4) project conceptualization is made easier; (5) increased ability to print out design details from 5D software enables greater analysis capability. |
| Singapore | (Qian, 2012) | 60 | (1) improved forecasting; (2) less project risks; (3) better company image; (4) less mistakes and errors; (5) better project control. |

| Country | Study | Total benefits identified | Benefits of BIM adoption |
|---|---|---|---|
| Pakistan | (Mostafa et al., 2020) | 6 | (1) early identification of long completion time; (2) shortening the procurement schedule; (3) exploring design constraints for fabricators; (4) reduce differences between design and manufacturing models; (5) reduce the fabrication cycle time. |
| | (Masood et al., 2014) | 7 | (1) reduced construction cost; (2) reduced construction time; (3) improve quality; (4) reduced human resources; (5) reduce contingencies. |
| UK | (Bryde et al., 2013) | 9 | (1) cost reduction or control; (2) time reduction or control; (3) communication improvement; (4) coordination improvement; (5) quality increase or control. |
| Turkey | (Seyis, 2019) | 41 | (1) planning the tasks and responsibilities in a timely manner; (2) promoting collaboration and coordination in early design phase; (3) automatic implementation of design changes into 3D CAD model; (4) decreasing uncertainties in the processes by clarifying risks; (5) reducing time variances in the processes. |
| India | (Diaz, 2016) | 10 | (1) enhancing the project performance; (2) efficient planning and scheduling; (3) detailing the project stages; (4) generating multiple planned scenarios; (5) being used for project bidding purposes. |

### Underlying rationale

BIM has been acknowledged as one of the most appropriate platforms for the AEC industry, which is considered to be multi-organizational and multi-disciplinary, helping resolve construction performance challenges during the planning, designing, construction, operation, and maintenance stages of the entire project life cycle (Li et al., 2017). In the literature review, relevant studies were explored to identify BIM adoption and implementation in construction projects. Although many studies discussed BIM benefits, there is a gap in the literature regarding specific benefits for project stakeholders. Besides, although the developed countries are harvesting the fruits of the benefits of adopting BIM for the construction industry, the adoption and implementation of BIM for construction projects in Vietnam are very much limited. Therefore, the goal of this study was to determine and evaluate the benefits of BIM adoption for each project stakeholder. To achieve the goal, two main objectives were set:
- To identify the most significant benefits of BIM adoption for project stakeholders.
- To evaluate the most significant benefits of BIM adoption for project stakeholders.

The results of this study are expected to be useful for policymakers, governments, construction enterprises, and other stakeholders in their quest to boost the current uptake of BIM in various construction projects not only in Vietnam but also in other countries with the same socio-economic or cultural circumstances.

The literature review was conducted by collecting and studying relevant research papers considering the various benefits of BIM adoption in the construction industry. These papers reported the top significant BIM benefits. In the course of the study, we revised all benefits by eliminating the replicates, refining the statements, and sharing the updated list with professionals in the construction industry to evaluate the presented benefits and finalize the list. Thus, a long list of benefits was shortened to include the 30 substantial benefits of BIM adoption in construction projects for four main project stakeholders: owners, designers, facility managers, and contractors. The benefits of BIM adoption in construction projects and their related sources are shown in Table 2.

### Methodology

#### 1.1. Questionnaire survey and respondents

The literature review was carried out to articulate issues regarding the benefits of BIM adoption and implementation in the construction industry with a particular emphasis on the Vietnamese construction sector. The review also aimed at identifying the potential BIM benefits in construction projects. As a result, a total of 30 significant benefits of BIM adoption for construction project stakeholders were identified in the study. These BIM benefits were tabulated in the form of a questionnaire. The questionnaire was composed of two main parts. The first part contained demographics of the respondents and project characteristics. Its main purpose was to describe the respondents in order to effectively ensure reliability and strengthen research findings. The second part included the list of the identified benefits.

Respondents were selected for the survey based on their previous participation in or direct implementation of construction projects adopting BIM tools in Vietnam. Based on their experience, they evaluated the degree of BIM adoption benefits importance in construction projects following a 5-point Likert scale (i.e.,1 — not important, 2 — somewhat important, 3 — neutral, 4 — important, 5 — very important).

Table 2. Benefits of BIM for construction project stakeholders

| Code | Benefits of BIM adoption | References |
|---|---|---|
| *OB* | *Benefits for Owners* | |
| OB1 | Easier to choose investment options | (Eastman et al., 2011; Mesároš and Mandičák, 2017) |
| OB2 | Improve operation and construction management | (Ashcraft, 2008; Hoang et al., 2020; Olawumi and Chan, 2019a; Seyis, 2019) |
| OB3 | Early design assessment to ensure project requirements are met | (Azhar, 2011; Mesároš & Mandičák, 2017) |
| OB4 | Maximize project performance | (Bryde et al., 2013; Diaz, 2016; Enegbuma and Ali, 2011; Olawumi and Chan, 2019a) |
| OB5 | Better marketing of project by making effective use of 3D renderings and walk-through animations | (Azhar, 2011; Eastman et al., 2011) |
| OB6 | Low financial risk because of reliable cost estimates and reduced number of change orders | (Azhar, 2011; Eastman et al., 2011) |
| *DB* | *Benefits for Designers* | |
| DB1 | Improve efficiency of design options | (Ashcraft, 2008; Enegbuma and Ali, 2011; Hong et al., 2019; Ibrahim et al., 2019; Olawumi and Chan, 2019; Saka et al., 2019; Seyis, 2019) |
| DB2 | Improve the quality of design drawings | (Ibrahim et al., 2019; Memon et al., 2014; Olawumi and Chan, 2019; Saka et al., 2019) |
| DB3 | Easy conflict detection | (Diaz, 2016; Ibrahim et al., 2019; Matarneh and Hamed, 2017; Saka et al., 2019; Stanley and Thurnell, 2014) |
| DB4 | Minimize conflicts/changes | (Al-Ashmori et al., 2020; Ashcraft, 2008; Hong et al., 2019; Ibrahim et al., 2019; Matarneh and Hamed, 2017; Newton and Chileshe, 2012b; Olawumi and Chan, 2019) |
| DB5 | Easy to adjust design changes | (Al-Ashmori et al., 2020; Ibrahim et al., 2019; Seyis, 2019; Sholeh et al., 2020) |
| DB6 | Easy quantity take-off and cost estimation | (Bryde et al., 2013; Chan et al., 2019b; Hong Duyen et al., 2018; Newton and Chileshe, 2012b; Seyis, 2019) |
| DB7 | Reduce design time and costs | (Ibrahim et al., 2019; Seyis, 2019; Stanley and Thurnell, 2014) |
| DB8 | Easy energy efficiency evaluation of options | (Ashcraft, 2008; Hoang et al., 2020; Olawumi and Chan, 2019; Saka et al., 2019; Seyis, 2019) |
| DB9 | Cooperation and commitment of professional bodies | (Chan et al., 2019b; Ibrahim et al., 2019; Qian, 2012) |
| DB10 | Easy product transfer | (Azhar, 2011; Mesároš and Mandičák, 2017; Qian, 2012) |
| *FB* | *Benefits for Facility Managers* | |
| FB1 | Easy planning and resource mobilization | (Al-Ashmori et al., 2020; Chan et al., 2019a; Diaz, 2016; Ibrahim et al., 2019; Olawumi and Chan, 2019; Seyis, 2019) |
| FB2 | Project management and execution improvement | (Azhar, 2011; Eastman et al., 2011) |
| FB3 | Easier to coordinate contractors and stakeholders | (Chan et al., 2019b; Eastman et al., 2011) |
| FB4 | Easier to track and supervise design, construction, and operation | (Al-Ashmori et al., 2020; Ibrahim et al., 2019) |
| FB5 | Predicting potential hazards and solving them | (Ibrahim et al., 2019; Stanley and Thurnell, 2014) |

| Code | Benefits of BIM adoption | References |
|------|--------------------------|-----------|
| FB6 | Convenient for managing project data | (Enegbuma and Ali, 2011; Hong et al., 2019; Ibrahim et al., 2019; Olawumi and Chan, 2019; Qian, 2012; Saka et al., 2019; Seyis, 2019) |
| FB7 | Better management and operation of facilities | (Azhar, 2011; Eastman et al., 2011; Meadati et al., 2010) |
| FB8 | Operational simulation for maintainability | (Azhar, 2011; Eastman et al., 2011; Meadati et al., 2010; Mesároš and Mandičák, 2017) |
| *CB* | *Benefits for Contractors* | |
| CB1 | Easy clash detection | (Diaz, 2016; Ibrahim et al., 2019; Matarneh and Hamed, 2017; A. Saka et al., 2019; Stanley & Thurnell, 2014) |
| CB2 | Minimize construction errors | (Ashcraft, 2008; Ibrahim et al., 2019; Mostafa et al., 2020; Qian, 2012; Saka et al., 2019; Seyis, 2019) |
| CB3 | Convenient for handing over works | (Azhar, 2011) |
| CB4 | Convenient for planning and resource provisioning | (Al-Ashmori et al., 2020; Chan et al., 2019a; Diaz, 2016; Ibrahim et al., 2019; Olawumi and Chan, 2019; Seyis, 2019) |
| CB5 | Construction time saving | (Bryde et al., 2013; Chan et al., 2019a; Hong et al., 2019; Ibrahim et al., 2019; Masood et al., 2014; Mostafa et al., 2020; Qian, 2012; Saka et al., 2019; Seyis, 2019) |
| CB6 | Construction cost saving | (Ashcraft, 2008; Bryde et al., 2013; Chan et al., 2019a; Diaz, 2016; Hoang et al., 2020; Hong et al., 2019; Ibrahim et al., 2019; Masood et al., 2014; Olawumi and Chan, 2019; Qian, 2012; Saka et al., 2019) |

Out of 250 questionnaires distributed among construction practitioners, only 168 were filled in. Answers with incomplete data or missing values were removed. Finally, 159 valid questionnaires were collected (age average — 32.5, SD = 4.528), this represented an approximately 63.6% usable response rate.

### 1.2. Survey results

Among 159 valid answers, 78.62% respondents were male and 21.37% were female. Most of them — 151 respondents (94.97%) — had bachelor's degrees. Only seven respondents (4.40%) had master's degrees, and only one respondent had a PhD (0.63%). This is relevant to the years of their experience in the construction industry. More than a half — 93 respondents (58.49%) — had 1–5 years of experience. Other groups had experience of 6–10 (22.01%), 11–15 (10.06%), and 16–20 years (2.52%). Besides, 11 respondents (6.92%) had more than 20 years of experience.

In terms of organizations involved in construction projects, the majority — 81 respondents — worked at contractor companies, accounting for 50.84% of the total. Those organizations were followed by design enterprises, with 66 respondents (41.51%), and 12 owners (7.55%). In terms of job position, the majority were designers (64 respondents, accounting for 40.25% of the total). The share of project managers/facility managers was 22.01% (35 respondents);

while estimators (35 respondents) and site engineers (24 respondents) accounted for 22.01% and 15.09%, respectively.

In terms of construction characteristics, most of the projects were related to building (106 projects, 66.67%), followed by industrial ones (28 projects, 17.61%). Infrastructure projects accounted for 10.06% (16 projects) while the figure for transportation was only 5.66% (9 projects). Among these projects, 90 (56.60%) were private-financed, 57 (31.45%) were public-financed, and the rest 12 projects (7.55%) were financed using offshore funds. More than a half of the projects (102 projects, 64.15%) were medium to big scale (≥ 15 VND billions), and 50 projects (31.45%) were small scale (≤ 15 VND billions), while only 7 projects (4.40%) were nationally important.

### Data analysis

#### 1. Internal consistency of the questionnaire

Cronbach's alpha is a measure the reliability of internal consistency that assumes the same thresholds but yields lower values than the composite reliability. We aimed to determine Cronbach's alpha so as to confirm that the criteria associated with the Likert's scale measure each variable that was intended to be measured (which is the importance of each benefit of BIM adoption in construction projects for stakeholders). The study of (Vaske et al., 2017) explained that Cronbach's alpha measures the extent to which answers to survey questions correlate with

each other, which means $\alpha$ estimates the proportion of variance that is systematic or consistent in a set of survey responses. The standard for evaluating the level of relevance of the model is a value where Cronbach's alpha is higher than 0.7. Then questionnaires are generally accepted as accurate (Fang et al., 2004; Hai et al., 2022; Hair et al., 1998). The 'Cronbach's Alpha if item deleted' option makes it possible to examine whether the removal of any items would enhance the reliability of a specific variable scale that showed an unsatisfactory

Cronbach's alpha value (i.e., the score less than 0.3). Cronbach's alpha coefficient can be determined by Eq. (1) as follows:

$$Cronbach\text{'}s\ alpha\ \alpha\ = \frac{N.C}{v+(N-1).C}, \qquad (1)$$

where $N$ represents the number of item indicators; $C$ the coefficient of correlation of the average non-redundant indicator (i.e., the mean of the lower or upper triangular matrix); and $v$ is the average variance.

Table 3. Results of Cronbach's alpha test of internal consistency

| Code | Cronbach's Alpha if Item Deleted | Cronbach's Alpha |
|---|---|---|
| OB1 | 0.895 | 0.913 |
| OB2 | 0.886 | |
| OB3 | 0.880 | |
| OB4 | 0.896 | |
| OB5 | 0.928 | |
| OB6 | 0.898 | |
| DB1 | 0.939 | 0.947 |
| DB2 | 0.940 | |
| DB3 | 0.940 | |
| DB4 | 0.941 | |
| DB5 | 0.941 | |
| DB6 | 0.942 | |
| DB7 | 0.940 | |
| DB8 | 0.942 | |
| DB9 | 0.943 | |
| DB10 | 0.941 | |
| FB1 | 0.945 | 0.948 |
| FB2 | 0.938 | |
| FB3 | 0.940 | |
| FB4 | 0.939 | |
| FB5 | 0.941 | |
| FB6 | 0.939 | |
| FB7 | 0.940 | |
| FB8 | 0.946 | |
| CB1 | 0.899 | 0.904 |
| CB2 | 0.880 | |
| CB3 | 0.898 | |
| CB4 | 0.880 | |
| CB5 | 0.885 | |
| CB6 | 0.878 | |

As demonstrated in Table 3, the results of Cronbach's alpha for the components are 0.913, 0.947, 0.948, and 0.904, respectively. These values are higher than 0.7, thereby reliability is acceptable. The observed variables have Cronbach's alpha if item is deleted > 0.3, thus they are closely related to

other variables; these variables are all measuring the same construct and therefore there will be no basis for removing any item.

**2. Kaiser–Meyer–Olkin test and Bartlett's test of sphericity**

The Kaiser–Meyer–Olkin Measure of Sampling

Adequacy and Bartlett's Test of Sphericity were adopted to assess if exploratory factor analysis is reasonable. Bartlett's test for testing the null hypothesis assumed that the extracted principal components or factors did not make unique contributions to the outcome being investigated or are significantly correlated with each other. The following is recommended: $0.5 \leq KMO \leq$ and Sig < 0.05 (Bryman and Cramer, 2011; Hair et al., 1998). As shown in Table 4, the result of the KMO test indicated a coefficient value of 0.937 > 0.5, which is a strong measure of sampling adequacy. This demonstrated that the partial correlations or multicollinearity structures between the factors were sufficient to justify aggregating the variables into related sets for extraction of the principal components. Bartlett's Test of Sphericity with Sig = 0.00 < 0.05 proves that the observed variables have an overall correlation with each other. Hence, the result reinforced the four principal components' reliability and validity extracted from the 30 observed variables.

Table 4. Results of KMO and Bartlett's tests

| Kaiser–Meyer–Olkin Measure of Sampling Adequacy | | 0.937 |
|---|---|---|
| Bartlett's Test of Sphericity | Approx. Chi-Square | 4952.620 |
| | df | 435 |
| | Sig | 0.000 |

### 3. Factor loadings

Variables with eigenvalue less than 1 do not have better function in summarizing information than original factors. Hence, variables are only extracted if eigenvalue is more than 1 and are accepted if variance extracted is more than 50%. In other words, the software statistically defined a group of factors as highly intercorrelated when the group had eigenvalue of at least 1. The other components, with eigenvalue less than 1, were considered as "scree" and assumed not to represent any real traits underlying the 30 variables. Factor loadings describe how much correlation exists between observed variables and underlying factors. These values should be more than 0.3 (Bryman and Cramer, 2011; Hair et al., 1998).

Table 5. Factor loadings on the four components

| Code | Component | | | |
|---|---|---|---|---|
| | DB | FB | CB | OB |
| DB2 | 0.754 | | | |
| DB4 | 0.746 | | | |
| DB1 | 0.743 | | | |
| DB7 | 0.692 | | | |
| DB10 | 0.667 | | | |
| DB3 | 0.664 | | | |
| DB9 | 0.634 | | | |
| DB6 | 0.618 | | | |
| DB5 | 0.555 | 0.504 | | |
| DB8 | 0.524 | | | |
| FB6 | | 0.736 | | |
| FB1 | | 0.708 | | |
| FB7 | | 0.691 | | |
| FB4 | | 0.688 | | |
| FB3 | | 0.686 | | |
| FB2 | | 0.685 | | |
| FB8 | 0.518 | 0.565 | | |
| FB5 | | 0.516 | | |

| Code | Component | | | |
|---|---|---|---|---|
| | DB | FB | CB | OB |
| CB2 | | | 0.754 | |
| CB6 | | | 0.713 | |
| CB4 | | | 0.675 | |
| CB1 | | | 0.653 | |
| CB5 | | | 0.556 | |
| OB5 | 0.518 | | 0.547 | |
| CB3 | | | | |
| OB4 | | | | 0.815 |
| OB1 | | | | 0.799 |
| OB3 | | | | 0.741 |
| OB2 | | | | 0.723 |
| OB6 | | | | 0.618 |
| Initial eigenvalues | 17.686 | 1.793 | 1.405 | 1.121 |
| % of variance | 58.954 | 5.975 | 4.682 | 3.736 |
| Cumulative % | 58.954 | 64.929 | 69.611 | 73.347 |

Table 5 provides the results for three extracted components and principal variables loaded on the four components (i.e., DB — Benefits for Designers, FB — Benefits for Facility Managers, CB — Benefits for Contractors, and OB — Benefits for Owners). The four underlying categories of variables accounted for 73.347 % of the total cumulative variance. It is more than 50%, which proves that the variation of the observed variables is considered acceptable. Table 5 shows that all observed variable correlations are more than 0.3, indicating a robust inter-item correlation within each principal component. It also demonstrates a strong representation of the variables by the extracted elements. Exploratory factor analysis was conducted to analyze the relationships among the correlated variables and reduce the data, which helped to confirm the structure of the model. Factors with loading below 0.50 (cut-off for significance) or incidence of cross-loading were found to be weak indicators of the constructs and therefore were not included in the components (Cho et al., 2009; Field, 2013). On that basis, several problematic factors were omitted from all items, including DB5 — easy to adjust design changes, CB3 — convenient for handing over works, FB8 — operational simulation for maintainability, and OB5 — reduce time solving conflicts.

### Discussion

This section will discuss the benefits of BIM implementation in construction projects for stakeholders based on data analysis results. The analysis is divided into four primary parts as follows: benefits of BIM adoption for architectural and structural design units, benefits of BIM adoption for facility management units, benefits of BIM adoption for contractors, and benefits of BIM adoption for project owners, which are discussed in this section.

### 1. Benefits of BIM adoption for architectural and structural design units

As demonstrated in Table 5, 10 variables loaded strongly and positively on the DB component, of which there was only one item cross-loading on another component, accounting for 33.3% of the total number of variables. This component explains 58.954% of the total variance among 30 variables. This means that analysis of the underlying benefits of BIM adoption in the order of their relative loading coefficients could confirm the valuable BIM implementation in construction projects. The most prominent benefit within the cluster of benefits for architectural and structural design units is 'improve the quality of design drawings'. This finding was further supported by studies of (Al-Ashmori et al., 2020; Ashcraft, 2008; Chan et al., 2019b; Enegbuma and Ali, 2011; Ibrahim et al., 2019; Mostafa et al., 2020), which revealed that one of the primary advantages of BIM adoption was improved drawing quality. This may be because building proposals can be rigorously analyzed, simulations performed quickly, and performance benchmarked, enabling improved and innovative solutions; documentation output is flexible and exploits automation (Azhar, 2011).

The surveyed respondents evaluated 'minimize conflicts/changes' as the second influential benefit for designers. This result is in the line with the findings of several previous studies (Diaz, 2016; Ibrahim et al., 2019; Matarneh and Hamed, 2017;

Saka et al., 2019; Stanley and Thurnell, 2014), which demonstrated that BIM is capable of detecting potential conflicts and minimizing drawing changes during the design phase. Clash avoidance is a key part of the design and construction process. During the design process, every BIM module or user shall assess design decisions and clashes to see if there is any problem early in the design stage (Ibrahim et al., 2019). Detecting clashes and minimizing conflicts and changes during construction are two of the top ways engineers say BIM adds value to a project (Matarneh and Hamed, 2017).

Implementing BIM in construction projects also brings several benefits for architectural and structural design units such as 'improve efficiency of design options', 'reduce design time and costs', 'easy product transfer', 'cooperation and commitment of professional bodies', and 'easy quantity take-off and cost estimation'. In fact, with an appropriate price database, the construction costs will be significantly saved. This utility is especially meaningful in the design phase of a project when the designs often change, and the investor urgently needs information to choose the option in time (Ashcraft, 2008; Chan et al., 2019b; Saka et al., 2019; Seyis, 2019; Stanley and Thurnell, 2014). The study of (Ashcraft, 2008) indicated that the model contains necessary information on quantity and estimated cost, avoiding processing of material take-offs manually, thus reducing error and misunderstanding.

The early design and pre-construction phases are the most important stages in deciding on the sustainability characteristics of a building (Azhar et al., 2009). In the early stages of design development, traditional Computer-Aided Design (CAD) planning environments usually lack the capacity to conduct sustainability analyses. Usually, construction performance evaluations are carried out after the architectural design and construction documents have been created. This failure to consistently evaluate sustainability during the design process results in inefficient retroactive design adjustment to meet a set of performance criteria (Schlueter and Thesseling, 2009). Access to a comprehensive collection of data regarding the shape, materials, context, and systems of a building is needed to realistically evaluate building performance in the early design and pre-construction phases. Since BIM enables multi-disciplinary data to be superimposed within a single model, it provides an opportunity to integrate sustainability measures into the design process (Autodesk, 2008). Azhar (Azhar, 2011) found that by conducting BIM-based sustainability analyses, data for up to 17 LEED® (Leadership in Energy and Environmental Design, a green building ranking system used in the USA) credits can be obtained in the design process. This implies that a building knowledge model can be used for LEED® research

as a by-product, thereby saving considerable time and energy.

### 2. Benefits of BIM adoption for facility management units

As shown in Table 5, the FB component received the second-highest factor loading with 8 of the 30 variables, accounting for 26.7% of the items. This reveals that BIM adoption in construction projects can bring eight primary benefits for facility management units. This component accounts for 5.975% of the variance among the 30 items. The most prominent benefit within this cluster is 'convenient for managing project data'. "With the BIM database, any information about an equipment is just one click away", as Reddy (2011) stated. In the past, buildings would be turned over to facility managers with boxes and piles of manuals and warranties from the owner. In order to obtain data on product details, warranties, product life cycle, maintenance controls, replacement costs, installation and repair procedures, and even place an order for a replacement online, facility managers can now click on any equipment or fixture (Jordani, 2010). Developments in mobile phones and tablets (such as iPhone® and iPad®) and Virtual Reality (AR) have made it possible to gain full information about a building by simply pointing the device to it. An AR-based program, InfoSPOT®, developed at the Georgia Institute of Technology, Atlanta, Georgia, was reported by Joyce (2012), which enables facility managers to quickly obtain "on the spot" information about equipment using their smartphones.

The second prominent benefit for facility management units is 'easy planning and resource mobilization'. This is because BIM provides project management with a visual model and integrated elements such as construction progress, labor chart, and construction cost development chart, helping managers with easy tracking and supervision. Moreover, monitoring and tracking progress during the project life cycle significantly influenced the practitioners' decision to enhance mutual trust, respect, and personal commitments to cooperation (Al-Ashmori et al., 2020). Besides, implementing BIM in construction projects can bring other benefits for the facility management, such as 'project management and execution improvement', 'easier to coordinate contractors and stakeholders', 'easier to track and supervise design, construction, and operation', 'predicting potential hazards and solving them', 'better management and operation of facilities', and 'operational simulation for maintainability'. The challenge of managing a project is to ensure project success, and the key to achieve it is risk management at the earliest stages before it becomes costlier (Abdullah et al., 2015). Facility management departments can use BIM for renovations, space planning, and maintenance operations (Azhar, 2011). Thanks to BIM models, potential hazards are not

only anticipated at the early stage, but they are also solved automatically by the software.

### 3. Benefits of BIM adoption for contractors

The constructor is the third principal component receiving benefits of BIM implementation in construction projects. This cluster includes six variables (20.00% of the total) and explains 14.682% of the total variance among 30 variables. Contractors and subcontractors can use BIM for many tasks such as quantity take-off and cost estimation (Duyen et al., 2018); early identification of design errors through clash detections; construction planning and constructability analysis; onsite verification, guidance, and tracking of construction activities; offsite prefabrication and modularization; site safety planning; value engineering and implementation of lean construction concepts; and communication with the project owner, designer, subcontractors and workers on site (Hardin and McCool, 2015; Nguyen et al., 2021; Nguyen Van et al., 2021; Van Tam et al., 2018). According to the analysis results, 'minimize construction errors' and 'construction cost saving' are the most prominent benefits for contractors when adopting BIM in construction projects. These findings were supported by (Ibrahim et al., 2019) who explained that construction errors, besides causing cost-related waste, strongly affects the project's sustainability. Implementation of BIM in the construction phase will be able to reduce error, rework and waste for better sustainability for construction since it is connected to the database.

Implementing BIM in construction projects also can bring several other benefits for constructors, such as 'easy clash detection', 'convenient for handing over work', 'convenient for planning and resource provisioning', and 'construction time saving'. The study of (Azhar et al., 2012) presented a case study illustrating the use of BIM by the general contractor (GC) to minimize design errors via clash detections. The project was a $35 million academic building at the campus of Emory University, Atlanta, Georgia, USA. The architect of the project designed the architectural model. The GC received drawings of 2D structural and MEP structures from project engineers and turned them into 3D BIM models. The GC was able to save approximately $259,000 by combining all 'single' BIM models and through clash detections in the pre-construction phase.

### 4. Benefits of BIM adoption for project owners

As provided in Table 5, only 5 variables were loaded in this cluster, accounting for 16.67% of the total; explaining 3.736 % of the total variance among 30 variables. In projects where BIM technologies and processes are implemented, owners can gain considerable benefits (Eastman et al., 2011; Reddy, 2011). The most prominent benefit for project owners is 'maximize project performance'.

This result is in line with some previous studies such as (Chan et al., 2019b; Diaz, 2016; Mohd Noor et al., 2018; Olawumi and Chan, 2019; Seyis, 2019), which affirmed that the main advantage of BIM is an increase in building performance and quality. Project performance was also considered as an item giving most benefits towards the project quality (Mohd Noor et al., 2018). The surveyed respondents evaluated 'easier to choose investment options' as the second prominent benefit for project owners. Besides, several other benefits of BIM adoption in this cluster include 'improve operation and construction management', 'early design assessment to ensure project requirements are met', 'better marketing of project by making effective use of 3D renderings and walk-through animations', and 'low financial risk because of reliable cost estimates and reduced number of change orders'. In fact, 3D renderings can be easily generated in a house with little additional effort (Azhar, 2011). The study of (Chan et al., 2019b) indicated that BIM implementation improves project quality variables by facilitating the ease of assessment of construction materials and work processes. An organization's policy or strategy toward integrating and implementing BIM in their work processes aims to reduce financial risk and improve their competitive advantages.

### Conclusions, contributions, and limitations

BIM represents a new paradigm within the architecture, engineering, and construction (AEC) industry, one that encourages integration of the roles of all stakeholders on a project. Implementing BIM in the construction industry can bring valuable benefits for project stakeholders. The survey showed that construction practitioners belong to four primary clusters of project stakeholders receiving benefits of BIM adoption in construction projects: architectural and structural design units (10 benefits), facility management units (8 benefits), contractors (6 benefits), and owners (6 benefits). The reliability and validity of the research design and findings were evaluated via prescribed quality assurance tests, including Cronbach's alpha test of internal consistency, KMO measure of sampling adequacy, Bartlett's test of sphericity, and factor loadings. The analysis of the test results confirmed the reliability and validity of the research design and findings.

According to the findings, 'improve the quality of design drawings' and 'minimize conflicts/changes' are the most significant BIM benefits for architectural and structural design units. Meanwhile, 'convenient for managing project data' and 'easy planning and resource mobilization' are benefits that facility management units gained most from BIM. As for contractors, 'minimize construction errors' and 'construction cost saving' were the most prominent BIM benefits. For owners, BIM's two most striking

benefits are 'maximize project performance' and 'easier to choose investment options'.

The main contribution of this study to the existing body of knowledge is the investigation of the benefits of BIM implementation and adoption for project stakeholders. In the context of the Vietnamese construction industry, this study contributes to filling a crucial knowledge gap by providing information on various manageable BIM benefits to boost BIM in construction projects and attain high performance in a typical developing economy setting.

The main limitation of this study is that it was conducted only in the Vietnamese construction industry context. It seems rather modest compared to many countries and construction projects applying BIM technology around the world. This was a snapshot view of BIM adoption benefits for stakeholders aimed to foster BIM implementation in the Vietnamese construction industry; hence, the findings are not future proof. Rapid changes driven by advanced technology would necessitate these benefits to be re-investigated and up to date with new and emerging critical benefits. In addition, this study does not provide quantitative parameters to help the readers understand the extent of the benefits (e.g., cost-saving, time saving) for project stakeholders in a specific project case. Therefore, further studies should consider the benefits of BIM implementation in construction projects at different levels such as industry level, enterprise level, project level, or activity level.

## References

Abbasnejad, B. and Moud, H. I. (2013). BIM and basic challenges associated with its definitions, interpretations and expectations. *International Journal of Engineering Research and Applications (IJERA)*, Vol. 3. Issue 2, pp. 287–294.

Abd Hamid, A. B., Mohd Taib, M. Z., Abdul Razak, A. N. N. and Embi, M. R. (2018). Building information modelling: challenges and barriers in implement of BIM for interior design industry in Malaysia. *IOP Conference Series: Earth and Environmental Science*, Vol. 40, 012002. DOI: 10.1088/1755-1315/140/1/012002.

Abdullah, N., Jabar, M. A., Sidi, F. and Yah, Y. (2015). Early prediction model to manage risks in earliest stages to increase project success. *Journal of Theoretical and Applied Information Technology*, Vol. 81, No. 3, pp. 413–419.

Abubakar, M., Ibrahim, Y. M., Kado, D. and Bala, K. (2014). Contractors' perception of the factors affecting Building Information Modelling (BIM) adoption in the Nigerian Construction Industry. *2014 International Conference on Computing in Civil and Building Engineering, June 23–25, 2014, Orlando, Florida, USA*. DOI: 10.1061/9780784413616.022.

Al-Ashmori, Y. Y., Othman, I., Rahmawati, Y., Mugahed Amran, Y. H., Abo Sabah, S. H., Rafindadi, A. D. and Mikić, M. (2020). BIM benefits and its influence on the BIM implementation in Malaysia. *Ain Shams Engineering Journal*, Vol. 11, Issue 4, pp. 1013–1019. DOI: 10.1016/j.asej.2020.02.002.

Ashcraft, H. W. (2008). Building information modeling: A framework for collaboration. *Construction Lawyer*, Vol. 28, No. 3.

Autodesk (2008). Improving building industry results through integrated project delivery and building information modeling. [online] Available at: https://damassets.autodesk.net/content/dam/autodesk/files/bim_and_ipd_whitepaper.pdf [Date accessed: 02.01.2021].

Azhar, S. (2011). Building information modeling (BIM): Trends, benefits, risks, and challenges for the AEC industry. *Leadership and Management in Engineering*, Vol. 11, No. 3, pp. 241–252.

Azhar, S., Brown, J. and Farooqui, R. (2009). BIM-based sustainability analysis: An evaluation of building performance analysis software. *45th ASC Annual Conference, April 1–4, 2009, Gainesville, Florida, USA*.

Azhar, S., Khalfan, M. and Maqsood, T. (2012). Building information modelling (BIM): now and beyond. *Australasian Journal of Construction Economics and Building*, Vol. 12, No. 4, pp. 15–28. DOI: 10.5130/ajceb.v12i4.3032.

Bryde, D., Broquetas, M. and Volm, J. M. (2013). The project benefits of Building Information Modelling (BIM). *International Journal of Project Management*, Vol. 31, Issue 7, pp. 971–980. DOI: 10.1016/j.ijproman.2012.12.001.

Bryman, A. and Cramer, D. (2011). *Quantitative data analysis with IBM SPSS 17, 18 & 19.* Hove, East Sussex: Routledge, *377 p.*

Carmona, J. and Irwin, K. (2007). BIM: who, what, how and why. *Building Operating Management*, Vol. 54, No. 10, pp. 37–39.

Chan, A. P. C., Ma, X., Yi, W., Zhou, X. and Xiong, F. (2018). Critical review of studies on building information modeling (BIM) in project management. *Frontiers of Engineering Management*, Vol. 5, Issue 3, pp. 394–406. DOI: 10.15302/J-FEM-2018203.

Chan, D. W. M., Olawumi, T. O. and Ho, A. M. L. (2019a). Critical success factors for building information modelling (BIM) implementation in Hong Kong. *Engineering, Construction and Architectural Management*, Vol. 26, Issue 9, pp. 1838–1854. DOI: 10.1108/ECAM-05-2018-0204.

Chan, D. W. M., Olawumi, T. O. and Ho, A. M. L. (2019b). Perceived benefits of and barriers to Building Information Modelling (BIM) implementation in construction: The case of Hong Kong. *Journal of Building Engineering*, Vol. 25, 100764. DOI: 10.1016/j.jobe.2019.100764.

Cho, K. M.., Hong, T. H. and Hyun, C. T. (2009). Effect of project characteristics on project performance in construction projects based on structural equation model. *Expert Systems with Applications*, Vol. 36, Issue 7, pp. 10461–10470. DOI: 10.1016/j.eswa.2009.01.032.

Dao, T.-N., Chen, P.-H. and Nguyen, T.-Q. (2021). Critical success factors and a contractual framework for construction projects adopting building information modeling in Vietnam. *International Journal of Civil Engineering*, Vol. 19, Issue 1, pp. 85–102, DOI: 10.1007/s40999-020-00542-3.

Dao, T.-N., Nguyen, T.-Q. and Chen, P.-H. (2020). BIM adoption in construction projects funded with state-managed capital in Vietnam: legal issues and proposed solutions. In: Ha-Minh, C., Dao, D., Benboudjema, F., Derrible, S., Huynh, D. and Tang, A. (eds.), *CIGOS 2019, Innovation for Sustainable Infrastructure*, Vol. 54. Singapore, Springer, pp. 1211–1216. DOI: 10.1007/978-981-15-0802-8_194.

Diaz, P. M. (2016). Analysis of benefits, advantages and challenges of building information modelling in construction industry. *Journal of Advances in Civil Engineering*, Vol. 2, No. 2, pp. 1–11. DOI: 10.18831/djcivil.org/2016021001.

Eastman, C., Teicholz, P., Sacks, R., & Liston, K. (2011). *BIM handbook: A guide to building information modeling for owners, managers, designers, engineers and contractors*. 2nd edition. Hoboken, New Jersey: John Wiley & Sons, *634 p.*

Enegbuma, W. I. and Ali, K. N. (2011a). A preliminary critical success factor (CSFs) analysis of building information

modelling (BIM) implementation in Malaysia. *Proceedings of the Asian Conference on Real Estate (ACRE 2011): Sustainable Growth, Management Challenges, October 3–5 October, Thistle Johor Bahru, Malaysia*.

Enegbuma, W. I. and Ali, K. N. (2011b). A preliminary study on building information modeling (BIM) implementation in Malaysia. In: Liu, S. Z., Javed, A. A., Ni, F. D. and Shen, A. W. (eds.), *Proceedings of 2011 3rd International Post Graduate Conference in Engineering (IPCIE2011), July 11–12, Hong Kong, Vol. 1*. Hong Kong: Hong Kong Polytechnic University, pp. 399–407.

Fallon, K. K. and Palmer, M. E. (2007). *General buildings information handover guide: Principles, methodology and case studies. An industry sector guide of the information handover guide series*. US Department of Commerce, National Institute of Standards and Technology, 89 p.

Fang, D., Li, M., Fong, P. S.-W. and Shen, L. (2004). Risks in Chinese construction market—contractors' perspective. *Journal of construction engineering and management*, Vol. 130, Issue 6, pp. 853–861. DOI: 10.1061/(ASCE)0733-9364(2004)130:6(853).

Field, A. (2013). *Discovering statistics using IBM SPSS statistics*. 4th edition. London: SAGE Publications, 952 p.

Grilo, A. and Jardim-Goncalves, R. (2010). Value proposition on interoperability of BIM and collaborative working environments. *Automation in Construction*, Vol. 19, Issue 5, pp. 522–530. DOI: 10.1016/j.autcon.2009.11.003.

Hai, D. T., Toan, N. Q. and Van Tam, N. (2022). Critical success factors for implementing PPP infrastructure projects in developing countries: the case of Vietnam. *Innovative Infrastructure Solutions*, Vol. 7, Issue 1, 89. DOI: 10.1007/s41062-021-00688-6.

Hair, J. F., Tatham, R. L., Anderson, R. E. and Black, W. C. (1998). *Multivariate data analysis*. 5th edition. Upper Saddle River, New Jersey: Prentice Hall, 730 p.

Hardin, B. and McCool, D. (2015). *BIM and construction management: proven tools, methods, and workflows*. 2nd edition. Hoboken, New Jersey: John Wiley & Sons, *416 p.*

Haron, A. T., Marshall-Ponting, A. J., Zakaria, Z., Nawi, M. N. M., Hamid, Z. A. and Kamar, K. A. M. (2015). An industrial report on the Malaysian building information modelling (BIM) taskforce: issues and recommendations. *Malaysian Construction Research Journal*, Vol. 17, No. 2, pp. 21–36.

Hoang, G. V., Vu, D. K. T., Le, N. H. and Nguyen, T. P. (2020). Benefits and challenges of BIM implementation for facility management in operation and maintenance face of buildings in Vietnam. *IOP Conference Series: Materials Science and Engineering*, Vol. 869, 022032. DOI: 10.1088/1757-899X/869/2/022032.

Hong, Y., Hammad, A. W. A., Sepasgozar, S. and Akbarnezhad, A. (2019). BIM adoption model for small and medium construction organisations in Australia. *Engineering, Construction and Architectural Management*, Vol. 26, Issue 2, pp. 154–183. DOI: 10.1108/ECAM-04-2017-0064.

Hong Duyen, D., Tam, N., Yen, N. and Hoai An, L. (2018). Application Building Information Modelling (BIM) in Quantity surveying: Learnt lessons from some countries in the world. *Journal of Science and Technology in Civil Engineering (STCE) - NUCE*, Vol. 12. No. 1, pp. 46–52. DOI: 10.31814/stce.nuce2018-12(1)-06.

Ibrahim, H. S., Hashim, N. and Jamal, K. A. A. (2019). The potential benefits of Building Information Modelling (BIM) in construction industry. *IOP Conference Series: Earth and Environmental Science*, Vol. 385, 012047. DOI: 10.1088/1755-1315/385/1/012047.

Jordani, D. A. (2010). BIM and FM: The portal to lifecycle facility management. *Journal of Building Information Modeling*, Spring 2010, pp. 13–16.

Joyce, E. (2012). Augmented reality for facilities management edges closer to real-world applications. *Engineering News Record*.

Kerosuo, H., Miettinen, R., Paavola, S., Mäki, T. and Korpela, J. (2015). Challenges of the expansive use of Building Information Modeling (BIM) in construction projects. *Production*, Vol. 25, No. 2, pp. 289–297. DOI: 10.1590/0103-6513.106512.

Li, X., Wu, P., Shen, G. Q., Wang, X. and Teng, Y. (2017). Mapping the knowledge domains of Building Information Modeling (BIM): A bibliometric approach. *Automation in Construction*, Vol. 84, pp. 195–206. DOI: 10.1016/j.autcon.2017.09.011.

Masood, R., Kharal, M. K. N. and Nasir, A. R. (2014). Is BIM adoption advantageous for construction industry of Pakistan? *Procedia Engineering*, Vol. 77, pp. 229–238. DOI: 10.1016/j.proeng.2014.07.021.

Matarneh, R. and Hamed, S. (2017). Barriers to the adoption of building information modeling in the Jordanian building industry. *Open Journal of Civil Engineering*, Vol. 7, No. 3, pp. 325–335. DOI: 10.4236/ojce.2017.73022.

Meadati, P., Irizarry, J. and Akhnoukh, A. K. (2010). BIM and RFID integration: a pilot study. *2nd International Conference on Construction in Developing Countries (ICCIDC–II) "Advancing and Integrating Construction Education, Research & Practice", August 3–5, 2010, Cairo, Egypt*, pp. 570–578.

Memon, A. H., Rahman, I. A., Memon, I. and Azman, N. I. A. (2014). BIM in Malaysian construction industry: status, advantages, barriers and strategies to enhance the implementation level. *Research Journal of Applied Sciences,*

*Engineering and Technology*, Vol. 8, Issue 5, pp. 606–614. DOI: 10.19026/rjaset.8.1012.

Mesároš, P. and Mandičák, T. (2017). Exploitation and benefits of BIM in construction project management. *IOP Conference Series: Materials Science and Engineering*, Vol. 245, Issue 6, 062056. DOI: 10.1088/1757-899X/245/6/062056.

Mohd Noor, S. N. A., Junaidi, S. R. and Ramly, M. K. A. (2018). Adoption of building information modelling (bim): factors contribution and benefits. *Journal of Information System and Technology Management*, Vol. 3, Issue 10, pp. 47–63.

Mostafa, S., Kim, K. P., Tam, V. W. Y. and Rahnamayiezekavat, P. (2020). Exploring the status, benefits, barriers and opportunities of using BIM for advancing prefabrication practice. *International Journal of Construction Management*, Vol. 20, Issue 2, pp. 146–156. DOI: 10.1080/15623599.2018.1484555.

Newton, K. and Chileshe, N. (2012a). Awareness, usage and benefits of building information modelling (BIM) adoption – the case of the South Australian construction organisations. In: Smith, S. D (ed.), *Proceedings of the 28th Annual ARCOM Conference, 3–5 September 2012, Edinburgh, UK*. Edinburgh: Association of Researchers in Construction Management, pp. 3–12.

Newton, K. L. and Chileshe, N. (2012b). Enablers and barriers of building information modelling (BIM) within South Australian construction organisations. *Proceedings of the 37th Annual Conference of Australasian University Building Educators Association (AUBEA), July 4–6, 2012, Sydney, Australia*. Sydney: University of New South Wales. DOI: 10.13140/2.1.4964.1607.

Nguyen, V. T., Nguyen, B. N., Nguyen, T. Q., Chu, A. T. and Dinh, H. T. (2021). The impact of the COVID-19 on the construction industry in Vietnam. *International Journal of Built Environment and Sustainability*, Vol. 8, No. 3, pp. 47–61. DOI: 10.11113/ijbes.v8.n3.745.

Nguyen Van, T., Nguyen Quoc, T. and Le Dinh, L. (2021). An analysis of value chain in the Vietnam construction industry. *International Journal of Sustainable Construction Engineering and Technology*, Vol. 12, No. 3, pp. 12–23. DOI: 10.30880/ijscet.2021.12.03.002.

Oesterreich, T. D. and Teuteberg, F. (2019). Behind the scenes: Understanding the socio-technical barriers to BIM adoption through the theoretical lens of information systems research. *Technological Forecasting and Social Change*, Vol 146(C), pp. 413–431. DOI: 10.1016/j.techfore.2019.01.003.

Olawumi, T. O. and Chan, D. W. M. (2019a). An empirical survey of the perceived benefits of executing BIM and sustainability practices in the built environment. *Construction Innovation*, Vol. 19, Issue 3, pp. 321–342. DOI: 10.1108/CI-08-2018-0065.

Olawumi, T. O. and Chan, D. W. M. (2019b). Building information modelling and project information management framework for construction projects. *Journal of Civil Engineering and Management*, Vol. 25, No. 1, pp. 53–75. DOI: 10.3846/jcem.2019.7841.

Olawumi, T. O., Chan, D. W. M., Wong, J. K. W. and Chan, A. P. C. (2018). Barriers to the integration of BIM and sustainability practices in construction projects: A Delphi survey of international experts. *Journal of Building Engineering*, Vol. 20, pp. 60–71. DOI: 10.1016/j.jobe.2018.06.017.

Qian, A. Y. (2012). *Benefits and ROI of BIM for multi-disciplinary project management*. Singapore: National University of Singapore.

Reddy, K. P. (2011). *BIM for building owners and developers: making a business case for using BIM on projects*. Hoboken, New Jersey: John Wiley & Sons*, 230 p.*

Saka, A. B. and Chan, D. W. M. (2019). A scientometric review and metasynthesis of building information modelling (BIM) research in Africa. *Buildings*, Vol. 9, Issue 4, 85. DOI: 10.3390/buildings9040085.

Saka, A. B., Chan, D. W. M. and Olawumi, T. O. (2019). A systematic literature review of building information modelling in the architecture, engineering and construction industry - the case of Nigeria. *EDMIC 2019: Environmental Design and Management International Conference*, pp. 728–738.

Schade, J., Olofsson, T. and Schreyer, M. (2011). Decision-making in a model-based design process. *Construction Management and Economics*, Vol. 29, Issue 4, pp. 371–382. DOI: 10.1080/01446193.2011.552510.

Schlueter, A. and Thesseling, F. (2009). Building information model based energy/exergy performance assessment in early design stages. *Automation in Construction*, Vol. 18, Issue 2, pp. 153–163. DOI: 10.1016/j.autcon.2008.07.003.

Seyis, S. (2019). Pros and cons of using building information modeling in the AEC industry. *Journal of Construction Engineering and Management*, Vol. 145, Issue 8, 04019046. DOI: 10.1061/(ASCE)CO.1943-7862.0001681.

Sholeh, M. N., Nurdiana, A., Setiabudi, B. and Suharjono (2020). Identification of potential uses of Building Information Modeling (BIM) for construction supply chain management: preliminary studies. *IOP Conference Series: Earth and Environmental Science*, Vol. 448, 012064. DOI: 10.1088/1755-1315/448/1/012064.

Stanley, R. and Thurnell, D. P. (2014). The benefits of, and barriers to, implementation of 5D BIM for quantity surveying in New Zealand. *Construction Economics and Building*, Vol. 14, No. 1, pp. 105–117. DOI: 10.5130/AJCEB.v14i1.3786.

Succar, B. (2009). Building information modelling framework: A research and delivery foundation for industry stakeholders. *Automation in Construction*, Vol. 18, Issue 3, pp. 357–375. DOI: 10.1016/j.autcon.2008.10.003.

Tse, T.-C. K., Wong, K.-D. A. and Wong, K.-W. F. (2005). The utilisation of building information models in nD modelling: a study of data interfacing and adoption barriers. *Journal of Information Technology in Construction (ITcon)*, Vol. 18, Special Issue "From 3D to nD Modelling", pp. 85–110.

Van Tam, N., Diep, T. N., Quoc Toan, N. and Le Dinh Quy, N. (2021a). Factors affecting adoption of building information modeling in construction projects: A case of Vietnam. *Cogent Business & Management*, Vol. 8, Issue 1, 1918848. DOI: 10.1080/23311975.2021.1918848.

Van Tam, N., Huong, N. L. and Ngoc, N. B. (2018). Factors affecting labour productivity of construction worker on construction site: A case of Hanoi. *Journal of Science and Technology in Civil Engineering (STCE) - NUCE*, Vol. 12, No. 5, pp. 127–138. DOI: 10.31814/stce.nuce2018-12(5)-13.

Van Tam, N., Quoc Toan, N., Phong, V. V. and Durdyev, S. (2021b). Impact of BIM-related factors affecting construction project performance. *International Journal of Building Pathology and Adaptation,* ahead-of-print. DOI: 10.1108/IJBPA-05-2021-0068.

Vaske, J. J., Beaman, J. and Sponarski, C. C. (2017). Rethinking internal consistency in Cronbach's alpha. *Leisure Sciences*, Vol. 39, Issue 2, pp. 163–173. DOI: 10.1080/01490400.2015.1127189.

Wong, A. K. D., Wong, F. K. W. and Nadeem, A. (2009). Attributes of building information modelling and its development in Hong Kong. *HKIE Transactions*, Vol. 16, Issue 2, pp. 38–45. DOI: 10.1080/1023697X.2009.10668156.

# Technique and Technology of Land Transport in Construction

## DYNAMIC MODEL OF A RAILWAY LIFTING CRANE

Jan Vatulin, Denis Potakhov, Egor Potakhov*, Sergei Orlov

Emperor Alexander I St. Petersburg State Transport University
Moskovsky pr., 9, Saint Petersburg, Russia

*Corresponding author: epotakhov@mail.ru

**Abstract**

**Introduction**: Currently, mobile boom cranes equipped with telescopic boom equipment are widely used in construction, loading and unloading, as well as installation. **Purpose of the study**: We aimed to develop a dynamic model for a railway lifting crane, taking into account the interaction of its structural elements with each other and the bearing soil surface in a three-dimensional formulation. **Methods**: In the course of the study, we used Simulation and Motion modules of the SolidWorks software package, Klepikov's non-linearly deformable soil model, and Lagrange's equation of the second kind. **Results**: As a result, we developed a numerical analytical 3D model describing dynamic loading and deformation of the "mobile boom crane – foundation" system in a three-dimensional formulation. The model takes into account the following: the internal bending deformation and the interaction of the mating structural elements of a crane (telescopic sections, telescoping hydraulic cylinders, and outriggers), hoist rope rigidity, grillage (framework of sleepers) influence, elastic and plastic properties of the base platform soil, and action of inertial loads on the structural elements of the lifting crane.

**Keywords**

Railway lifting crane, crane model, numerical dynamic model.

## Introduction

Currently, mobile boom cranes (MBCs) equipped with telescopic boom equipment are widely used in construction, loading and unloading, as well as installation (Aleksandrov, 2000). They came into common use due to their high mobility and lifting capacity, the possibility of operation in confined spaces, considerable lifting height and load/attachment lifting and lowering speed, simplified transportation, etc.

It is a known fact that most lifting crane failures are related to dynamic loads causing heavy wear of contacting elements, breakdown of load-bearing metal structures and components of mechanisms, critical deformations, etc. (Aleksandrov et al., 1986). In MBC operation, crane elements experience dynamic loading from the simultaneous action of various loads caused by inertial forces during the rotation of the rotary platform and load lifting/lowering, a pliable foundation, bending stiffness of boom equipment, clearances between the contacting elements, load swinging on a flexible hoist rope, meteorological factors, etc. It has been established that the dynamics of the telescopic boom equipment of a lifting crane significantly affect the dynamic loads of outriggers (Qian et al., 2017; Shcherbakov et al., 2009; Shelmich, 1996).

The load-bearing capacity and gradient of the foundation significantly affect the stability of a lifting crane when loaded. Thus, MBC operating instructions pay a lot of attention to the operating site (MBC location in relation to the pit depending on the type of soil; permissible specific soil loading at the operating site, site preparation methods).

To determine the exact maximum loading of individual lifting crane components, it is important to consider a lifting machine as a system of inter-related elements with the maximum possible number of constituents, taking into account the maximum possible number of loading factors.

To perform capital or emergency works (emergency damage control on track; replacement, loading, and unloading of structural railway track elements, etc.), railway lifting cranes are used.

The operation of railway lifting cranes is distinguished by the fact that such cranes rest on special elements — a framework of sleepers (grillage) (Petukhov et al., 1985; Muzhichkov et al., 1978), which are installed on the subgrade shoulder when cutting a niche in the subgrade area and part of the ballast section, and reduce the average pressure of the outriggers on the ground.

Dynamic loading from rolling stock as well as exposure to atmospheric precipitation, alternating

freezing and thawing, moistening and drying, contamination with particles of goods transported (coal, ore, salts, and other minerals), corrosion, etc. result in layer motion and changes in the railway track substructure and its characteristics.

Changes in the soil structure affect the load-bearing capacity and stability of the soil mass (Ishihara, 1996; Savinov, 1979). Ground motion promotes the development of uneven settlements of structures (Ishihara, 1996; Savinov, 1979) (including railway tracks). As a result, the top layers of the soil mass with the grillage may deform in the direction from the longitudinal axis of the railway track to the subgrade shoulder, thus leading to additional loads on the outriggers, which affects the loading of the lifting machine in general.

Thus, layer motion and changes in the base (foundation) structure and characteristics can have a negative impact on the operation of railway lifting machines mounted on that foundation.

The pliability of the supporting elements, clearances between the sections of the telescopic boom (structural and those formed as a result of wear of the supporting elements and outriggers), bending deformation of the extended telescopic sections and telescoping hydraulic cylinders significantly affect the oscillatory processes with regard to the MBC and load. Oscillations result in the formation of dynamic loading and heavy wear of mating surfaces, as well as increase load swinging and the time of its stabilization, which makes it difficult to ensure accurate load positioning. As a result, the MBC output decreases. This effect is most noticeable in railway cranes during track works performed when taking possession of the line.

We aimed to develop a dynamic model for a railway lifting crane, taking into account the interaction of its structural elements with each other and the bearing soil surface in a three-dimensional formulation.

**Subject, tasks, and methods**

It is rather difficult to conduct experimental studies when trying to achieve the limiting state in actual MBCs. This is due to significant economic losses, a decrease in the operating life of crane equipment, and high potential site hazards. In this regard, to determine the parameters of dynamic loading on the MBC elements, a numerical experiment seems the most reasonable. Simulation makes it possible to save considerable physical resources, significantly reduce the development time during design, analyze loading on the elements of a lifting machine with no damage to the object of the study or changes in its operating life, and avoid danger to life and health of the machine maintenance personnel, designers, and researchers.

The numerical simulation procedure has two stages: developing a virtual model and conducting a numerical experiment with regard to loading modes. The analytical dynamic model of the MBC system shall adequately reflect the basic physical and mechanical characteristics of the actual boom crane elements.

Simulation is carried out in SolidWorks Simulation (module for structural analysis using the finite element method) and SolidWorks Motion (module for comprehensive dynamic and kinematic structural analysis) (Alyamovsky, 2015; Kurowski, 2017).

The virtual 3D model of a lifting crane of the "MBC – foundation" system is based on the structure of the Sokol 80.01M railway boom crane (Fig. 1). Bogies as well as elements not presented in the model in terms of design (power unit engine, rotation mechanism, hook assembly, automatic coupler, winch hydraulic motor, winch, counterbalance, operator's cab, etc.) are accounted for by concentrated and distributed masses and forces.

The developed numerical dynamic model of the "MBC – foundation" system in SolidWorks Motion conventionally consists of three levels (Table 1) and can be adjusted according to the following:

– the geometric and mass inertia characteristics of lifting crane elements;

– the correspondence between the reactions of the lifting crane model outriggers with the reactions obtained using methods described by Gokhberg (1988) and Vainson (1989);

– stiffness and strength characteristics of elements, parts, and assemblies of the lifting machine and framework of sleepers;

– the theory of soil mechanics;

– the system of differential equations for free and forced oscillations of the telescopic boom section, load, and frame, with account for foundation pliability.
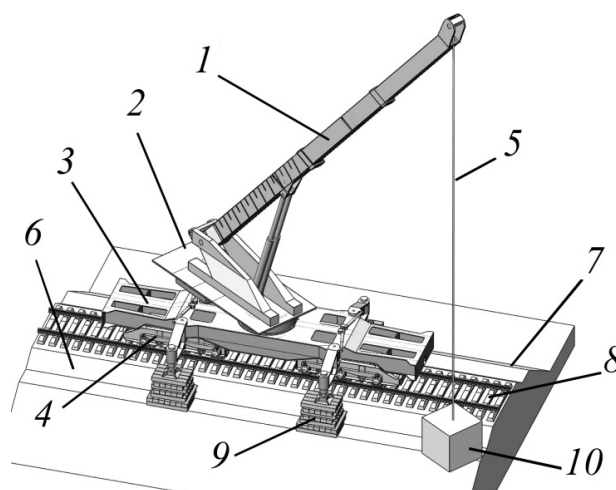


Fig. 1. Numerical dynamic model of the
"MBC – foundation" system.
Lifting crane numerical model:
1 — a telescopic boom, 2 — a rotary platform,
3 — a crane platform, 4 — a bogie, 5 — a hoist rope.
Railway track section model: 6 — a ballast section,
7 — a subgrade, 8 — assembled rails and sleepers.
Other elements: 9 — a framework of sleepers, 10 — a load

Due to the fact that, in SolidWorks Motion, elements of mechanical systems are considered rigid, structural deformations are not taken into account. To simulate bending deformation in structures, a "fictitious" joint (Hooke's joint) is used, which is equipped with viscoelastic elements (springs and a damper) (Fig. 2). The location of the joints is determined based on the results of lifting crane frequency and modal analysis: the "fictitious" joints are placed in the areas corresponding to the instantaneous centers of rotation, speed, and acceleration of the structure: two in the telescopic boom, two in each telescoping hydraulic cylinder (Fig. 2), and one in each outrigger. The parameters of the "fictitious" joint are set in such a way so as to ensure convergence of displacements (deformations) and oscillation modes of the dynamic model in the Motion module with the displacements in the Simulation static strength analysis and oscillation modes in the Simulation modal analysis.

The numerical model of the framework of sleepers consists of two elements connected with a spherical joint. One of the elements is in contact with soil, and the other element has two Kelvin–Voigt models in two planes where the parameters of these models correspond to the pliability of the framework of sleepers.

A nonlinearly deformable model developed by Klepikov (1996), taking into account purely elastic and residual (plastic) deformations, is used as a mathematical model of soil in the "MBC – foundation"

numerical system for foundation simulation.

Klepikov (1996) suggested an equation for general determination of the case of non-homogeneous foundation represented by any analytical model:
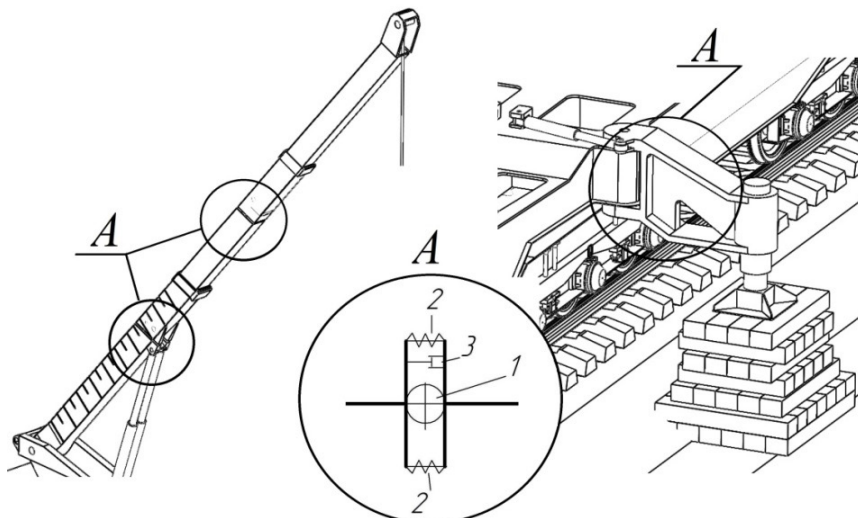
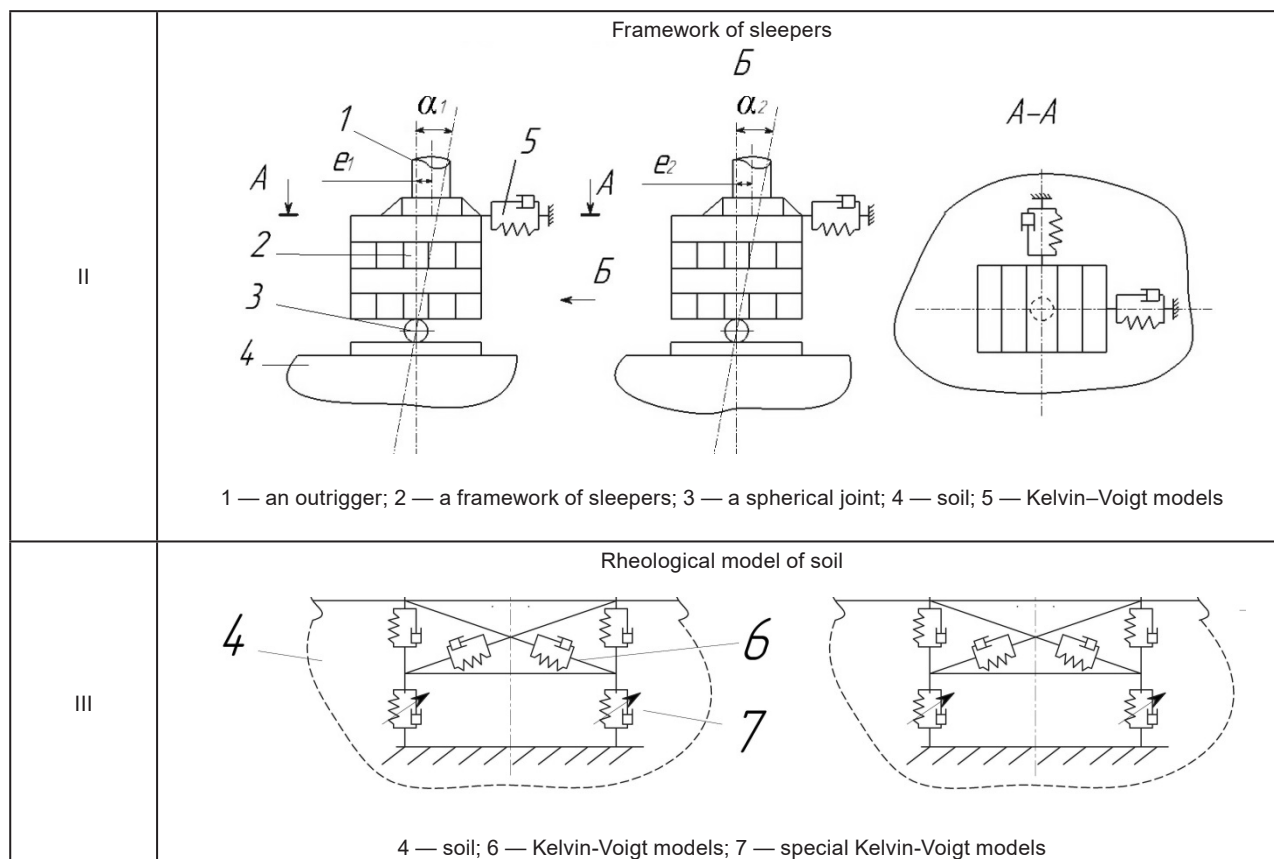$$s = \frac{\bar{s}(1 - \bar{p}/p_u)p}{\bar{p}(1 - p/p_u)},$$

where $\bar{s}$ — the foundation surface settlement at pressure $\bar{p}$ under the foundation bottom, not exceeding the design resistance R of subgrade soil; $p$ — the average pressure uniformly distributed on the foundation surface; $P_u$ — the ultimate pressure on the foundation, corresponding to the exhaustion of its load-bearing capacity.

The settlement $\bar{s}$ is determined considering the shape of the foundation bottom, availability of heterogeneous soil layers, and depth of the compressed foundation.

The rheological model of soil consists of vertical, inclined, and special Kelvin–Voigt models. The horizontal components of the Kelvin–Voigt models simulate shear resistance. The vertical components of the Kelvin–Voigt models simulate the elastic properties of the soil foundation. The special Kelvin–Voigt models were developed to simulate the plastic properties of soil base since they do not feature recovery of deformations after load removal. The parameters of the given elements in the numerical rheological model of soil are adjusted according to Klepikov (1996).

Table 1. Levels of the numerical dynamic model

| Level | Analytical model |
|---|---|
| I | Lifting crane <br>  <br> A — "fictitious" joints: 1 — a spherical joint, 2 — a spring, 3 — a damper |

1 — an outrigger; 2 — a framework of sleepers; 3 — a spherical joint; 4 — soil; 5 — Kelvin–Voigt models

4 — soil; 6 — Kelvin-Voigt models; 7 — special Kelvin-Voigt models

During the analysis of dynamic processes, multi-mass systems of a real-life object with a large number of degrees of freedom are usually reduced to simplified dynamic models (analytical models) that consist of several concentrated reduced masses interconnected by viscoelastic links (springs and a damper) (Gokhberg, 1988; Vainson, 1989; Yablonsky and Noreyko, 2003). The motion of dynamic mathematical models is described by systems of differential equations. Based on their solution, conclusions are drawn about the loads acting on the elements of the object under consideration, as well as the motion of those elements.

Since the motion of the MBC elements is of a spatial nature, the analytical mathematical model of the "MBC – foundation" system is represented in the form of a system of equations where the first subsystem of equations describes the motion of the object under consideration in the vertical plane and the second subsystem of equations describes the motion of the object under consideration in the horizontal plane.

Two separate multi-mass dynamic models of the MBC elements are formed: horizontal and vertical models, including masses of the load, middle and upper sections, piston and rod of the upper telescoping hydraulic cylinder, piston and rod of the lower telescoping hydraulic cylinder, frame, outriggers, and frameworks of sleepers. The reduced masses are connected by viscoelastic links (Kelvin–Voigt models). The frameworks of sleepers and the

foundation are also connected with viscoelastic elements. Two separate subsystems of differential equations, based on Lagrange's equation of the second kind, are composed: the first one describes the motion of the load and MBC elements in the vertical plane, and the second one describes the motion of the load and MBC elements in the horizontal plane. The equations include the kinetic and potential energies of the system as well as the Rayleigh dissipation function.

The general solution of the system of differential equations is based on the sum of the general integral of the corresponding system of homogeneous equations and the particular integral of the analyzed non-homogeneous system. The first solution describes free oscillations of the object under consideration, and the second solution describes forced oscillations of the object under consideration (Yablonsky and Noreyko, 2003).

**Results and discussion**

As a result of the studies, we have developed an analytical 3D model describing dynamic loading and deformation of the "MBC – foundation" system in a three-dimensional formulation. The model takes into account the following: the internal bending deformation and the interaction of the mating structural elements of a crane (telescopic sections, telescoping hydraulic cylinders, and outriggers), hoist rope rigidity, grillage (framework of sleepers) influence, elastic and plastic properties of the base platform soil, and action of inertial loads on the
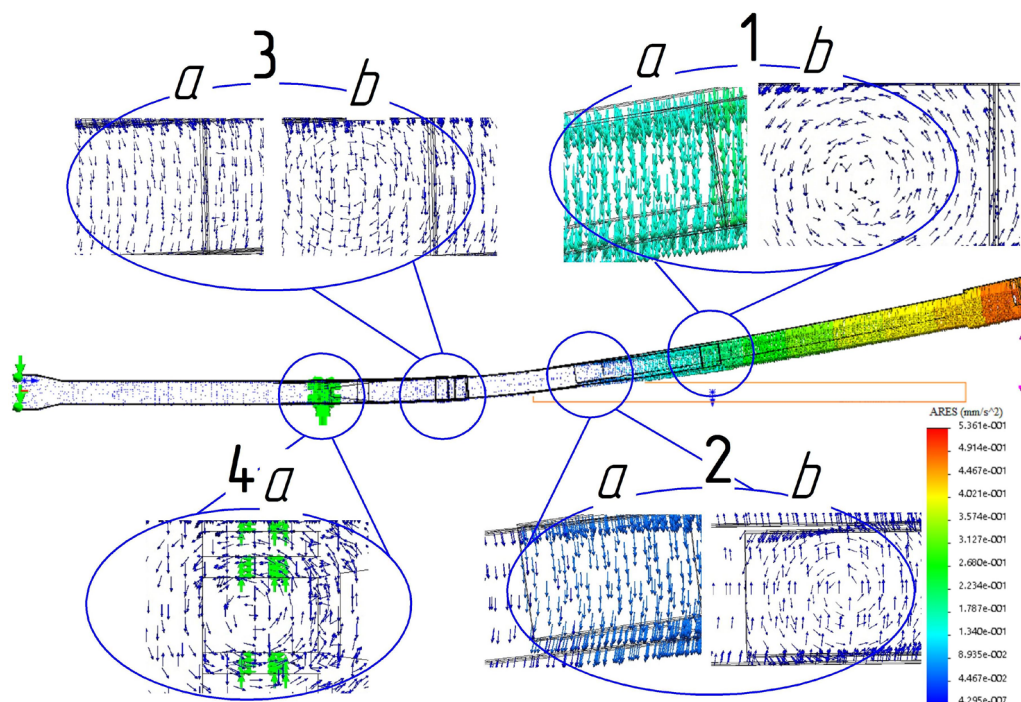
Fig. 2. Vector representation of the acceleration of oscillatory processes in the telescopic boom in the horizontal plane:
1, 2, 3, 4 — areas of instantaneous centers of rotation, speed, and acceleration; a — the basis vector; b — the short-term vector

structural elements of the lifting crane.

**Conclusions**

Currently, mobile boom cranes equipped with telescopic boom equipment are widely used in construction, loading and unloading, as well as installation. It is a known fact that most lifting machine failures are related to dynamic loads. It is rather difficult to conduct experimental studies when trying to achieve the limiting state in actual lifting cranes. This is due to significant economic losses, a decrease in the operating life of crane equipment, and high potential site hazards. In this regard, to determine the parameters of dynamic loading on the MBC elements, we have performed a numerical simulation in SolidWorks Simulation and SolidWorks Motion.

As a result of the studies, we have developed a numerical analytical 3D model describing dynamic loading and deformation of the "MBC – foundation" system in a three-dimensional formulation. The model takes into account the following: the internal bending deformation and the interaction of the mating structural elements of a crane (telescopic sections, telescoping hydraulic cylinders, and outriggers), hoist rope rigidity, grillage (framework of sleepers) influence, elastic and plastic properties of the base platform soil, and action of inertial loads on the structural elements of the lifting crane. The developed analytical spatial model makes it possible to obtain temporal dependencies for the kinematic and dynamic parameters of the lifting crane elements, counter-forces (reaction forces) of the mating components of the system in the dynamic loading mode during lifting machine operation on a pliable foundation. It seems possible to determine the nature of loading in any arbitrary point (or a set of points) of the analytical model, considering the mutual influence of the bending deformation of the crane elements and the rigidity of the platform.

The concept of analytical spatial model development can be extrapolated to all types of lifting machines with any type of foundation.

The results of the studies will improve the accuracy of simulating lifting crane operation and crane elements loading, which, in turn, will improve lifting machines' operational safety. Besides, it is possible to upgrade the developed mathematical model: by adding new or replacing existing structural and "fictitious" elements (viscoelastic elements, joints, sections, load, outriggers, etc.); by adding various types of external loads; by changing the position and motion modes of the elements; and by applying control systems and optimization methods.

**References**

Aleksandrov, M. P. (2000). *Hoisting machines*. Moscow: Publishing House of Bauman Moscow State Technical University – Vysshaya Shkola, 552 p.

Aleksandrov, M. P., Kolobov, L. N., Lobov, N. A., Nikolskaya, T. A. and Polkovnikov, V. S. (1986). *Hoisting machines*. Moscow: Mashinostroyenie, 400 p.

Alyamovsky, A. A. (2015). *SolidWorks Simulation. Engineering analysis for professionals: tasks, methods, recommendations*. Moscow: DMK Press, 562 p.

Gokhberg, M. M. (ed.) (1988). *Handbook on cranes. In 2 volumes. Vol. 1 Characteristics of materials and loads. Basics of analysis for cranes, their drives, and metal structures*. Moscow: Mashinostroyenie, 536 p.

Ishihara, K. (1996). *Soil behavior in earthquake geotechnics (Oxford Engineering Science Series, 46)*. Oxford: Clarendon Press, 350 p.

Klepikov, S. N. (1996). *Analysis of structures on a deformable foundation*. Kiev: Research Institute for Building Structures, 203 p.

Kurowski, P. (2017). *Engineering analysis with SolidWorks Simulation 2017*. Mission, KS: SDC Publications, 200 p.

Muzhichkov, V. I. and Rednikov, V. A. (1978). *Railway lifting cranes*. 4th edition. Moscow: Transport, 433 p.

Petukhov, P. Z., Ksyunin, G. P. and Serlin, L. G. (1985). *Special cranes*. Moscow: Mashinostroyenie, 248 p.

Qian, J. B., Bao, L. P., Yuan, R. B. and Yang, X. J. (2017). Modeling and analysis of outrigger reaction forces of hydraulic mobile crane. *International Journal of Engineering*, Vol. 30, Issue 8, pp. 1246–1252.

Savinov, O. A. (1979). *Modern structures of foundations for machines and their analysis*. 2nd edition. Leningrad: Stroyizdat, Leningrad Department, 200 p.

Shcherbakov, V. S., Zyryanova, S. A. and Korytov, M. S. (2009). *System for automated modeling of a lifting boom crane*. Omsk: Siberian State Automobile and Highway University (SibADI), 106 p.

Shelmich, R. R. (1996). Dynamic loads and stability of a truck crane on an elastic foundation. *Construction and Road Building Machinery*, No. 4.

Vainson, A. A. (1989). *Hoisting and transporting machines*. 4th edition. Moscow: Mashinostroyenie, 536 p.

Yablonsky, A. A. and Noreyko S. S. (2003). *Oscillation theory course*. Saint Petersburg: Lan, 256 p.

# ДИНАМИЧЕСКАЯ МОДЕЛЬ ЖЕЛЕЗНОДОРОЖНОГО ГРУЗОПОДЪЕМНОГО КРАНА

Ян Семенович Ватулин, Денис Александрович Потахов, Егор Александрович Потахов*, Сергей Васильевич Орлов

Петербургский государственный университет путей сообщения Императора Александра I
Московский пр., 9, Санкт-Петербург, Россия

*E-mail: epotakhov@mail.ru

**Аннотация**
В настоящее время для выполнения различных строительных, погрузо-разгрузочных и монтажных работ широкое используются самоходные стреловые краны, оснащенные телескопическим стреловым оборудованием. **Цель исследования:** Разработка динамической модели железнодорожного грузоподъемного крана с учетом взаимодействия конструктивных элементов крана между собой и с грунтовой опорной поверхностью в трехмерной постановке. **Методы:** Модули Simulation и Motion программного комплекса SolidWorks, нелинейно-деформируемая модель грунта С.Н. Клепикова, уравнение Лагранжа второго рода. **Результаты:** Разработана численная расчетная 3D-модель, которая отражает динамическое нагружение и деформирование системы «стреловой самоходный кран – основание» в трехмерной постановке, учитывая: собственную изгибную деформацию и взаимодействие сопряженных конструктивных элементов крана (телескопические секции, гидроцилиндры телескопирования, аутригеры), жесткость грузового каната, влияние шпальной клети, пластические и упругие свойства грунта опорной площадки, действие инерционных нагрузок на элементы и узлы грузоподъемного крана.

**Ключевые слова**
Железнодорожный грузоподъемный кран, модель крана, численная динамическая модель.

# Guide for Authors
# for submitting a manuscript for publication in the «Architecture and Engineering»

The journal is an electronic media and accepts the manuscripts via the online submission. Please register on the website of the journal http://aej.spbgasu.ru/, log in and press "Submit article" button or send it via email aejeditorialoffice@gmail.com.

Please ensure that the submitted work has neither been previously published nor has been currently submitted for publication in another journal.

**Main topics of the journal:**

1. Architecture
2. Civil Engineering
3. Geotechnical Engineering and Engineering Geology
4. Urban Planning
5. Technique and Technology of Land Transport in Construction

**Title page**

The title page should include:

The title of the article in bold (max. 90 characters with spaces, only conventional abbreviations should be used); The name(s) of the author(s); Author's(s') affiliation(s); The name of the corresponding author.

**Abstract and keywords**

Please provide an abstract of 100 to 250 words. The abstract should not contain any undefined abbreviations or unspecified references. Use the IMRAD structure in the abstract (introduction, methods, results, discussion).

Please provide 4 to 6 keywords which can be used for indexing purposes. The keywords should be mentioned in order of relevance.

**Main text**

It should have the following structure:

1) Introduction,
2) Scope, Objectives and Methodology (with subparagraphs),
3) Results and Discussion (may also include subparagraphs, but should not repeat the previous section or numerical data already presented),
4) Conclusions,
5) Acknowledgements (the section is not obligatory, but should be included in case of participation of people, grants, funds, etc. in preparation of the article. The names of funding organizations should be written in full).

**General comments on formatting:**

- Subtitles should be printed in Bold,
- Use MathType for equations,
- Tables should be inserted in separate paragraphs. The consecutive number and title of the table should be placed before it in separate paragraphs. The references to the tables should be placed in parentheses (Table 1),
- Use "Top and Bottom" wrapping for figures. Figure captions should be placed in the main text after the image. Figures should be referred to as (Fig. 1) in the text.

**References**

The journal uses Harvard (author, date) style for references:

**Reference list**

The list of references should only include works that are cited in the text and that have been published or accepted for publication. Personal communications and unpublished works should only be mentioned in the text. Do not use footnotes or endnotes as a substitute for a proper reference list. All references must be listed in full at the end of the paper in alphabetical order, irrespective of where they are cited in the text. Reference made to sources published in languages other than English or Russian should contain English translation of the original title together with a note of the used language.

**Peer Review Process**

Articles submitted to the journal undergo a double blind peer-review procedure, which means that the reviewer is not informed about the identity of the author of the article, and the author is not given information about the reviewer.
On average, the review process takes from one to three months.